Synthesis, Characterization and Optical Properties of Rare Earth – Transition Metal Based Environmentally Friendly Red and Yellow Pigments

Thesis submitted to

Cochin University of Science and Technology

for the award of the degree of

Doctor of Philosophy

in

Chemistry

under

The Faculty of Science

By

SANDHYA KUMARI L.

DEPARTMENT OF ELECTRON MICROSCOPY

MATERIALS SCIENCE AND TECHNOLOGY DIVISION

NATIONAL INSTITUTE FOR INTERDISCIPLINARY SCIENCE AND TECHNOLOGY (NIIST)

THIRUVANANTHAPURAM - 695019, KERALA, INDIA

2012

...Dedicated to

my son Goutham...

DECLARATION

I hereby declare that the Ph.D thesis entitled "**Synthesis, Characterization and Optical Properties of Rare Earth – Transition Metal Based Environmentally Friendly Red and Yellow Pigments**" is an independent work carried out by me at the Materials Science and Technology Division, National Institute for Interdisciplinary Science and Technology (NIIST)-CSIR, Thiruvananthapuram, under the supervision of **Dr. P. Prabhakar Rao** (Guide), Senior Principal Scientist and **Dr. Peter Koshy** (Co-Guide), Rtd. Chief Scientist, for the degree of Doctor of Philosophy in chemistry of the Cochin University of Science and Technology and it has not been submitted anywhere else for any other degree, diploma or title.

Sandhya Kumari L.

Thiruvananthapuram
August 2012

NATIONAL INSTITUTE FOR INTERDISCIPLINARY SCIENCE AND TECHNOLOGY (NIIST)

Council of Scientific & Industrial Research (CSIR)
(Formerly Regional Research Laboratory)
Industrial Estate P.O., Thiruvananthapuram – 695 019
Kerala, INDIA

August 2012

CERTIFICATE

This is to certify that the thesis entitled "**Synthesis, Characterization and Optical Properties of Rare Earth – Transition Metal Based Environmentally Friendly Red and Yellow Pigments**" is an authentic record of the bonafide research work carried out by **Mrs. Sandhya Kumari L.** at the Materials Science and Technology Division of National Institute for Interdisciplinary Science and Technology (NIIST)-CSIR, Thiruvananthapuram for the degree of Doctor of Philosophy in Chemistry of Cochin University of Science and Technology under our guidance and supervision.

Dr. P. Prabhakar Rao
(Guide)
Senior principal Scientist
National Institute for Interdisciplinary Science and Technology (NIIST)
Thiruvananthapuram

Dr. Peter Koshy
(Co-Guide)
Rtd. Chief Scientist
National Institute for Interdisciplinary Science and Technology (NIIST)
Thiruvananthapuram

Acknowledgements

This thesis is a culmination of many years of effort where I have been accompanied and supported by many. One of the joys of completion is to look over the journey past and remember all those who have helped and supported me along this long but fulfilling road.

First and foremost I offer my sincerest gratitude to my supervisor, Dr. P. Prabhakar Rao, who has supported me throughout my thesis with his patience and knowledge. He has been supportive since the day I began working on the pigments as a postgraduate. His expertise, understanding, and patience, added considerably to my graduate experience. His suggestions always added another dimension of perfection to my work. I am grateful to you for introducing me to research and the mentorship provided over the years which prepared me for this doctoral work.

I am indebted to my co-guide Dr. Peter Koshy, without whose motivation and encouragement I would not have a research career. He provided me with direction, technical support and became more of a mentor and friend, than a guide. It was through his persistence, understanding and kindness that I continued my research work and was encouraged to apply for Senior Research Fellowship. I doubt that I will ever be able to convey my appreciation fully, but I owe him my eternal gratitude. One simply could not wish for a better or friendlier supervisor.

I would like to convey my gratitude to Dr. Suresh Das, Director, NIIST, Thiruvananthapuram and former directors Dr. T. K. Chandrashekar and Dr. B. C Pai for the infrastructural facilities provided.

I sincerely thank Dr. M. T. Sebastian, Dr. K. G. K. Warrier, and Dr. U. Syamaprasad for extending the research facilities.

I would like to express my gratitude to Dr. M. L. P. Reddy, Scientist, Chemical Sciences and Technology Division, NIIST, Thiruvananthapuram for guiding me during my NMITLI project period.

I express my gratitude to Dr. A. Ananthakumar and Dr. J. D. Sudha for their help during my research.

I would like to thank Mr. M. R. Chandran for all the help and support and for SEM works. A very special thanks goes out to Mr. M. R. Nair for his selfless affection and for his constant moral support. I would like to thank Mrs. Lucy Paul for helping me out with the SEM works, Mr. V. Sreekantan and Mr. Shanoj for their untiring and immediate help. I also thank Mr. S. Velusamy for TG/DTA analysis and Mr. Kiran Mohan for TEM analysis.

In my daily work I have been blessed with a friendly and cheerful group of fellow students. Words are inadequate to express my heartfelt gratitude to my colleagues Mrs. Anjuthara, Dr. V. Jayasree, Mrs. A.V. Anjana, Dr. K. S. Sibi, Dr. M. Deepa, Mr. A. N. Radhakrishnan, Mrs. Mariyam Thomas, Mr. S. K. Mahesh, Ms. S. Sumi, Mrs. S. Sameera, Ms. K.S. Mary Linsa, Mr. D. S. Vaisakhan Thampi, Mrs. V. R. Reshmi, Ms. T. Linda Francis, Ms. Vineetha James and Ms. S. Divya with whom I have spent many memorable occasions and who have been very helpful and supportive both in personal and academic.

I express my thanks to Dr. V. S. Vishnu, Dr. Giable George and Ms. Sheethu Jose for their help.

Special thanks to Mr. S. K. Mahesh and Ms. S. Sumi for proof reading this thesis.

I acknowledge the Council of Scientific and Industrial Research, New Delhi for the award of Senior Research Fellowship, NMITLI, CSIR and Kerala State Council for Science

Technology and Environment, for the fellowship towards a project during the early stages of my research.

I take this opportunity to sincerely acknowledge all scientists, students and staff members of Materials Science and Technology Division for their help and support. I convey my special acknowledgments to Administrative section, Finance and Account section, Stores and Purchase Section, and Library and Information section for extending me various services to facilitate my research program.

Warmest thanks to my husband Shyam for always being by my side, supporting and encouraging me to be on track. He has been, always, my pillar, my joy and my guiding light. My family deserves special mention for their inseparable support and prayers. My parents' unconditional credit and support have sustained me throughout my life. I cannot ask for more from my father and mother, as they have both been wonderful parents to me and also for caring my son during my busy research period. I thank my beloved father, mother and my sister Soumya for their blessings and love. This thesis is specially dedicated to my son, Goutham.

I would like to thank everyone who was important to the successful realization of the thesis.

Finally, I praise God almighty for strengthening me throughout my life.

Sandhya Kumari L.

Contents

List of Tables

List of Figures

List of Abbreviations

ISO	International Organization for Standardisation
DIN	Deutsches Institute fur Normung (German Standards Organisation)
CIE	Commission Internationale de l'Eclairage
AN	Adams–Nickerson
VB	Valence Band
CB	Conduction Band
RE	Rare Earth
Ln	Lanthanide
UV	Ultraviolet
vis	Visible
ISR	Integrating Sphere
NIR	Near Infrared
LD	Lethal Dose
XRD	X–Ray Diffraction
SEM	Scanning Electron Microscope
TEM	Transmission Electron Microscope
HRTEM	High Resolution Transmission Electron Microscope
EDS	Energy Dispersive Spectrometer
PTFE	Poly–tetrafluoroethylene
ASTM	American Society for Testing and Materials
TG	Thermogravimety

DTA	Differential Thermal Analysis
PMMA	Poly (methyl methacrylate)
CN	Co-ordination Number
CT	Charge Transfer
PDF	Powder diffraction File
HOMO	Highest Occupied Molecular Orbital
LUMO	Lowest Unoccupied Molecular Orbital

PREFACE

Inorganic pigments are widely used in various applications such as paints, inks, plastics, rubbers, ceramics, enamels and glasses. Unfortunately, many of the inorganic pigments which are currently used for industrial applications comprise of toxic metal ions like cadmium, lead, chromium and cobalt. The use of these metal ions is becoming increasingly strictly controlled, indeed banned by legislation in many countries due to their high toxicity. Further, there is a need to add specialty or smart applications to the pigments employed as exterior coatings. Rising energy cost continues to drive advances in new technologies designed to improve energy efficiency across the globe. One such technology is the use of specialty infrared reflective pigments which impart color to an object and reflect the invisible heat from the object to minimize heat build-up, when exposed to solar radiation. NIR reflective pigments coated on the external walls of a building can reduce energy consumption, which makes the interior of the building cooler. Hence, there is a strong incentive to develop new colored NIR reflecting pigments to substitute for industrial pigments that are based on toxic metals hazardous to health and environment.

The primary objective of the present investigation is to design and develop non–toxic rare earth – transition metal based red and yellow inorganic pigments as viable alternatives to the traditional toxic pigment formulations. The second objective of this work is to study the structural, morphological and optical properties of pigments and explore their coloring mechanism and band gap tuning. In addition, testing of the synthesized pigments for coloring applications in plastics and investigations on the NIR-reflecting properties to reduce the heat build-up have been carried out. The thesis is well organized into six chapters and the details of the studies are given below.

A general introduction to inorganic pigments, their classification, application and theories behind the color properties have been documented in chapter 1. The introductory

chapter highlights the need for the development of new rare earth based inorganic pigments as alternatives to the existing toxic pigments based on heavy metals. Further, a detailed overview on the recent developments on the red and yellow pigments has also been incorporated in this chapter. At the end of the chapter, the importance of NIR reflecting pigments for use as cool colorants to reduce the heat build-up are highlighted, reviewing relevant literature followed by the background and objectives of the present study.

Chapter 2 describes the results on the synthesis, characterization and optical properties of red pigments Based on CeO_2–MO_2–Pr_6O_{11} (M = Fe, Mn, Zr, Si and Sn) for the coloration of plastics. The designed products were characterized by XRD, SEM, TEM, UV–vis diffuse reflectance spectroscopy and CIE-$L^*a^*b^*$ 1976 color scales. The substitution of transition metals in Pr-substituted CeO_2 produces wide range of colors from bright cream to brick–red and dark–brown. It was observed that small substitutions of transition metals into $Ce_{0.95}Pr_{0.05}O_2$ system shift their absorption edge towards the higher energy side as the co-substitution of metal ion increases or praseodymium decreases for cerium with change in band gap. The band gap engineering in ceria is highlighted in this chapter with respect to the substitution of different transition metals and praseodymium. The coloring performance of the synthesized pigments was tested for its coloring application in a substrate material like PMMA.

Chapter 3 embodies the results on the synthesis and characterization of Pr - substituted $TiCeO_4$ pigments, displaying colors ranging from white to brick red. The coloring mechanism is based on the strong absorptions of the pigments in the visible region, which could originate from the introduction of an additional energy level from the $4f^1$ electron of praseodymium between O_{2p} valence band and Ce_{4f} conduction band. The utility value of the designed colorants in surface coating applications has been evaluated and the results are also given in this chapter.

Chapter 4 deals with the synthesis and optical studies of RE-substituted Bi_2MoO_6 (RE = Y, Pr, Nd, Sm, Tb and Yb) yellow and green pigments for coloration of plastics as alternatives to lead, cadmium and chromium colorants. The effect of substitution of various RE^{3+} ions at the Bi site of the Bi_2MoO_6 on its optical properties has also been examined and highlighted in this chapter. The results revealed that substitution of different RE in Bi_2MoO_6 lowers the energy level of RE 4*f* bands continuously with increasing the number of 4*f* electrons and thereby increasing the band gap. The designed pigments consist of non-toxic elements and further found to be thermally and chemically stable. The yellow and greenish yellow pigments were found to be interesting alternatives to existing toxic pigments for coloration of plastics.

In chapter 5, preparation, characterization and optical properties of inorganic pigments based on M^{5+} (M= Nb, Ta and P) substituted $BiVO_4$ is presented in detail. The effect of pentavalent metal ions on the optical properties of $BiVO_4$ is highlighted in this chapter. The NIR reflectance of the designed pigments has also been evaluated for possible use as “cool pigment”. Most importantly, the designed pigments not only exhibit bright yellow hue but also possess high NIR solar reflectance (~90%) in the wavelength range 700–2500 nm.

Chapter 6 presents the conclusions drawn from the study of optical properties of ceria based red and bismuth based yellow pigments which will help in the design of environmentally friendly inorganic pigments with multifunctionality. This chapter also contains the future scope of the present study including band structure studies of the developed pigments using Density Functional Theory and photochromic study of molybdenum and vanadium based colorants.

CHAPTER 1

Inorganic Pigments, Classification and Theory of Color

Advances in paint technology continue to consume and demand inorganic pigments which are environmentally friendly and more targeted to specific uses. Also there is a need to add specialty or smart applications to the pigments employed as exterior coatings. Designing new inorganic functional materials for emerging applications in the field of energy and environment rely on fundamental understanding of structure-property correlations as well as band gap engineering. Rising energy cost continues to drive advances in new technologies designed to improve energy efficiency across the globe. One such technology is the use of multifunctional pigments which impart color to an object, and reflect the invisible heat from the object to minimize heat build-up, when exposed to solar radiation. The details about inorganic pigments, their classification, application and an understanding of the changing role of multifunctional pigments in today's global market place have been summarized. Scientific theory about color is also traced in this chapter. This is followed by a state of art literature survey about red, yellow and NIR reflecting pigments and ends with the objectives of the present investigation.

1.1 Pigments

According to accepted standards, the word “pigment” means a substance consisting of small particles that is practically insoluble in the applied medium and is used on account of its coloring and protective properties. Both pigments and dyes are included in the general term “coloring materials”, which denote all materials used for coloring properties. The characteristic that distinguishes pigments from soluble organic dyes is their low solubility in solvents and binders (Buxhaum 1993). Pigments are defined as "colored, black, white, or fluorescent particulate organic or inorganic solids which are essentially, physically and chemically unaffected by the vehicle or substrate in which they are incorporated”. They alter appearance by selective absorption and/or by scattering of light. Pigments can be classified by their chemical composition, and optical or technical properties.

The development of inorganic pigments has been one of the major commercial pursuits of man from time immemorial. One of the reasons for their popularity is their high temperature stability. They score over organic pigments in this regard (Furukawa *et al.* 2006). In general, inorganic pigments are capable of providing excellent resistance to heat, light, weathering, solvents and chemicals, and in those respects they can offer technical advantage over most organic pigments. Inorganic pigments are high refractive index materials which are capable of giving high opacity while organic pigments are of low refractive index and consequently transparent (Christie 2001). Inorganic pigments have been in use right from ancient times. One of the most customary examples is the use of iron oxide as a coloring agent (produces red color) for pottery and other earthenware. About 2000 BC, natural ocher was burnt, sometimes in mixtures with manganese ores, to produce red, violet, and black pigments for pottery (Buxbaum and Pfaff 2005). Arsenic sulfide and Naples yellow (lead antimonate) were the first clear yellow pigments. Ultramarine and artificial lapis lazuli (Egyptian blue and cobalt aluminum spinel) were the first blue pigments (Berke 2007). On the other hand, they commonly lack the intensity and brightness of color of typical organic pigments. Organic pigments are

characterized by high color strength and brightness. There is, however, a range of high performance organic pigments which offer excellent durability while retaining their superior color properties but these tend to be rather more expensive. The ability either to provide opacity or to ensure transparency provides a further contrast between inorganic and organic pigments.

The colored pigments have found a wide variety of applications in various fields such as paints, varnishes, plastics, artists ‘colors, printing inks for paper and textiles, leather decoration, building materials (cement, renderings, concrete bricks and tiles), imitation leather, floor coverings, rubber, paper, cosmetics, ceramic glazes, and enamels (Buxbaum 2003). Nowadays use of pigments is increasing as in the case of glasses, glazes and ceramics there are no alternatives to inorganic pigments for coloring (Jansen and Letschert 2000). The paint industry uses high quality pigments almost exclusively. An optimal, uniform particle size is important because it influences gloss, hiding power, tinting strength, and lightening power. Paint films must not be too thick; therefore pigments with good tinting strength and hiding power combined with optimum dispersing properties are needed. The coloring properties (e.g., color, tinting strength or lightening power and hiding power) are important in determining application efficiency and hence economics. The following properties are also important:

1. *General chemical and physical properties:* chemical composition, moisture and salt content, content of water soluble and acid soluble matter, particle size, density, and hardness.
2. *Stability properties:* resistance toward light, weather, heat, and chemicals, anticorrosive properties and retention of gloss.
3. *Behavior in binders:* interaction with the binder properties, dispersibility, special properties in certain binders, compatibility, and solidifying effect (Buxbaum 2003; Escribano *et al.* 2001)

Research in the field of ceramic pigments is nowadays oriented toward the enlargement of the chromatic set of colors together with an increased thermal and

chemical stability. Synthesis of these pigments requires knowledge in various fields of modern science like chemical preparation, optical characterization, crystallography, solid state chemistry, color characterization and manipulation of band gap. The "doping" of an oxide powder by metal species, different from the reticular ions, is one of the most frequently adopted practices to provoke modifications both of the bulk features of a material and its surface composition and reactivity (Jatia *et al.* 1994; Tabora and Davis 1995). The substitution of Al^{3+} for Si^{4+} in zeolites, for example, is well known to affect the environment of the zeolite cavity, generates Broensted acid sites and rule consequently the material selectivity and catalytic activity (Gorte 1999). Oxide based allochromic ceramic pigments are another large class of materials obtained by framework substitution of guest metal species in the host lattice of an oxide. The structural features of the oxide matrix (e.g. TiO_2, ZrO_2, Al_2O_3 etc.) play a primary role in imposing the chromatic performance of the pigment which is a complex function of reticular accommodation and metal ion valence dimension. As for zeolites, also in the case of pigments, the framework incorporation of the metal may provoke modifications of several properties of the phase, for example of the interfacial reactivity, surface composition, particle morphology and band gap (Andrade *et al.* 1986; Roncari *et al.* 1996). The possibility to control and modulate these latter aspects is very relevant in the case of a ceramic pigment.

1.2 Classification of Pigments

Pigments are broadly classified into different categories such as natural, synthetic, organic, inorganic, pearlescent, luminescent etc. Inorganic pigments contain various types of metal ions in the form of carbonates, sulphides, silicates and oxides (Smith 2002). The nature of the metal plays a vital role in the color of the pigments.

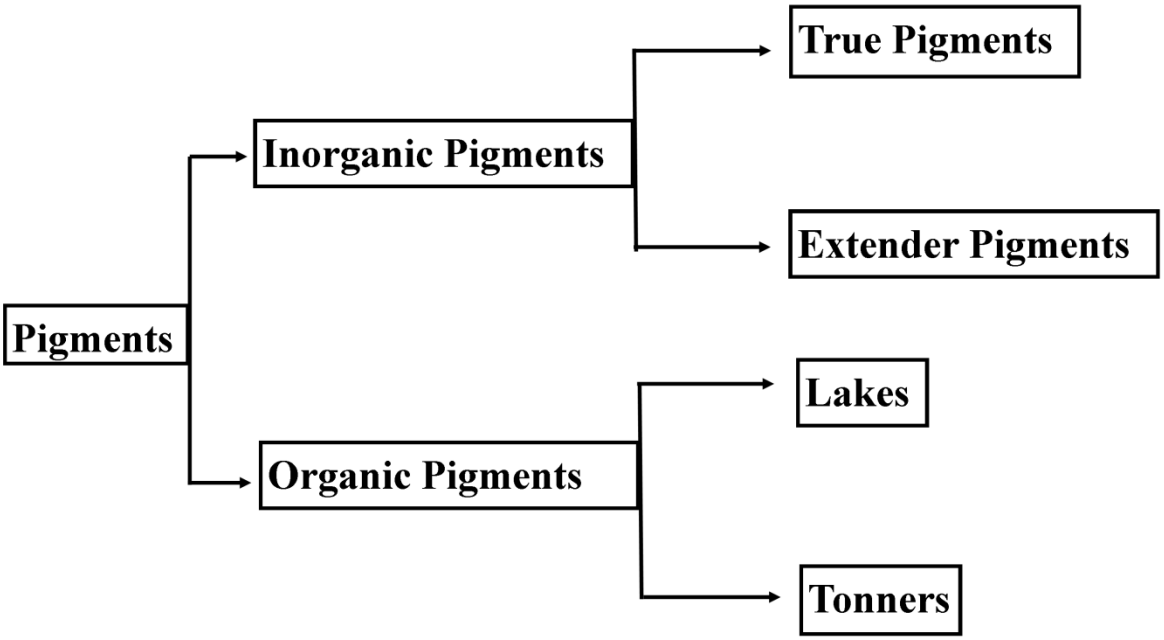

Fig. 1.1. Schematic representation of classification of pigments.

Pigments are generally classified into organic and inorganic pigments (Fig. 1.1). The naturally occurring organic pigments are mainly of historical interest and are no longer used. In the manufacture of organic pigments, certain materials become insoluble in the pure form, whereas, others require a metal or an inorganic base to precipitate them. The coloring materials, which are insoluble in the pure form, are known as toners and those, which require a base, are called lakes. Synthetic organic pigments are very finely textured and provide clean and intense colors. However, both light fastness and heat stability of organic pigments are generally lower than that of inorganic pigments. Many inorganic pigments are found in nature as minerals. The light stability, degree of opacity and chemical resistance of natural inorganic pigment are normally very high. Extenders or extender pigments are white inorganic minerals that are relatively deficient in both color and opacity and are commonly used to replace the more expensive prime pigments. These pigments are also referred to as inert pigments because of their optically inert behavior in surface coatings. The extenders commonly used by the surface coatings

industry include the following: Calcite (Whiting), Silica, Kaolin (Clay), Talc and Barytes. Calcites are naturally occurring calcium carbonate deposits. The lowest cost grades are ground limestone or the mixed calcium magnesium carbonate ore, dolomite.

Based on coloristic and chemical considerations, as recommended by ISO and DIN, inorganic pigments can be classified as given in Table 1.1 (Buxbaum and Pfaff 2005).

Table 1.1. Classification of inorganic pigments.

Term	Definition
White pigments	Nonselective light scattering (TiO_2 and ZnS pigments)
Colored pigments	Selective light absorption and selective light scattering (Fe_2O_3 red and yellow, cadmium pigments, ultramarine pigments, chrome yellow and cobalt blue)
Black pigments	Nonselective light absorption (carbon black and iron oxide black)
Effect pigments	Regular reflection or interference
Pearl luster pigments	Regular reflection on highly refractive parallel pigment platelets (titanium dioxide on mica)
Metal effect pigments	Regular reflection on mainly flat and parallel metallic pigment particles (aluminum flakes)
Interference pigments	The optical effect is due to interference (iron oxide on mica)
Luminescent pigments	The optical effect is caused by the capacity to absorb radiation and to emit it as light of a longer wavelength
Fluorescent pigments	Light of longer wavelength is emitted (Ag doped ZnS)
Phosphorescent pigments	Light of longer wavelength is emitted within several hours after excitation (Cu doped ZnS)

1.3 Theory of Color

Pigments are materials that change the color of transmitted or reflected light due to wavelength selective absorption. When white light falls on a sample, the light may be totally reflected, in which case the substance appears white or the light may be totally absorbed, in which case the substance will appear black. If only a portion of the light is absorbed and the balance is reflected, the color of the sample is determined by the reflected light (Fig 1.2), i.e. if violet is absorbed, the sample appears yellow-green and if yellow is absorbed, the sample appears blue. The colors are described as complementary. However, many substances which appear colorless do have absorption spectra and their absorption take place in the infrared or ultraviolet and not in the visible region. Table 1.2 illustrates the relationship between light absorption and color.

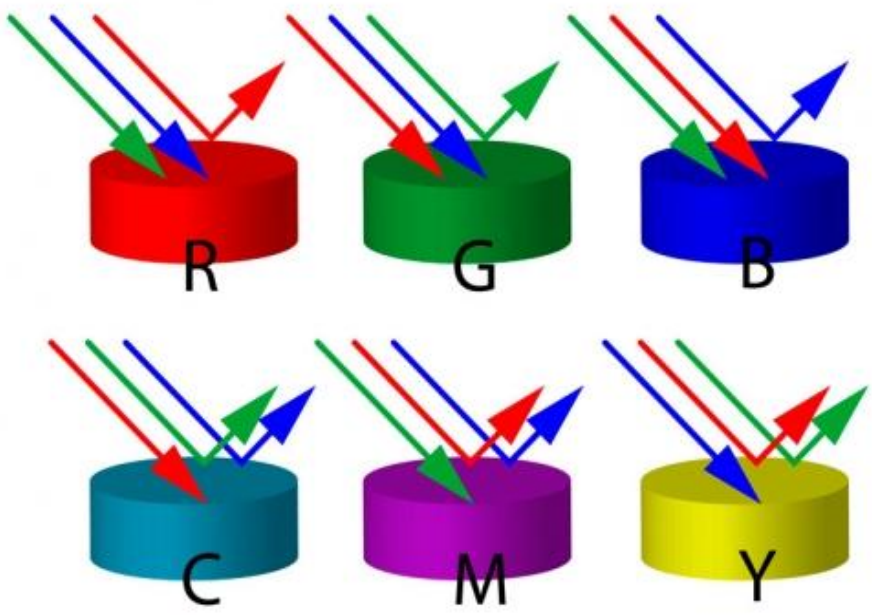

Fig. 1.2 Absorption and reflection of light.

Table 1.2. Relationship between light absorption and color.

Wavelength [nm]	Absorbed color	Complementary color
600-680	red	blue-green
580-600	orange	greenish blue
550-580	yellow-green	purple
500-550	green	red-purple
480-500	bluish green	red
450-480	greenish blue	orange
420-450	blue	yellow
380-420	violet	yellow-green

A close relationship exists between the color of a substance and its electronic structure. A molecule or ion will exhibit absorption in the visible or ultraviolet region when radiation causes an electronic transition within its structure. Thus, the absorption of light by a sample in the ultraviolet or visible region is accompanied by a change in the electronic state of the molecules in the sample. The energy supplied by the light will promote electrons from their ground state orbitals to higher energy excited state orbitals or antibonding orbitals. The energy difference ΔE, between the electronic ground state and excited state is given by Planck's relationship

$$\Delta E = h\nu \tag{1.1}$$

where h is the Planck's constant and ν is the frequency of light absorbed.

Alternatively, the relationship may be expressed as

$$\Delta E = hc/\lambda \tag{1.2}$$

where c is the velocity of light and λ is the wavelength of light absorbed. Thus there is an inverse relationship between the energy and the wavelength of light that the pigment absorbs.

The absorption of light generally arises due to any one of the following properties

- Charge transfer between anionic and cationic component of the pigment.
- Intervalence transition
- Charge transfer between valence and conduction band

It is commonly stated that there are fifteen specific cause of color, arising from a variety of physical and chemical mechanisms. These mechanisms may be collected in to four groups to explain the visual effects we designate as color.

- Color from ligand field effects: color from transition metal compounds and impurities.
- Color from molecular orbitals: color from organic compounds and from charge transfer.
- Color from band theory: color from metals, semiconductors, doped semiconductors and color centers.
- Color from geometrical and physical optics: color from scattering, dispersion, interference and diffraction.

Color best explained by the crystal field formalism involves predominantly ionic crystals containing ions with unpaired electrons. These usually originate in elements with partially filled *d* shells such as V, Cr, Mn, Fe, Co, Ni and Cu, or in elements with partially filled *f* shells such as the lanthanides and actinides. Transition and Rare earth elements are the universal choice of elements for preparing pigments. Compounds of these elements are naturally colored due to the presence of partially filled *d* (transition metals) and *f* (rare earths) sub shells (Petoud *et al.* 2003). Color can arise from them due

to two possible grounds. One reason is the *d-d* electronic transitions within the transition metal ions that give rise to many of the familiar colors of transition metal compounds, e.g. the blue and green color associated with different copper (II) complexes. Many gemstones' distinctive colors come from the presence of transition metals as impurities in an otherwise transparent crystal lattice. In solids with unpaired *d/f* shells, due to the quantization of energy, there exists different energy levels and electronic transitions between these levels depend on the following parameters : the valence state, the symmetry of the ion's environment (i.e. the coordination polyhedron of charges which produces the "crystal field," also sometimes called the "ligand field") including any distortions from ideal tetrahedral, octahedral, etc. and the strength of the crystal field, i.e., the nature and strength of the bonding. In the crystal field or ligand field effect, the field exerted by the host crystal on the guest impurity fixes the energy levels of the latter as a photon absorber. In another way, the chemical bonding between the host crystal and guest impurity always involves the donation of electrons from the host crystal to empty energy levels in the metal impurity, binding the metal to the crystal.

The molecular orbital formalism applies to several different types of situations where electrons are involved which are not simply located on single atoms or ions as in the crystal field formalism, but must be considered to be present in multi centered orbits. The results vary depending on whether metal-metal, metal-nonmetal, or nonmetal-nonmetal centers are involved. In the latter two cases the type of bonding is predominantly covalent. The result of a molecular orbital treatment is similar to that of a crystal field treatment; both formalisms result in a set of energy levels and associated transition probabilities. Charge transfer effects also, in which an electron is transferred between an anion and cation, are often responsible for intense colors in permanganate (purple) and chromates (yellow). In $PbCrO_4$, CrO_4^{2-} molecular units are covalently bonded. A molecular orbital treatment shows that there are excited states, corresponding to the transfer of electrons from the oxygen to the central metal, i.e. O - Cr in this case. The result is a broad absorption at the blue end of the spectrum and the transmittance of

the other wavelengths, leading to an orange color. As in crystal field calculations, the point symmetry and geometric distortions of the molecular group and the strength of bonding are important parameters. Charge transfer transitions usually have high transition probabilities (Laporte allowed), thus giving intense colors, and tend to dominate crystal field transition colors, although they may also occur in the ultraviolet part of the spectrum.

In solids, there is an additional source of color, which involves the transition of electrons between energy bands (West 1989). According to band theory, the electrons in solids behave differently than those in individual atoms. In a single atom, an electron can occupy one of several distinct energy levels. When light strikes the surface, electrons in a lower energy level can be excited to a higher energy level. The distance between the levels represents the relative energy required to excite an electron. As atoms are brought closer together, these distinct energy levels interact. The low energy and high energy levels overlap separately. As the number of neighboring atoms increases, more overlap occurs and bands of low and high energy replace the distinct energy levels. The excitation of electrons (by visible light) into the conduction band leads to absorption of selected wavelengths. Thus the color of these pigments is due to those radiation that have been not been absorbed, hence reflected, by the pigment. A pigment appears white when it reflects or scatters all the colors falling on it. The absorption or reflectance of light, in turn, depends upon the band gap between the valance band and the conduction band. Indeed, the technique followed for obtaining a desired color is by tuning the band gap of the compound to a specific value. This is normally carried out by suitable doping in the host lattice. Doping introduces impurity energy levels in the band gap of the host compound. These impurity levels absorb specific wavelengths producing the desired color. Thus, in order to obtain a particular color there must be a proper choice of host lattice and dopant atom.

The common oxidation states of lanthanides are +3. In addition to this stable +3 state some of these lanthanides shows variable valency. Because of the variable electronic configuration of the rare earths, they are known to give color effect while in solution. The color appears to depend on the number of *f* electrons. The color of ions containing n*f* electrons is about the same as those of with (14-n) *f* electrons. This shows that 4*f* electrons are the main cause of color. Light absorption by Ln^{3+} (lanthanide) ions, and their resulting colors are most often due to *f*→*f* transitions and less commonly, *f*→*d* transitions. i.e, the absorption bands in the visible region of electronic spectra of rare earth ions arise because of the absorption of light in the visible range resulting in the transition of electrons of the ions from the lower energy *f* orbital to the higher energy *f* orbital. A rare earth ion thus appears to be of the color, which is complementary to the color of the light absorbed. This type of change in the arrangement of *f* electrons due to absorption of light is called *f*→*f* transition. While the lanthanide ions with unoccupied, half filled, or completely filled 4*f* shells (La^{3+}, Gd^{3+} , Lu^{3+}) are colorless, and the immediate adjacent ions (Ce^{3+}, Tb^{3+}, and Eu^{3+}, Yb^{3+}) are almost colorless., the remaining ions of the rare earth series exhibit characteristic colors for which the intensity increases as the distance from these limiting cases increases. The next neighbors (Pr^{3+}, Dy^{3+}, or Sm^{3+}, Tm^{3+}) are yellow to green and almost all of the remaining members of the series (Nd^{3+}, Pm^{3+}, Er^{3+}) have red to violet coloration. In lanthanides, spin orbit coupling is more important than crystal field splitting. The color of lanthanides arises from *f*→*f* transitions. Since the electronic transitions within the *f* orbital are Laporte forbidden, the intensities of the spectral bands associated within the *f*→*f* transition may be low. However, the intensities of charge transfer bands can be high.

The pigments derived from rare earths show their characteristic color also due to charge transfer electronic transition between a donor and acceptor with the metal ion playing generally the role of an acceptor (Rao and Reddy 2007). Dopants based on rare earth elements in mixed oxide systems offer opportunity to tune the color response through manipulation of energy gaps and delocalization phenomena in conduction and

valence bands (Silversmith *et al.* 2006). In the case of ceramic pigments, the rare earths play a very important role. Because of the electronic configuration characteristics of rare earths and the transition elements, these are known to give the coloring effects while in solid solution. This property of rare earths and transition metals is made use of in making ceramic pigments, where in both metal ions gets linked up in a compound like Pr^{3+} substituted zirconium silicate and changes its absorption spectrum giving a colored compound. Many rare earth elements have high spectral purity relative to transition element derived colorants owing to the relaxation phenomenon of an electronically excited state. Cerium and praseodymium are the most common rare earth metals in use for ceramic pigment manufacturing.

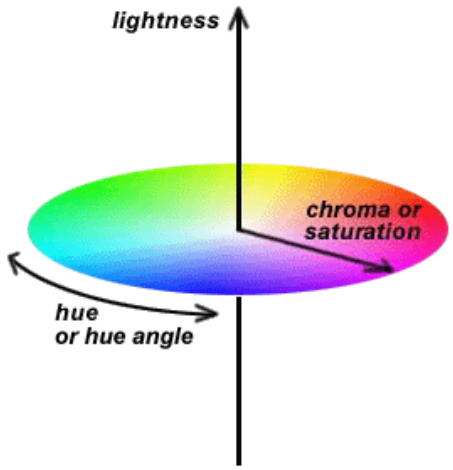

Fig. 1.3. The concept of color space.

When color is assessed on the basis of reflectance measurements, it is common to consider the three relevant attributes of perception of color as hue, chroma (saturation) which is the "colorfulness" or richness of color and lightness which refers to the amount of reflected light. These three attributes can be described using the concept of color space, which shows the relationship of colors to one another and illustrates the three dimensional nature of color as portrayed in Fig. 1.3

The hue of a particular color is represented in a color circle. The three additive primaries red, green and blue are equally spaced around the color circle. The three subtractive primaries; yellow, magenta and cyan are located between the pairs of additive primaries from which they are obtained by mixing. The second attribute, chroma increases with distance from the center of the circle. The third attribute, lightness requires a third dimension that is at right angles to the plane of the color circle. The achromatic colors, white and black, are located at either extremes of the lightness scale. Colorimetry is the science and technology used to quantify and describe physically the human color perception. The basis for colorimetry was established by CIE (Commission Internationale de l'Eclairage; International Commission on Illumination) (Ohno 2000). Mathematical approaches which make use of the concept of color space for the color measurement and specification are now well known. In one of the most important of these approaches, the CIE $L^*a^*b^*$ equation for the measurement of color differences makes use of the visually uniform $L^*a^*b^*$ space.

The principles of colorimetry are based on the fact that all color stimuli can be simulated by additively mixing only three selected color stimuli (Buxbaum and Pfaff 2005; Volz 2001). A color stimulus can, however, also be produced by mixing the spectral colors. After defining three reference stimuli, the trichromatic principle allows a three–dimensional color space to be built up in which the color coordinates (tristimulus values) can be interpreted as components of a vector. For pure white light, the CIE tristimulus values are calculated as

$$X = \int_{400}^{700} \bar{x}(\lambda)\rho(\lambda)d(\lambda) \tag{1.3}$$

$$Y = \int_{400}^{700} \bar{y}(\lambda)\rho(\lambda)d(\lambda) \tag{1.4}$$

$$Z = \int_{400}^{700} \bar{z}(\lambda)\rho(\lambda)d(\lambda) \tag{1.5}$$

where $\bar{x}, \bar{y}$ and $\bar{z}$ are the CIE tristimulus values of the spectral colors and are called the CIE spectral tristimulus values (color matching function).If light other than pure white light is used for illumination, $\rho(\lambda)$ must be replaced with the product of $\rho(\lambda)$ and $S(\lambda)$. The three CIE tristimulus values will then depend on the spectral reflectance $\rho(\lambda)$ and the spectrum of the illuminant $S(\lambda)$ as follows:

$$X = \int_{400}^{700} \bar{x}(\lambda)\rho(\lambda)S(\lambda)d(\lambda) \tag{1.6}$$

$$Y = \int_{400}^{700} \bar{y}(\lambda)\rho(\lambda)S(\lambda)d(\lambda) \tag{1.7}$$

$$Z = \int_{400}^{700} \bar{z}(\lambda)\rho(\lambda)S(\lambda)d(\lambda) \tag{1.8}$$

The CIE chromaticity coordinates (x, y, and z) are given by

$$x = \frac{X}{X+Y+Z} \tag{1.9}$$

$$y = \frac{Y}{X+Y+Z} \tag{1.10}$$

$$z = 1 - x - y \tag{1.11}$$

These are treated as coordinates in the color plane and define the CIE chromaticity diagram (Fig. 1.4). The chromaticity coordinates x and y are used to specify the saturation and hue of any color. The CIE spectral tristimulus value $y(\lambda)$ corresponds

to the lightness sensitivity curve of the human eye.A third color variable is specified in addition to *x* and *y*, namely the CIE tristimulus value *Y*, which is a measure of lightness.

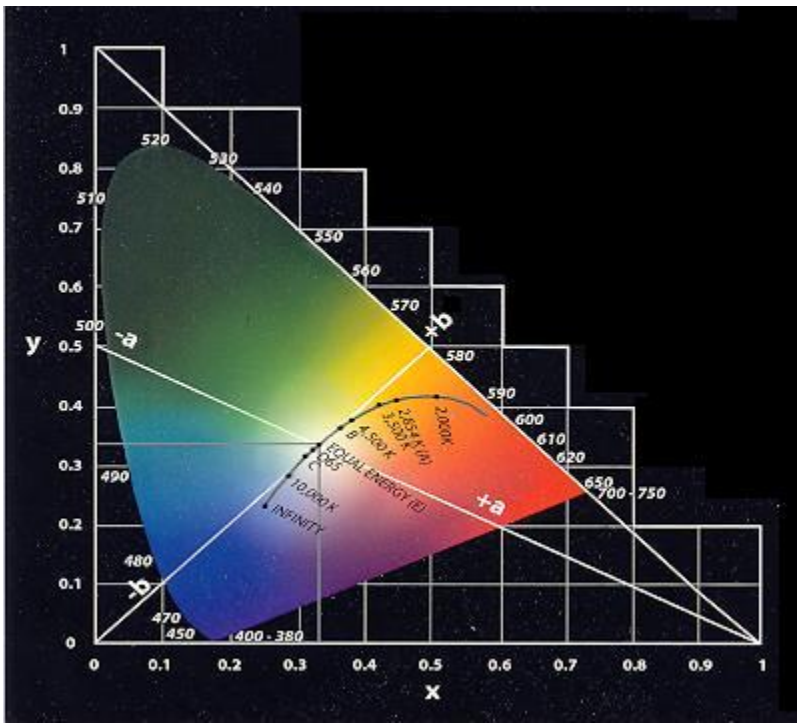

Fig. 1.4. CIE 1976 chromaticity diagram.

This system allows exact measurement of color with worldwide agreement. However, this is not sufficient for the testing of pigments, because small color differences usually have to be determined and evaluated. To determine color difference objectively, one needs to start with a concept that plays an idealized role in the physiology of colors, the concept of "absolute color space", which can be thought of as a three–dimensional arrangement of color stimuli such that the distance between two color stimuli in an arbitrary spatial direction corresponds to the perceived difference. A color space with these properties cannot be derived on a purely theoretical basis; its structure must be determined experimentally through color matching tests on samples having small color differences. Such a type of color space can be based on the color qualities; lightness, hue,

and saturation. Among such several systems, the most widespread color system is probably the Munsell system. Lightness, hue and saturation are termed value, hue and chroma respectively in the Munsell system.

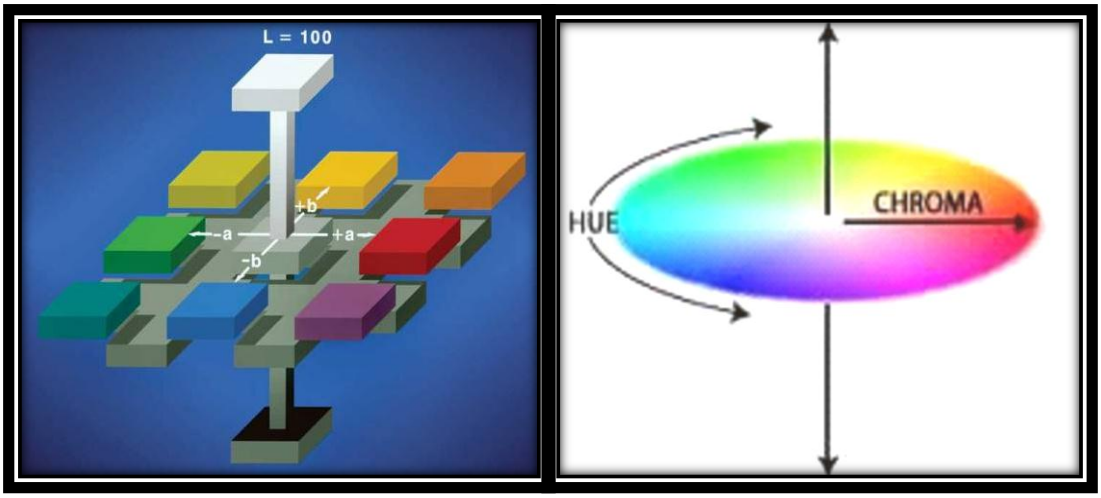

Fig. 1.5. CIE 1976 color scale.

For the quantitative determination of color differences, the transformation relationships between the CIE system (which has to be used for color measurement) and the physiologically equidistant color system must be established. Color differences can then be calculated in the latter system. A large number of color difference systems have been developed, mainly as needed for industrial color testing. The Adams–Nickerson (AN) system, well known for many decades and derived from the Munsell system, was recommended for pigment testing by DIN and later worldwide by the CIE. CIE $L^*a^*b^*$ color space is perceptually uniform. The three coordinates are denoted by L^*, a^* and b^* where L^* is the vertical lightness axis [black (0) to white (100)], a^* is the green (–ve) to red (+ve), and b^* is the blue (–ve) to yellow (+ve) axis (Fig. 1.5). The color locus in the color plane (a^*, b^* plane) can also be described as polar coordinates as C^* (chroma) and $h°$(hue angle), where

$$C^* = \sqrt{(a^*)^2 + (b^*)^2} \tag{1.12}$$

$$h° = \tan^{-1}\left(\frac{b^*}{a^*}\right) \tag{1.13}$$

To calculate the CIE $L^*a^*b^*$ coordinates, X, Y, and Z are first converted into the functions X^*, Y^*, and Z^* by using a relationship that approximately take account of the physiologically equidistant lightness steps.

$$X^* = \sqrt[3]{\frac{X}{X_n}}; \quad (1.14) \qquad Y^* = \sqrt[3]{\frac{Y}{Y_n}}; \quad (1.15) \qquad Z^* = \sqrt[3]{\frac{Z}{Z_n}} \quad (1.16)$$

where X_n, Y_n *and* Z_n are the CIE tristimulus values of the illuminant, especially a standard illuminant.

For radicands ≤0.008856, these equations become

$$X^* = 7.787\frac{X}{X_n} + 0.138 \tag{1.17}$$

$$Y^* = 7.787\frac{Y}{Y_n} + 0.138 \tag{1.18}$$

$$Z^* = 7.787\frac{Z}{Z_n} + 0.138 \tag{1.19}$$

The $L^*a^*$and b^* can then be calculated as

$$L^* = 116Y^* - 16 \tag{1.20}$$

$$b^* = 200\ (Y^* - Z^*) \tag{1.21}$$

$$a^* = 500\ (X^* - Y^*) \tag{1.22}$$

The components of the color difference are obtained as differences between the test sample (T) and the reference pigment (R).

$$\Delta E^*_{ab} = \sqrt{(\Delta L^*)^2 + (\Delta a^*)^2 + (\Delta b^*)^2} \tag{1.23}$$

where $$\Delta L^* = L^*_T - L^*_R \tag{1.24}$$

$$\Delta a^* = a_T^* - a_R^* \tag{1.25}$$

$$\Delta b^* = b_T^* - b_R^* \tag{1.26}$$

A significant advantage of the CIE system is that the color difference can be broken down into components in another way: into brightness, chroma and hue, corresponding to the arrangement in the color space.

Lightness difference, $\Delta L^* = L_T^* - L_R^*$ (1.27)

Chroma difference, $\Delta C_{ab}^* = C_{ab(T)}^* - C_{ab(R)}^* = \left(\sqrt{(a_T^*)^2 + (b_T^*)^2} - \sqrt{(a_R^*)^2 + (b_R^*)^2}\right)$ (1.28)

Hue difference, $\Delta H_{ab}^* = \sqrt{\left(\Delta E_{ab}^*\right)^2 - \left(\Delta L^*\right)^2 - (\Delta C_{ab}^*)^2}$ (1.29)

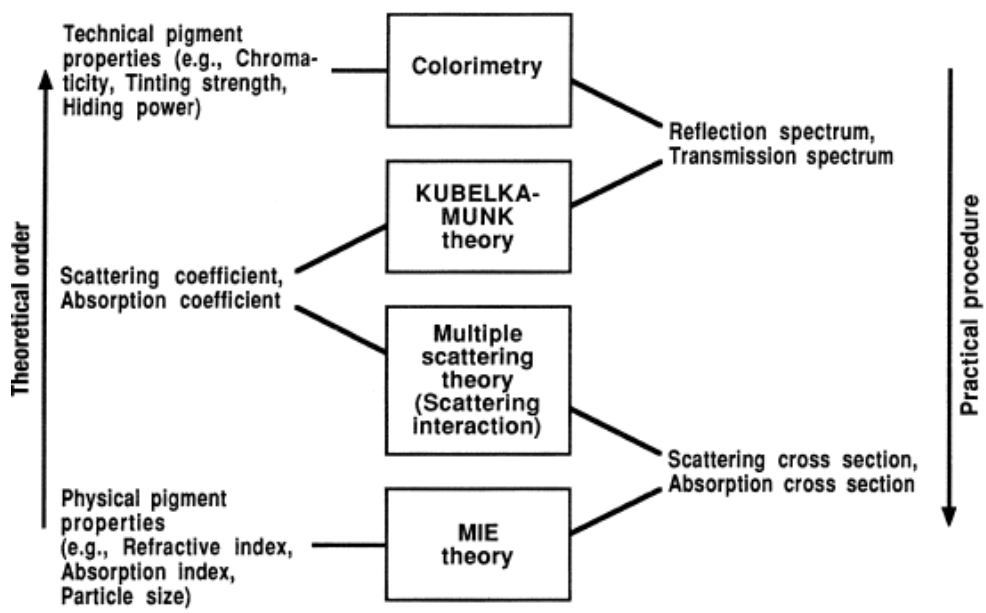

Fig. 1.6. Schematic diagram showing the relation between color properties and theoretical fundamentals.

Modern testing of coloring materials is able to establish an almost perfect connection between the color stimulus (and hence the optical properties of pigments) and

the fundamental physical quantities. Fig. 1.6 represents a schematic diagram connecting the color properties and the theoretical fundamentals (Volz 2001).

Colorimetry relates the perceived color quality to the color stimulus and this in turn, to the spectral reflectance $\rho(\lambda)$.

Kubelka–Munk theory relates $\rho(\lambda)$ to the scattering coefficient, absorption coefficient, and coating thickness. The theory is based on the fact that the optical properties of a film which absorbs and scatters light may be described by two constants: the absorption coefficient K and the scattering coefficient S. In a simplification, the flux of the diffuse incident light is represented by a single beam L+, and the flux of the light scattered in the opposite direction by a beam L−. Each beam is attenuated by absorption and scattering losses, but reinforced by the scattering losses of the respectively opposite beam. The absorption and scattering losses are determined quantitatively by the two coefficients K and S. A simple system of two linked differential equations can be written. These can be integrated for the valid boundary conditions at the incident light side, and at the opposite side. Solutions for the transmittance τ and the reflectance ρ are obtained from these integrals as a function of the absorption coefficient K, the scattering coefficient S and the film thickness h of a given substrate.

The most important and widely used quantity derived from the Kubelka–Munk theory is the reflectance of an opaque (infinitely thick) film that is described by a very simple equation:

$$\frac{K}{S} = \frac{(1-\rho_\infty)^2}{2\rho_\infty} \tag{1.30}$$

From this expression (Kubelka–Munk function) it follows that, within the range of validity of the theory, ρ_∞ depends only on the ratio of the absorption coefficient to the scattering coefficient, and not on their individual values. The equation 1.30 has been most

useful where reflectance measurements are used to obtain information about absorption and scattering (e.g., in textile dyeing, thin layer chromatography and IR spectroscopy).

This theory is especially useful for computer color matching of pigmented systems: absorption and scattering coefficients are combined additively using the specific coefficients of the components multiplied by their concentrations (Buxbaum and Pfaff 2005).

Multiple scattering theory relates scattering coefficient to the scattering cross section of the individual particle and the pigment concentration (The absorption coefficient is directly proportional to the absorption cross section and pigment concentration).

Mie theory, finally relates scattering coefficient and absorption coefficient to the particle size, wavelength, refractive index and absorption index; the last two optical properties being constants of the material.

1.4 Red Pigments

There is a current need to develop environmentally friendly inorganic pigments to replace the ones containing toxic elements such as Cd, Co, Cr, Hg, Pb, Sb and Se that are hazardous to health and environment (Smith 2002). In this sense, the development of rare earth based red pigments with good color characteristics is of great importance for the pigment industry, because of the limitations imposed on the use of toxic pigments by the current technological and environmental requirements. To date the pigment industry used red pigments on a large scale which includes: $CdS_{1-x}Se_x$ (Fig. 1.7) (cadmium sulfoselenide); $ZrSiO_4:Fe^{3+}$ (iron oxide in zircon matrixes); $Al_2O_3:Cr^{3+}$ (corundum); $ZnAl_2O_4:Cr^{3+}$, $CaSnSiO_5:Cr^{3+}$ (sphene); $MnAl_2O_4.Cr^{3+}$ (spinel) and $Y_2Sn_{2-x}Cr_xO_{7-\delta}$ (Emiliani and Corbara 1999; Radostin *et al.* 2002; Richard and Douglas 1994). The utility of these pigments in ceramic industry can be improved by encapsulating some of these pigments in a zircon matrix. Fe_2O_3–$ZrSiO_4$ and $CdS_{1-x}Se_x$ -$ZrSiO_4$ heteromorphic pigments, based on inclusion of hematite or cadmium sulfoselenide respectively in to the

zircon structure are employed traditionally. Zircon crystals protect the occluded red Fe_2O_3 or $CdS_{1-x}Se_x$ chromophore crystals from vitreous phases. However, the resulting color of both pigments does not achieve the desired color intensity and/or pure shades (García *et al.* 2001; Llusar *et al.* 2001). Among these cadmium and lead based pigments are being expelled from the market due to toxicity issues.

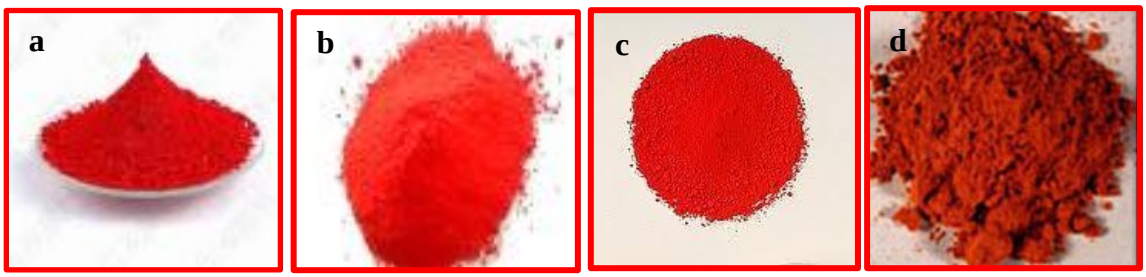

Fig. 1.7. Red pigments: (a) Cadmium red, (b) Molybdate red, (c) Vermillion and (d) Realgar.

Recently, many rare earth and transition metal based environmentally safer inorganic pigments have been proposed by several researchers (Candeia *et al.* 2006; Giable *et al.* 2006; Martos *et al.* 2008; Rao and Reddy 2007). Among the several candidates for the alternative nontoxic red pigments, CeO_2 and its related materials have been attracted because of the opacity, low toxicity and high temperature stability. CeO_2 promotes opacity in ceramic glazes and cerium sulfide has substituted the orange and red colors based on the cadmium sulfoselenide pigment used in the ceramic and painting industries (Gauthier *et al.* 2003). CeO_2 is a fluorite structured oxide that can form extensive solid solutions with a variety of alien cations while retaining the fluorite crystal structure. Ln–CeO_2 (Ln = Pr, Tb, Eu) and M–CeO_2 solid solutions (M = Cr or In) have been reported as low toxicity red ceramic pigments (García *et al.* 2001; Llusar *et al.* 2010). CeO_2 and related ceria based solid solutions (Fig. 1.8) have become interesting low toxicity alternatives (George *et al.* 2006; Kumari *et al.* 2008; Nunes *et al.* 2008; Rao and Reddy 2007; Sulcova and Trojan 1999; Sulcova *et al.* 1998) to other traditionally used orange red ceramic pigments. Indeed, the choice of available reddish ceramic

pigments is restricted either to pigments involving toxicity problems associated to Cd, Pb and Cr (García *et al.* 2001) or to pigments which lack sufficient color purity and reproducibility, such as Fe_2O_3 included in a zircon matrix (Llusar *et al.* 2001). Terbium doped ceria red pigments have also been reported for use in ceramics (Llusar *et al.* 2010; Sulcova *et al.* 2010b). These pigments were prepared through both classical and non–conventional routes. The results disclose that nice reddish colors can be obtained at lower temperatures (400–1100 °C) as compared to traditional methods. Recently, a series of non-toxic inorganic pigments having the general formula $Y_2Ce_{2-x}Pr_xO_7$ displaying wide range of colors from cream to dark brown have been designed by simple calcination route (Vishnu and Reddy 2011). The pigments possess high NIR solar reflectance when coated on asbestos cement sheet rendering them as excellent candidates for use as 'cool pigments' (Fig. 1.9).

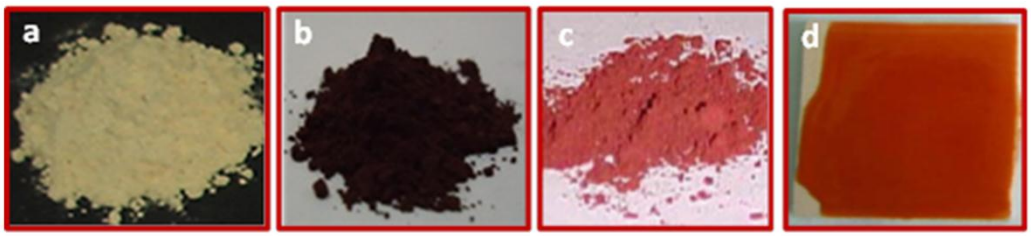

Fig. 1.8. Cerium based red pigments (a) CeO_2, (b) $Ce_{1-x}Pr_xO_2$, (c) (55%Fe_2O_3-40%CeO_2):5%Pr and (d) $Ce_{0.8}Tb_{0.2}O_{2-y}$.

Fig. 1.9. Photographs of $Y_2Ce_{2-x}Pr_xO_7$: (a) x = 0 (b) x = 0.1 (c) x = 0.3 and (d) x = 0.5 pigments.

Reddish yellow pigments based on $Ce_{10}Pr_xW_yO_z$, (where *x* and *y* varied from 0.075 to 0.6) solid solutions have been reported (Sreeram *et al.* 2008a). The use of tungsten gives a reddish yellow hue to the pigments with corresponding band gap energy around 2.2 eV. Recently, new insights on the structural and optical properties of praseodymium doped cerium–titanium mixed oxide systems as red pigments have been reported (Fernandez-Gonzalez *et al.* 2011). These nanostructured compounds were prepared by solvothermal method and well characterized. The experimental results suggest that, different colored materials ranging from yellow to red can be obtained by varying the firing temperature, quantity of praseodymium doping and pH of the reaction.

A new class of inorganic pigments have been reported based on the general formula $Ce_{1-(x+y)}Ti_xPr_yO_2$ (*x* ranges from 0.05 to 0.195 and *y* ranges from 0.005 to 0.15). These pigments have been synthesized by solid state route with a goal of preparing environmentally secure red colorants (George *et al.* 2006). The pigments display colors ranging from brick red to dark brown. It is suggested that the coloring mechanism is based on the shift of the charge transfer band of CeO_2 to higher wavelengths, introducing an additional electronic level by doping praseodymium. $Ce_{1-(x+y)}Ti_xPr_yO_2$ absorbs in the wavelength region below 600 nm producing a red color. Ceramic pigments with color hues varying from orange to brown based on Fe_2O_3 doped rare earth pigments synthesized by both solid state route and sol–gel methods have been disclosed (Dohnalova *et al.* 2008; Nunes *et al.* 2008). In the case of calcination route, the color of the pigment changes as the calcination temperature increases from 900 to 1000 °C. On the other hand, in sol–gel route, ceramic pigments free of secondary phases and with different red and brown colors were obtained after heat treatment at 800 °C for 2 h in air atmosphere.

In cerianite doped red pigments, the coloring mechanism is based on the shift of the charge transfer band of the semiconductor CeO_2 to higher wavelengths, introducing an additional electronic level by doping. CeO_2 crystallizes in the fluorite structure, where fcc packed Ce^{4+} ions are surrounded by eight oxygens, occupying alternate centres of

tetrahedral cavities in the fcc lattice. The 4*f* valence shell of Ce^{4+}([Xe]) in cerianite is empty, and that of O^{2-} ([Ne]$2s^2 2p^6$) is full: adjacent Ce^{4+} ions are virtually in contact in the fluorite lattice and, as a result, 4*f* orbitals overlap to form cationic conduction band; similarly, overlap of 2p orbitals of oxygen ions gives an anionic valence band. The band gap between the anionic band and the cationic band is 3.01 eV. The O_{2p} - Ce_{5d} excitation gap is larger for CeO_2. This suggests that the Ce-O bonds have a stronger ionic character and hence a smaller contribution of the Ce 5*d* and 4*f* orbitals in the VB, in CeO_2 (Goubin *et al.* 2004). By doping CeO_2 with Pr^{4+} ions, the $4f^1$ electron of the praseodymium valence shell introduces an additional electronic level of energy between the O^{2-} valence band and Ce^{4+} conduction band and hence a reduced band gap of 1.88 eV is observed. The CeO_2 band gap falls in indigo region of visible wavelengths, and a complementary light yellow color is observed. By contrast, Pr^{4+}–CeO_2 absorbs in the wavelength region below 600 nm producing a red color (Olazcuaga *et al.* 1984). Pr - doped CeO_2 ceramic pigments are interesting because they produce colors ranging from brick red to dark brown, depending on the quantity of praseodymium, synthesis conditions, and the calcination conditions (Aruna *et al.* 2001; Bondioli *et al.* 2005; Chaminade *et al.* 1988; Nahum *et al.* 2003; Sulcova and Trojan 2003a; Sulcova and Trojan 2003b). The substitution of other lanthanides such as La, Sm, Nd, and Gd in CeO_2–PrO_2 have also been investigated and yielded various hues ranging from pink-orange to yellow (Sulcova and Trojan 2001; Sulcova and Trojan 2003b; Sulcova and Trojan 2004). However, the serious problem associated with these pigments is the lack of thermal stability due to the reduction of Ce(IV) oxide to Ce(III) oxide accompanied by releasing oxygen and the color tends to turn orange. Hence, the above investigations have not improved the red hue of the pigment to form a viable alternate to traditional toxic red pigments. Thus, a serious need arises to search for environmentally friendly and viable materials for the replacement of toxic inorganic red pigments.

1.5 Yellow Pigments

Yellow color is particularly important in the pigment industry and the consumption of the yellow exceeds that of any other colored pigments. There are various important yellow pigment families: tin vanadia yellows, praseodymium zircon, zircon vanadia yellow, cadmium yellow and lead antimonite (Fig. 1.10). For decades $PbCrO_4$ was one of the most widely used yellow pigments, but concerns about the toxicity of both lead and chromate have significantly reduced its use. Chrome yellows, oranges, and molybdate oranges are used in a large number of different paint systems, which are restricted mostly to maintenance and industrial finishes, because of their toxicity and potential carcinogenic nature. Traditional use of these pigments has been decreasing as a result of environmental regulations. Thus, serious need arises to search for environmentally friendly and economically viable materials for the replacement of toxic inorganic yellow pigments.

Fig. 1.10. Yellow pigments: (a) Cadmium Yellow, (b) Lead antimonate, (c) Chrome yellow and (d) Zircon yellow.

Praseodymium yellow ($ZrSiO_4$:Pr) (Kato 1961) has been known as one of the environmentally benign inorganic colorants, which can be applied to paints, inks, plastics, rubbers, ceramics, enamels and glasses because of its thermal stability. However, this pigment requires high temperature calcinations (>1273 K) for the preparation, which tends to induce particle growth of the pigment. Hence, it is difficult to apply the praseodymium yellow to paints and inks in which fine dispersion of the pigment is

essential. There is a strong incentive to design new colorants based on inorganic materials to substitute for industrial pigments that are based on heavy elements hazardous to health and environment.

Less toxic, inorganic metal oxide yellow pigments, such as titanium–nickel yellow, bismuth vanadate, and their combinations with organic pigments, are being used increasingly as a replacement for lead chromate pigments (Trojan *et al.* 1996). Other yellow pigments commonly used such as $Pb_2Sb_2O_7$ and CdS are now being expelled from the market because of their toxicity. Cerium sulphide and its analogues (Fig. 1.11), such as the doped cerium sulphide, have been reported as safe replacements for potentially toxic cadmium sulphide pigments (Romero *et al.* 2000). Recently, many rare earth-based inorganic pigments have been proposed by several researchers (Jansen and Letschert 2000; Pailhe *et al.* 2009; Rao and Reddy 2007). The rare earth sulfides such as La_2S_3 (Yellow) (Adachi 1999), solid solutions mixed with $CaTaO_2N$ and $LaTaON_2$ (Jansen and Letschert 2000) that can be adjusted to the desired hue from yellow to red and nontoxic pigment $LiCeMo_2O_8$ (Odaki *et al.* 2008) have been reported. Compositions based on amorphous cerium tungstate, $Ce_{1-x}M_xW_2O_8$ (M=Zr or Ti, $0 \leq x \leq 0.6$), were synthesized and their color properties were characterized from the viewpoint of possible ecological inorganic pigments (Furukawa *et al.* 2006). The coloring mechanism is based on O_{2p}–Ce_{4f} and O_{2p}–W_{5d} double charge–transfer transitions. The optical absorption edge of these pigments depends on the Zr or Ti content, and the effective yellow hue was observed at $x = 0.2$ for both pigments (Fig. 1.12).

In recent years, several new bismuth compounds have been developed as a nontoxic substitute for lead. $BiVO_4$ pigments (Fig. 1.11) are relatively new pigment class that has gained steadily increasing importance over the last few decades. The pigments exhibit brilliant greenish-yellow to reddish - yellow shades with compositions ranging from pure $BiVO_4$ to the mixed pigment $4BiVO_4$ x $3Bi_2MoO_6$ (Erkens 1999). $BiVO_4$ compounds are nontoxic inorganic yellow pigment used in coating industry to

manufacture brilliant yellow, orange, red and green shades with good gloss and hiding power (Buxbaum 2003).

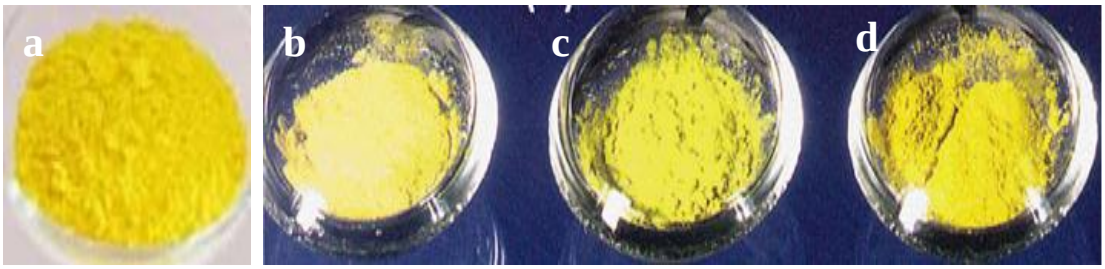

Fig. 1.11. Photographs of (a) $BiVO_4$ (b) $CePS_4$ (c) $Ce_4Si_3S_{12}$ and (d) $Ce_6Si_4S_{17}$.

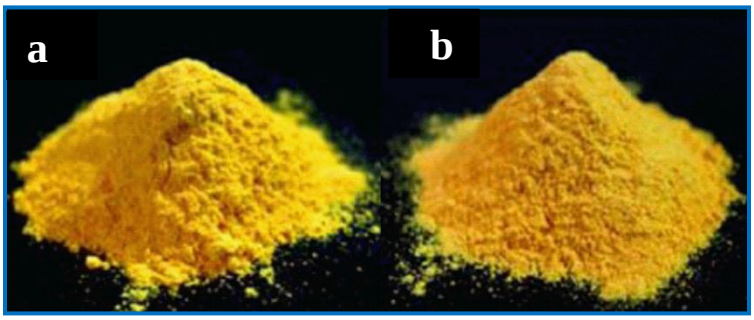

Fig. 1.12. Photographs of (a) $Ce_{0.8}Zr_{0.2}W_2O_8$ and (b) $Ce_{0.8}Ti_{0.2}W_2O_8$.

Fig. 1.13. Photographs of (a) $Ce_{0.43}Zr_{0.37}La_{0.20}O_{1.9}$, (b) $Ce_{0.43}Zr_{0.37}Bi_{0.20}O_{1.9}$ and (c) praseodymium yellow.

Pigments on the base of Bi_2O_3 seem to be interesting, because they provide interesting color hues from yellow to orange (Prabhakar Rao and Reddy 2004). Intense colors of these pigments are based on the incorporation of Ln ions into the host lattice of Bi_2O_3 (Mizoguchi *et al.* 1999; Prabhakar Rao and Reddy 2004; Sulcova *et al.* 2010a; Sulcova and Trojan 2006) and the Bi_2O_3 itself is a light yellow powder. Bi_2O_3 easily forms solid solutions with many other metal oxides. These doped systems exhibit a complex array of structures and properties dependent on the type of dopant, dopant concentration and the thermal history of the sample. The most widely studied systems are those involving rare earth metal oxides, Ln_2O_3, including yttria, Y_2O_3 (Bosacka *et al.* 2005; Sulcova and Trojan 2007). Rare earth metal ions are generally very stable, have similar chemical properties to one another and are similar in size to Bi^{3+}, making them all excellent dopants. Bismuth oxide is an important metal oxide semiconductor with a direct band gap of 2.8 eV (Krishna Reddy *et al.* 2009; Reddy *et al.* 2008; Shannon 1976). Recent investigations reveal that the toxic yellow pigments can be replaced by solid solutions of $(Bi_2O_3)_{1-x}(R_2O_3)_x$, R: Nd, Sm and Dy (Gonzalvo *et al.* 2001), $Bi_{2-x}Y_{x/2}Zr_{3x/8}O_3$ (Sulcova and Trojan 2008b), CeO_2-SiO_2-Bi_2O_3 (Imanaka *et al.* 2008)and CeO_2-ZrO_2-Bi_2O_3 (Fig. 1.13) (Masui *et al.* 2006).

1.6 Near–infrared reflective inorganic pigments

Overheating due to solar radiation negatively affects comfort in the built environment and contributes substantially to electrical consumption for air conditioning and release of green-house gases. Spectral solar power distribution (Fig. 1.14) shows that most of the sun's energy reaches the earth in the form of invisible heat induced IR radiation. Rising energy cost continues to drive advances in new technologies designed to improve energy efficiency across the globe. One such technology is the use of speciality infrared reflective pigments used to impart color to an object, and to reflect the invisible heat from the object to minimize heat build–up, when exposed to solar radiation. Ultimately the reflection of solar energy lowers the heat build–up resulting in reduction

on the load of the cooling system and therefore energy saving. NIR reflective pigments coated on the external walls of a building have been reported to reduce energy consumption, which makes the interior of the building cooler. Solar reflective granules for roofing applications have been reported by Shia et al (Shia *et al.* 2007). IR reflective screens useful in green houses, made using a polymer and reflective pigments, allow only visible light and reflect the NIR light. NIR reflective pigments can also be useful for camouflage applications, for example in textile printing (Gupta *et al.* 2001). Inorganic class of NIR reflectors are mainly metal oxides and are primarily useful in two major applications: (i) visual camouflage and (ii) reducing heat build–up on the surface of building roofing materials (Jeevanandam *et al.* 2007). The other reported inorganic pigments include (i) composites consisting of a coloring agent and a white pigment (e.g., TiO_2) coated with another non-NIR absorbing pigment, pigments based on rare earth manganese oxides, with an NIR reflectivity >50%, Cr_2O_3-Fe_2O_3 mixtures along with additives in a polymer with an NIR reflectance of about 68% (Modly 1986; Sliwinsky *et al.* 2002; Swiler and Axtell 2003; Swiler 2002).

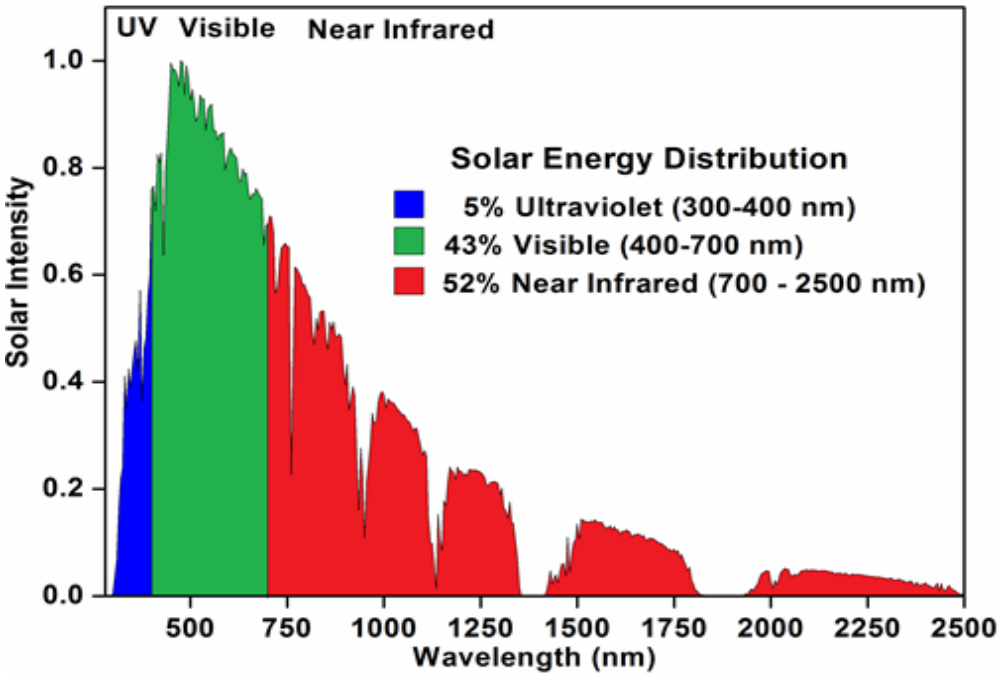

Fig. 1.14. Spectral solar power distribution.

Complex inorganic pigments based on mixed metal oxides (eg: chromium green, cobalt blue, cadmium stannate, lead chromate, cadmium yellow and chrome titanate yellow) which have been widely used in camouflage absorb visible light but reflect the NIR portion of the incident radiation (Levinson *et al.* 2005a; Levinson *et al.* 2005b; Levinson *et al.* 2007b). However many of these pigments encompass toxic metals and hence their use is restricted. Thus there is a strong incentive to develop new colored NIR reflecting pigments to substitute for industrial pigments that are based on heavy metals hazardous to health and environment. Recently lanthanide based NIR reflective pigments have been proposed as viable alternates to traditional toxic pigments due to their low toxicity (George *et al.* 2011; Sreeram *et al.* 2008b; Swiler and Axtell 2003). Most of the NIR reflective inorganic pigments particularly yellow (eg. cadmium yellow, lead chromate, chrome titanate yellow etc.) contain toxic metals and hence their consumption is being limited. Quite a few infrared reflective inorganic pigments have been reported recently; mostly as patents, which is an indication of their vast potential applications (Swiler and Axtell 2003; Swiler 2002).

1.7 Objectives of the present investigation

Inorganic pigments are currently widely used in numerous industries, especially in those of paints, inks, plastics, rubbers, ceramics, enamels and glasses. The characteristics required for commercial use of pigments are: color tone and saturation, hiding power, tinting strength, brightness, non-reactivity, insolubility, chalking resistance, dispersibility, etc. (Buxbaum 1998; Escribano *et al.* 2001). However, conventional inorganic pigments used in these applications contain potentially toxic elements such as cadmium, cobalt, chromium, lead, antimony or selenium (Furukawa *et al.* 2006; Jansen and Letschert 2000). The use of these metal ions is becoming increasingly strictly controlled, indeed banned, by legislation in many countries because of their allegedly very high toxicity. Organic pigments have some limitations because of their thermal and ultraviolet radiation instabilities (Furukawa *et al.* 2006). Several researchers have proposed safe inorganic pigments based on metal oxides and

compounds, but only a few effective pigments have been developed (Sulcova *et al.* 1998). Inorganic pigments in yellow, orange, red and maroon colors are always insufficiently represented for the coloring of plastics, paints and ceramics (Prabhakar Rao and Reddy 2004). Materials that are environmentally friendly and economically viable are the focus of much research in order to replace potentially toxic inorganic pigments (Trojan *et al.* 1996). Thus, serious economic and industrial need continues to exist for substitute inorganic pigments devoid of the above disadvantages and drawbacks.

Rare earth elements offer a vast opportunity for development of environmentally secure alternatives for many of the eco constrained colorants (García *et al.* 2001). The industrial utilization of rare earths is growing very rapidly because of their known low toxicity. The main industrial application in the field of rare earths is the ceramic industry, which consumes up to 31% world production of rare earth compounds. India is rich in rare earth resources and possesses 3% of the total rare earth reserves in the world. Pigments possessing the ability to confer high solar reflectance have received considerable attention in recent years. The specialty infrared reflective pigments which impart color to an object and reflect the invisible heat from the object to minimize heat build-up, when exposed to solar radiation is nowadays used to improve the energy efficiency. Quite a few NIR reflective inorganic pigments have been reported recently; mostly as patents, which is an indication of their vast potential applications. However, most of the NIR reflective inorganic pigments particularly yellow (e.g., cadmium yellow, lead chromate, chrome titanate yellow, etc.) contain toxic metals, and hence their consumption is being limited. Replacing conventional pigments with environmentally benign cool pigments that absorb less NIR radiation can yield colored coatings similar in color but with higher NIR reflectance.

It is clear from the literature review that there exists a large number of rare earth based inorganic pigments. However, their color properties are not satisfactory as compared to the existing industrially used toxic pigments. Further, the synthesis procedure employed for the preparation of many of these pigments involves the use of

toxic and inflammable gases. Furthermore, many of the rare earth based pigments exhibit poor thermal and chemical stability, which hinders their use in real world applications. In addition, the demand for infrared reflective pigments that can be used in the coating formulation to reduce the heat build-up of the buildings, roofs, cars etc. is increasing. Thus it has been always a challenging task to develop new class of inorganic pigments that are both non–toxic and environmentally unimpeachable, while preserving or even exceeding the optical, thermal and chemical characteristics of the existing commercial pigments.

Thus, the objectives of the present investigation are as follows:

- To develop less toxic rare earth – transition metal based red and yellow inorganic pigments as viable alternatives to the traditional toxic pigment formulations.
- Study the structure, morphology and optical properties of pigments and understand their coloring mechanism and band gap tuning for the design of pigments with good chromatic properties.
- Testing of the synthesized pigments for coloring applications in plastics and glazes and investigations on the NIR- reflecting properties.
- To develop environmentally benign NIR reflective colored inorganic pigments based on rare earths and their application towards building roofing materials as ‘cool pigments’.

CHAPTER 2

Red Pigments Based on CeO_2–MO_2–Pr_6O_{11} (M = Fe, Mn, Zr, Si and Sn): Solid Solutions for Coloration of Plastics

A series of novel environmentally benign reddish brown pigments based on CeO_2–PrO_2 co-substituted with different metal ions such as Fe^{3+}, Mn^{4+}, Zr^{4+}, Si^{4+} and Sn^{4+} have been synthesized and characterized using XRD, SEM, UV–vis diffuse reflectance spectroscopy and CIE–1976 *L*a*b color scales. The coloring mechanism is based on the shift of charge transfer band of CeO_2 to higher wavelength by co-substitution of Pr^{4+} and tetravalent metal ions in ceria. $M^{3+/4+}$substitution blue shifts the absorption edge of Pr – substituted ceria and show various shades of reddish brown color. The solid solutions absorb the visible blue and green below 600 nm efficiently, which is originated from the shift of charge transfer band of CeO_2 by co-substitution of transition metal and praseodymium. The substitution of M^{4+} and/or Pr^{4+} for Ce^{4+} in CeO_2 gently changed the band gap from 3.01 eV to 1.88 eV. The reduction in band gap is caused by the introduction of an additional energy level between the O^{2-} valence band and Ce^{4+} conduction band from the $4f^1$ electron of the praseodymium valence shell and hybridization of the vacant orbital of transition metal with Ce 4*f* conduction band. This results in a change of the color from bright cream to reddish brown. The thermal and chemical stabilities of the pigments have also been examined. Utility of the designed pigments for the coloration of plastics is also evaluated.**

Sandhya Kumari et al. ***J. Alloys Compound.*** 461 (2008) 509-515.

Sandhya Kumari et al. ***J. Am. Ceram. Soc.*** 93 (2010) 1402-1408.

Sandhya Kumari et al. ***Ceram. Inter.*** 38 (2012) 4009–4016.

2.1 Introduction

There is a current need to develop environmentally friendly inorganic pigments to replace the ones containing toxic elements such as Cd, Co, Cr, Hg, Pb, Sb and Se that are hazardous to health and environment based on their lethal dose (LD_{50}) exposure limits (Smith 2002). Among the several candidates for the alternative nontoxic red pigments, CeO_2 and its related materials have been attracted because of the opacity, low toxicity, and high temperature stability. CeO_2 promotes opacity in ceramic glazes and cerium sulfide has substituted the orange and red colors based on the cadmium sulfoselenide pigment used in the ceramic and painting industries (Gauthier *et al.* 2003). CeO_2 is a fluorite structured material that can form extensive solid solutions with a variety of alien cations while retaining the fluorite crystal structure. Ln–CeO_2 (Ln = Pr, Tb, Eu) and M–CeO_2 solid solutions (M = Cr or In) have been reported as low toxicity red ceramic pigments (García *et al.* 2001). Pr-doped ceria is employed in the ceramic industry since 1960 as red ceramic pigment. In response to growing concerns demanding environmentally benign and commercially viable ceramic pigments (Furukawa *et al.* 2006; Jansen and Letschert 2000; Sreeram *et al.* 2007), Pr- CeO_2 and related ceria based solid solutions have become interesting low toxicity alternatives (George *et al.* 2006; Rao and Reddy 2007; Sulcova and Trojan 2003a) to other traditionally used orange-red ceramic pigments. Indeed, the choice of available reddish ceramic pigments is restricted to pigments involving toxicity problems (associated to Cd, Pb and Cr). The coloring mechanism of red ceria pigments is already discussed in previous chapter.

CeO_2 easily forms solid solutions with other rare earth elements and with elements belonging to the transition-metal series. Among rare earth elements, CeO_2-Ln_2O_3 (Ln = La, Pr, Sm, Gd, and Tb) systems have been extensively investigated and their effects have been closely monitored (Miki *et al.* 1990; Shuk *et al.* 1999). Regarding transition/nontransition elements, CeO_2 easily forms solid solutions with ZrO_2 (Reddy *et al.* 2003a; Yashima *et al.* 1994), MnO_x (Imamura *et al.* 1996) and SiO_2 (Reddy *et al.*

2003b) and each has its own uniqueness. When designing CeO_2 based mixed oxides, especially for colorants, several factors must be considered, such as the effect of dopant concentration, thermal stability and the presence of a single phase.

It is well known in the literature that small amounts of tetravalent ions i.e., Zr^{4+}, Hf^{4+}, Ti^{4+}, Si^{4+} etc., are normally introduced into the ceria cubic structure to increase its thermal stability (Reddy and Khan 2005; Reddy *et al.* 2005). Further, the advantage is that Pr has a larger ion radius than Zr, Sn and Si; therefore, the introduction of a small amount of Zr/Sn/Si into the CeO_2–PrO_2 solid solution should lead to the stabilization of cubic modification (Liu *et al.* 2007). Substitution of transition metal like Cr, Mn and Fe in CeO_2 in fluorite structure was also studied for oxygen storage capacity (Gupta *et al.* 2009). Optical properties of oxide materials based on silica and ceria have attracted attention. For example, cerium-silicon solid solutions are intensively investigated from the viewpoint of their potential applications as stable luminescent materials for phosphors, scintillators and detectors (Kepinski *et al.* 2002). Optical absorption properties of the silica-coated CeO_2 materials have also been reported in recent works (Tago *et al.* 2003). The high stability of CeO_2 and SiO_2 has been guaranteed for a long time as well as high durability against humidity, and therefore, they have potential to be used as new pigments (Masui *et al.* 2004). Keeping these facts in mind, the main attention was focused on the pigment synthesis based on CeO_2 doped by small amounts of praseodymium and transition metal to achieve good red color characteristics in plastics. In this chapter, new safer red pigments having the formula $Ce_{0.95}M_xPr_{0.05-x}O_2$, (M = Mn, Zr, Si and Sn; x = 0, 0.01, 0.02, 0.03, 0.04 and 0.05), $Ce_{0.9}Fe_xPr_{0.1-x}O_{2-\delta}$ (x = 0.02, 0.04, 0.06, 0.08 and 0.095) and $Ce_{0.8}Fe_xPr_{0.2-x}O_{2-\delta}$ (x = 0.04, 0.08, 0.12, 0.16 and 0.19) have been synthesized by solid state reaction of the respective oxides. These pigments were characterized for their structural and optical properties and evaluated their coloring performance by dispersing pigments in a polymer matrix like Poly methyl methacrylate (PMMA).

2.2 Experimental Section

2.2.1 Materials and Methodology

Solid solutions in different stoichiometric compositions: $Ce_{0.95}M_xPr_{0.05-x}O_2$, (M = Mn, Zr, Si and Sn; x = 0, 0.01, 0.02, 0.03, 0.04 and 0.05), $Ce_{0.9}Fe_xPr_{0.1-x}O_{2-\delta}$ (x = 0.02, 0.04, 0.06, 0.08 and 0.095) and $Ce_{0.8}Fe_xPr_{0.2-x}O_{2-\delta}$ (x = 0.04, 0.08, 0.12, 0.16 and 0.19) were synthesized by a solid state reaction, using precursor oxides, CeO_2, MnO_2, SiO_2, Fe_2O_3, ZrO_2, SnO_2 and Pr_6O_{11} (Sigma Aldrich, 99.99%) as the starting materials. Pr^{4+} substituted ceria is named as CP. Fe based compounds in the stoichiometry $Ce_{0.9}Fe_xPr_{0.1-x}O_{2-\delta}$ are named as Fe 2, Fe 4, Fe 6, Fe 8, Fe 9.5 and Fe 04, Fe 08, Fe 12, Fe 16, Fe 19 in the stoichiometry $Ce_{0.8}Fe_xPr_{0.2-x}O_{2-\delta}$. Zr and Sn based compounds are named as Zr 1, Zr 2, Zr 3, Zr 4, Zr 5 and Sn 1, Sn 2, Sn 3, Sn 4, Sn 5 respectively. Mn 1, Mn 2, Mn 3, Mn 4, Mn 5 and Si 1, Si 2, Si 3, Si 4, Si 5 are the names given for Mn and Si co-substituted Pr-CeO_2 respectively. (These nomenclatures are used in the figures and tables of the later part of the text). The raw materials were weighed according to the stoichiometry of the samples and then mixed thoroughly in an agate mortar and homogenized by wet mixing in acetone media. Then, the mixture was dried in an air oven at 100 °C for 1 h. This procedure of mixing and subsequent drying was repeated thrice to get a homogeneous mixture. The resultant powders were calcined in platinum crucibles in a high temperature electric furnace at 1300 °C for 6 h in air atmosphere. The heating of the furnace was programmed to increase the temperature initially at 10°C/min up to 1000 °C and afterwards the heating rate was decreased to 5 °C/min up to 1300 ^{o}C. The pigment compositions thus obtained were ground in an agate mortar in order to refine and homogenize the particle size. The phase purity and chromatic properties were not satisfactory below 1300 °C.

2.2.2 Characterization Techniques

The crystalline nature and phase purity of the samples were investigated using powder X-ray diffraction analysis (XRD) with Ni-filtered Cu-Kα ($K\alpha_1$ = 1.54060 Å, $K\alpha_2$

= 1.54443 Å) radiation using a PANalytical Philips X'pert Pro diffractometer. Data were collected by step scanning over a 2θ range from 10° to 90°. Morphology of the synthesized samples was recorded on a scanning electron microscope (SEM) JEOL JSM–5600 model, with an acceleration voltage of 15 kV. High resolution images of the samples were taken using transmission electron microscope (TEM) TECNAI $30G^2$ S-TWIN. Particle size distribution of the typical pigment sample was investigated in water medium with calgon as the dispersing agent using the Laser Scattering Particle Size Distribution Analyzer (CILAS 930 Liquid). The samples were ultrasonically homogenized for 180 s during measurement and the signal was evaluated on the basis of Fraunhofer bending.

The diffuse reflectance of the powdered pigment samples were measured (200 – 780 nm) with a UV–vis Spectrophotometer (Shimadzu UV–2450 with an integrating sphere attachment, ISR–2200) using barium sulphate as the reference. The measurement conditions were as follows: an illuminant D_{65}, 10° complementary observer and measuring geometry d/8°. The band gap values were calculated from the corresponding absorbance spectra by straight forward extrapolation method using the formula $E(eV) = hc/\lambda$ (where λ represents the wavelength in nm).

The color coordinates were determined by coupling analytical software (UVPC Color Analysis Personal Spectroscopy Software V3, Shimadzu) to the UV–2450 spectrophotometer. The CIE 1976 $L^*a^*b^*$ colorimetric method was used, as recommended by the Commission Internationale de l'Eclairage (CIE). In this method, L^* is the lightness axis [black (0) to white (100)], a^* is the green (–ve) to red (+ve), and b^* is the blue (–ve) to yellow (+ve) axis. The parameter chroma is defined as $C^* = \sqrt{(a^*)^2 + (b^*)^2}$. The hue angle, $h°$ is expressed in degrees and ranges from 0° to 360° and is calculated using the formula $h° = \tan^{-1}(b^*/a^*)$. For each colorimetric parameter of a sample, measurements were made in triplicate and an average value was chosen as the result. Typically, for a given sample, the standard deviation of the

measured CIE–*L*a*b** values is less than 0.10, and the relative standard deviation is not higher than 1%, indicating that the measurement error can be ignored.

Among the range of pigment compositions prepared, typically those pigment compositions from each system which exhibited better chromatic properties were selected to disperse in polymer matrix like PMMA for fabricating the pigmented compact and to test their coloring performance. PMMA is a known water-soluble polymeric material extensively used for cold extrusion of many inorganic oxides such as alumina and zirconia. The pigment (5 and 10 wt%) was ultrasonicated (250 W, Vibronics) in alcohol-water (1:4) mixture for 10 min to ensure complete dispersion of the pigment particles. A viscous solution of PMMA (95 and 90 wt%) was made using a conventional electrical coil heater. The pigment dispersion was slowly added with stirring and converted to a thick paste. The paste after 2 h curing was compressed uniaxially into a form of cylindrical disk using a hydraulic press at a pressure of 25 MPa. Both sides of the pigmented polymer were lapped using a fine grade emery sheet for obtaining a polished surface. The color coordinates of the pigmented compacts were examined to assess the coloration.

2.3 Results and Discussion

2.3.1 Powder X–ray diffraction studies

The powder XRD patterns of the samples in the series $Ce_{0.9}Fe_xPr_{0.1-x}O_{2-\delta}$ (x = 0.02, 0.04, 0.06, 0.08 and 0.095) and $Ce_{0.8}Fe_xPr_{0.2-x}O_{2-\delta}$ (x = 0.04, 0.08, 0.12, 0.16 and 0.19) are shown in Fig. 2.1 (a) and (b) respectively. All the patterns show the characteristic reflections of the cubic fluorite structure of CeO_2 (Space group - *Fm*3*m*, No. 225) and also in good agreement with the JCPDS No. 34-394 except minor variations in the cell parameter as expected. The unit cell parameter '*a*' decreases with increasing Fe^{3+} substitution for Pr^{4+} (Table 2.1 and 2.2) in good agreement with the effective ionic radii considerations (r_{Ce4+} = 0.97 Å, r_{Pr4+} = 0.96 Å and r_{Fe3+} = 0.78 Å) (Shannon 1976).

Further, the introduction of Fe^{3+} for Pr^{4+} creates oxygen vacancies in the lattice for maintaining the electrical neutrality of the system, producing the observed shrinkage of the cell. The unit cell parameter reported for CeO_2 is 5.41134 Å as per the JCPDS card No. 34-394. It is clear from the cell parameter data that the incorporation of Fe^{3+} in Pr^{4+} - CeO_2 decreases the lattice parameter progressively in both the compositions, $Ce_{0.9}Fe_xPr_{0.1-x}O_{2-\delta}$ and $Ce_{0.8}Fe_xPr_{0.2-x}O_{2-\delta}$. The crystallite size is calculated using Debye Scherrer formula, $D = 0.9\lambda/\beta\cos\theta$, where D is the particle size, λ is the wavelength of X-ray and β is the full width at half maximum of X-ray diffraction lines. The crystallite size of the pigments is found to be 32-68 nm for $Ce_{0.9}Fe_xPr_{0.1-x}O_{2-\delta}$ and 32-87 nm for $Ce_{0.8}Fe_xPr_{0.2-x}O_{2-\delta}$ samples.

Fig. 2.2 (a) and (b) show the powder XRD patterns of $Ce_{0.95}Zr_xPr_{0.05-x}O_2$ and $Ce_{0.95}Sn_xPr_{0.05-x}O_2$ (x = 0, 0.01, 0.02, 0.03, 0.04 and 0.05) compositions prepared at 1300°C by solid state reaction. The XRD patterns of $Ce_{0.95}Mn_xPr_{0.05-x}O_2$ and $Ce_{0.95}Si_xPr_{0.05-x}O_2$ (x = 0, 0.01, 0.02, 0.03, 0.04 and 0.05) pigments are shown in Fig. 2.3 (a) and (b). Since all the compositions are Ce rich, all the patterns show the characteristic reflections of the cubic fluorite structure of CeO_2 except minor variations in the d-spacings as expected. The intense and sharp peaks found in the diffraction pattern reveal the crystalline nature of the phase. This indicates that all the samples are homogeneous and the co-substitution of zirconium/tin forms solid solutions in Pr^{4+}-CeO_2 lattice. According to Vegard's rule (Aruna *et al.* 2001), which is a good generalization applied to solid solution formation, unit cell lattice parameter (a) varies linearly with composition (x). Equation (2.1) gives the relation between a and x when Pr^{4+} replaces Ce^{4+}.

$$a_x = 5.41134-0.0193x \qquad (2.1)$$

In the present case the 'a' parameter decreases when x increases that is with increasing concentration of co-substituents for Ce^{4+}, which is in good agreement with the effective ionic radii considerations in eight co-ordination (r_{Ce4+} = 0.97 Å, r_{Pr4+} = 0.96 Å, r_{Zr4+}= 0.84 Å, r_{Sn4+}=0.69 Å, r_{Si4+}=0.40 and r_{Mn4+}=0.53) (Table 2.3 and 2.4). It is clear from the

cell parameter that the incorporation of M^{4+} (M = Zr, Sn, Si, and Mn) for Pr^{4+} decreases the lattice parameter progressively in all the compositions: $Ce_{0.95}M_xPr_{0.05-x}O_2$ (M = Zr, Sn, Si and Mn; x = 0, 0.01, 0.02, 0.03, 0.04 and 0.05).

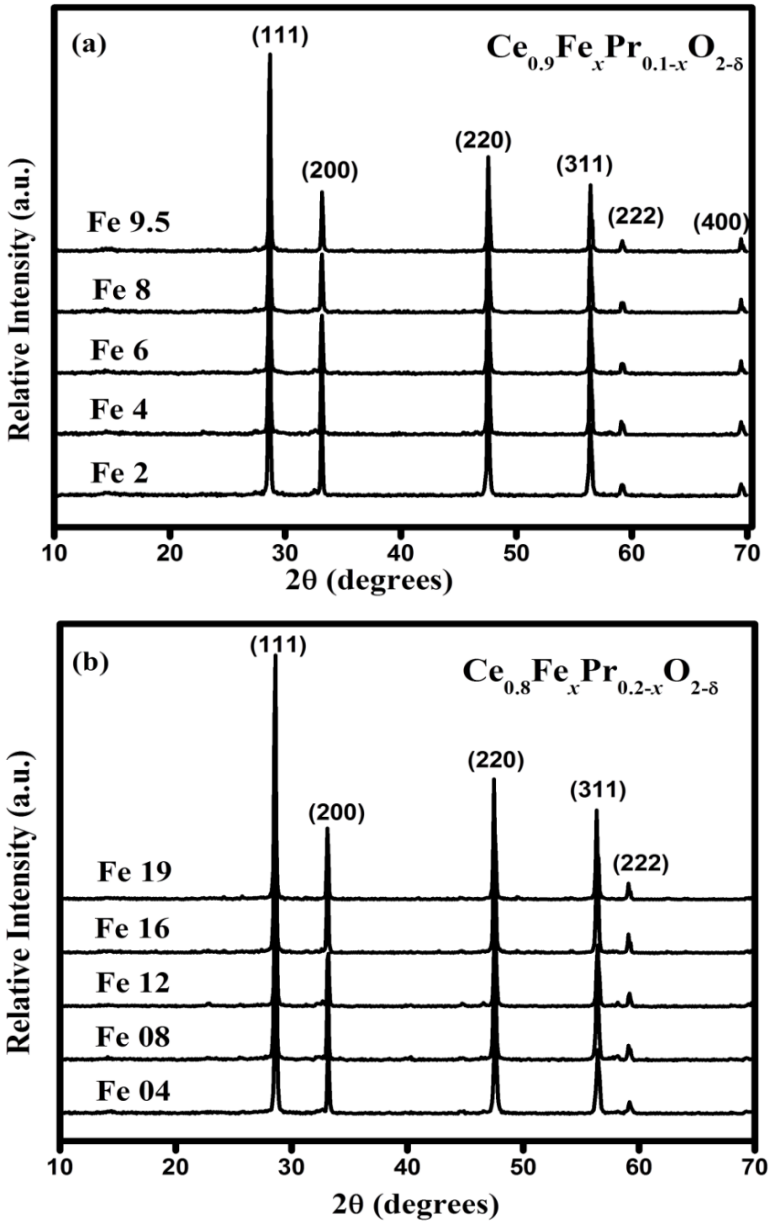

Fig. 2.1. Powder XRD patterns of (a) $Ce_{0.9}Fe_xPr_{0.1-x}O_{2-\delta}$ (x = 0.02, 0.04, 0.06, 0.08 and 0.095) and (b) $Ce_{0.8}Fe_xPr_{0.2-x}O_{2-\delta}$ (x = 0.04, 0.08, 0.12, 0.16 and 0.19) pigments.

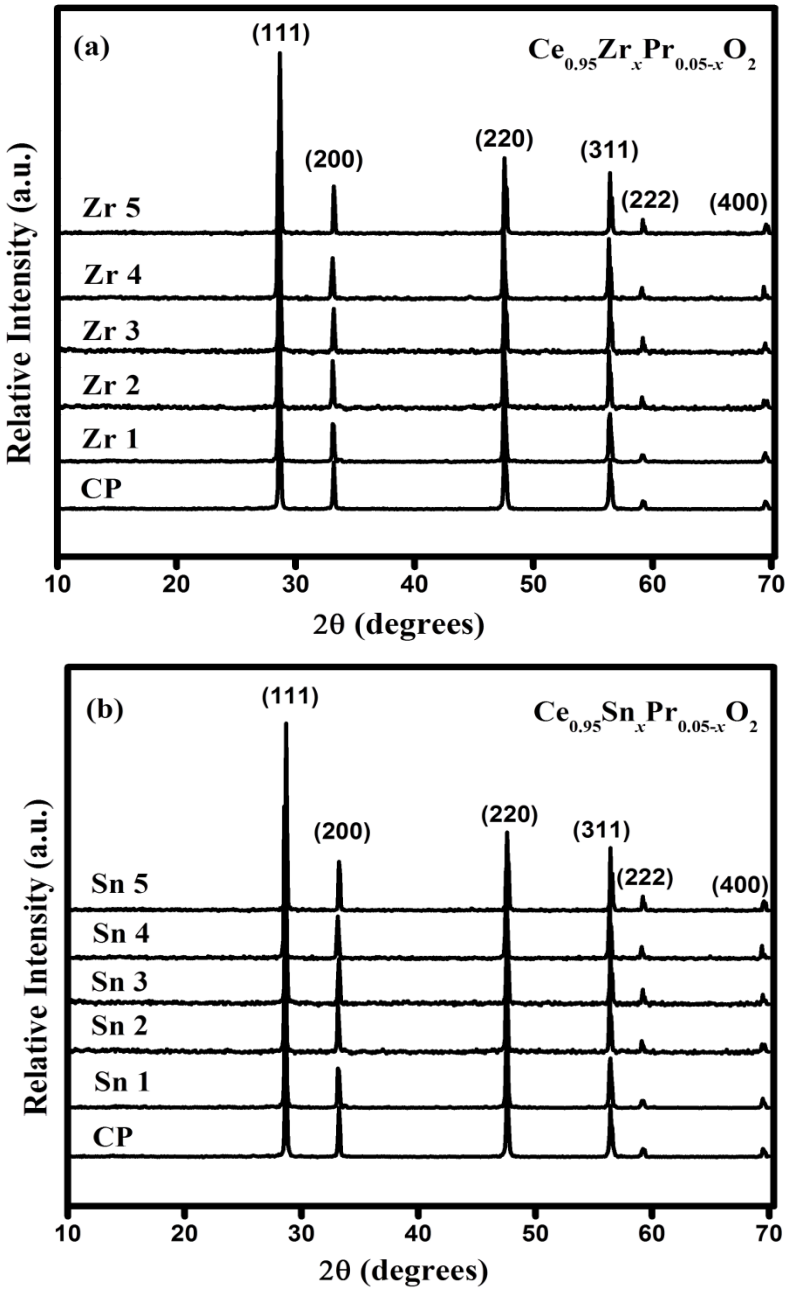

Fig. 2.2. Powder XRD patterns of (a) $Ce_{0.95}Zr_xPr_{0.05-x}O_2$ (x = 0, 0.01, 0.02, 0.03, 0.04 and 0.05) and (b) $Ce_{0.95}Sn_xPr_{0.05-x}O_2$ (x = 0, 0.01, 0.02, 0.03, 0.04 and 0.05) pigments.

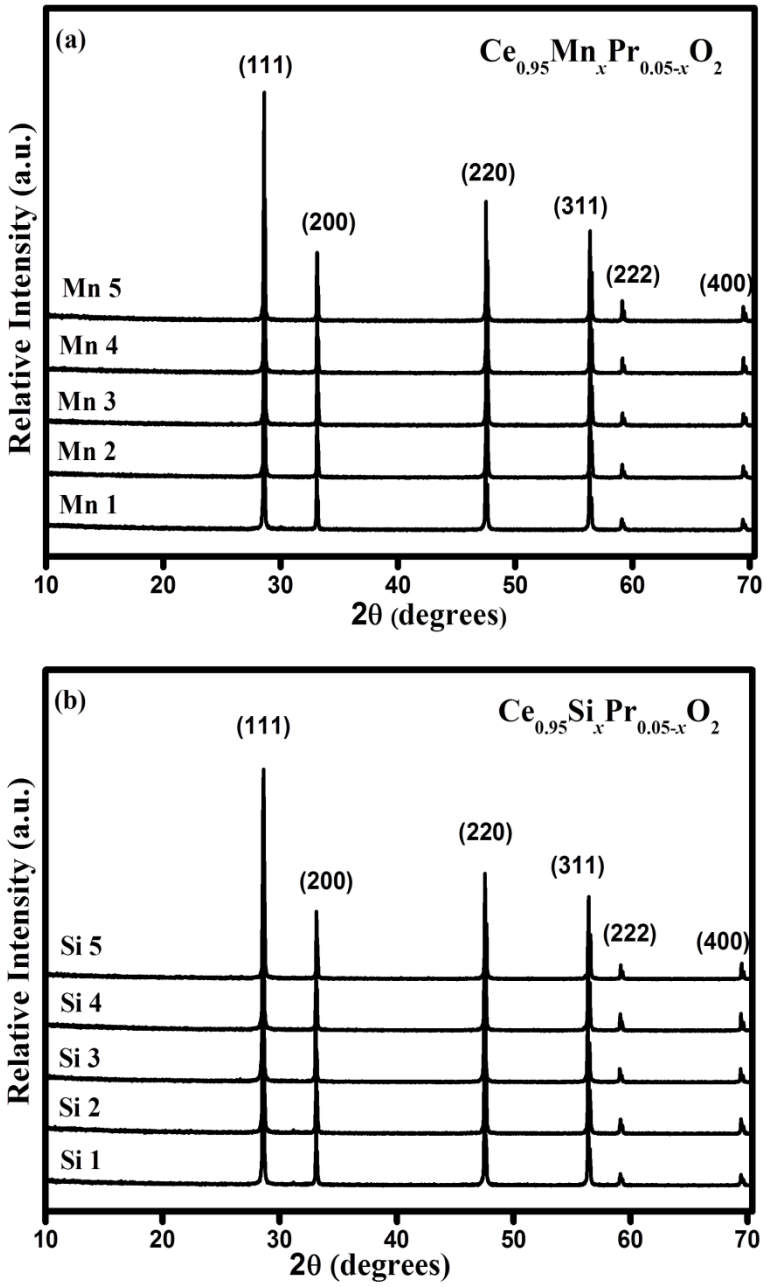

Fig. 2.3. Powder XRD patterns of (a) $Ce_{0.95}Si_xPr_{0.05-x}O_2$ (x = 0, 0.01, 0.02, 0.03, 0.04 and 0.05) and (b) $Ce_{0.95}Mn_xPr_{0.05-x}O_2$ (x = 0, 0.01, 0.02, 0.03, 0.04 and 0.05) pigments.

2.3.2 Morphological and micro chemical Analysis

Typical SEM photographs recorded for $Ce_{0.9}Fe_xPr_{0.1-x}O_{2-\delta}$ and $Ce_{0.8}Fe_xPr_{0.2-x}O_{2-\delta}$ (x = 0.04 and 0.08) pigment powders are given in Fig. 2.4. The crystalline nature of the samples can be noticed from the SEM photographs. All samples show particles in the 1-5 µm size range. However, some agglomeration of particles is seen in the SEM micrographs which are essentially clusters of particles. The effective solid solution formation was further checked by Energy dispersive spectrometer (EDS) analysis and correlated to the theoretical compositions. Typical microchemical analysis of the two compositions, $Ce_{0.9}Fe_{0.04}Pr_{0.06}O_{2-\delta}$ and $Ce_{0.8}Fe_{0.08}Pr_{0.12}O_{2-\delta}$ are shown in Fig. 2.5 (a) and (b) respectively and identifies the presence of all the expected elements. The stoichiometric formula calculated from the semiquantitative EDS results are in close agreement with the theoretical formulae. This further confirms the homogeneity of the phase formed.

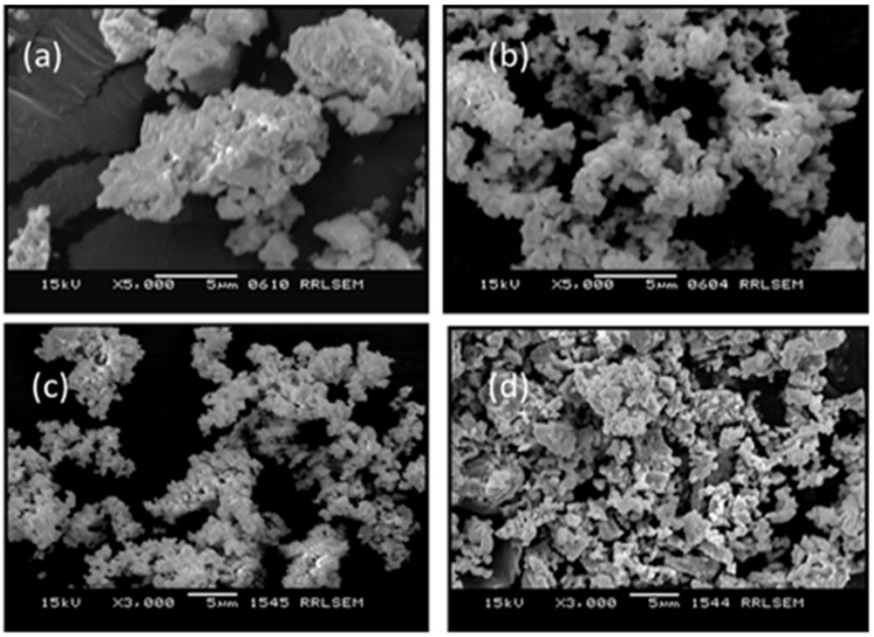

Fig. 2.4. SEM micrographs of the pigment compositions (a) $Ce_{0.9}Fe_{0.04}Pr_{0.06}O_{2-\delta}$, (b) $Ce_{0.9}Fe_{0.08}Pr_{0.02}O_{2-\delta}$, (c) $Ce_{0.8}Fe_{0.04}Pr_{0.16}O_{2-\delta}$ and (d) $Ce_{0.8}Fe_{0.08}Pr_{0.12}O_{2-\delta}$.

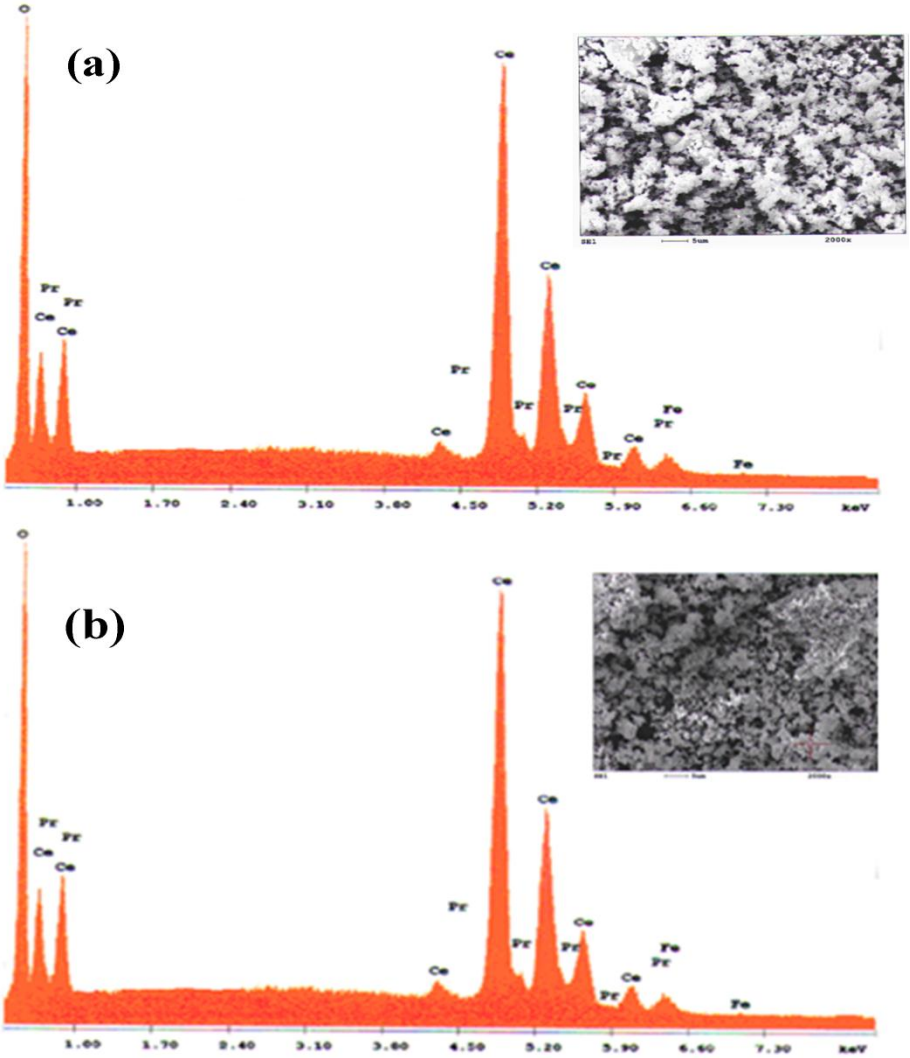

Fig. 2.5. EDS analysis of (a) $Ce_{0.9}Fe_{0.04}Pr_{0.06}O_{2-\delta}$ and (b) $Ce_{0.8}Fe_{0.08}Pr_{0.12}O_{2-\delta}$ pigments.

Typical SEM photographs recorded for $Ce_{0.95}Zr_xPr_{0.05-x}O_2$ and $Ce_{0.95}Sn_xPr_{0.05-x}O_2$ (x = 0.02 and 0.03) pigment powders are given in Fig. 2.6. All the samples show particles in 2-3 μm size range. Some aggregation of particles is seen in the SEM micrographs which are essentially clusters of particles. However, de-aggregation is observed to some extent with the increase of Zr/Sn content in the system. Fig. 2.7 (a) and (b) show the EDS

analysis of selected samples, $Ce_{0.95}Zr_{0.02}Pr_{0.03}O_2$ and $Ce_{0.95}Sn_{0.02}Pr_{0.03}O_2$ and identifies the presence of all the expected elements and confirms the homogeneity of the phase formed.

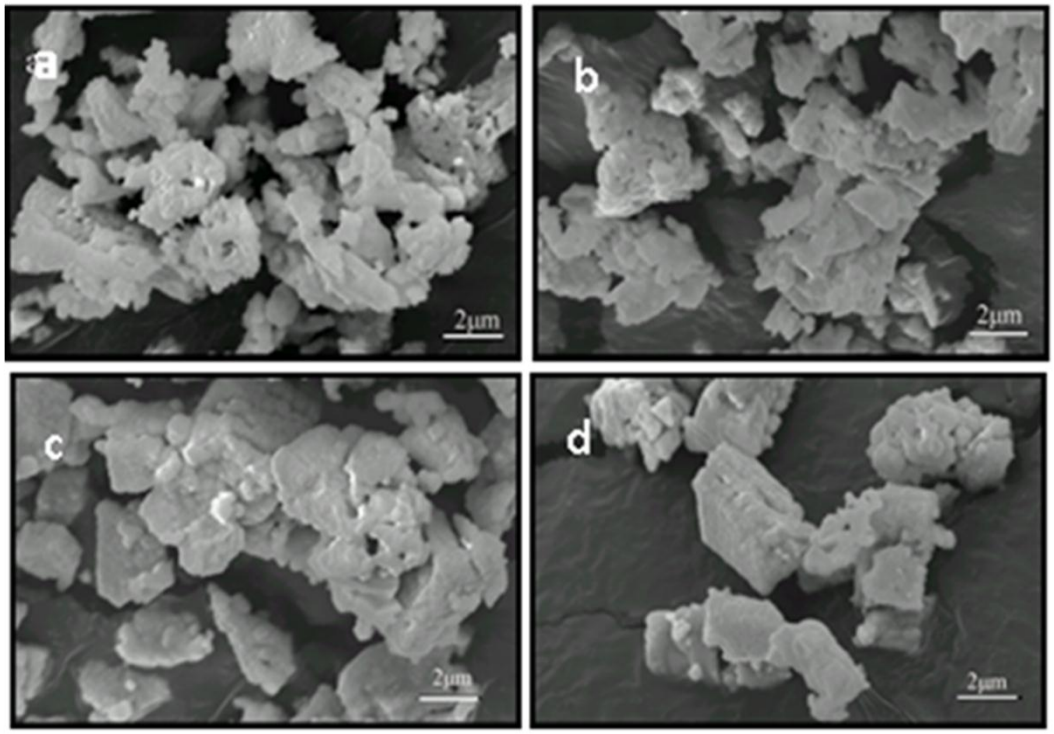

Fig. 2.6. SEM micrographs of (a) $Ce_{0.95}Zr_{0.02}Pr_{0.03}O_2$, (b) $Ce_{0.95}Zr_{0.03}Pr_{0.02}O_2$, (c) $Ce_{0.95}Sn_{0.02}Pr_{0.03}O_2$, and (d) $Ce_{0.95}Sn_{0.03}Pr_{0.02}O_2$ pigments.

In order to identify the distribution of constituent elements, elemental X-ray dot mapping analysis of the calcined ceramics was carried out. Fig. 2.8 and 2.9 shows the SEM micrographs and elemental mappings of chosen samples, $Ce_{0.95}Zr_{0.02}Pr_{0.03}O_2$ and $Ce_{0.95}Sn_{0.02}Pr_{0.03}O_2$. It is found that Zr, Sn and Pr atoms are homogeneously distributed in CeO_2 matrix.

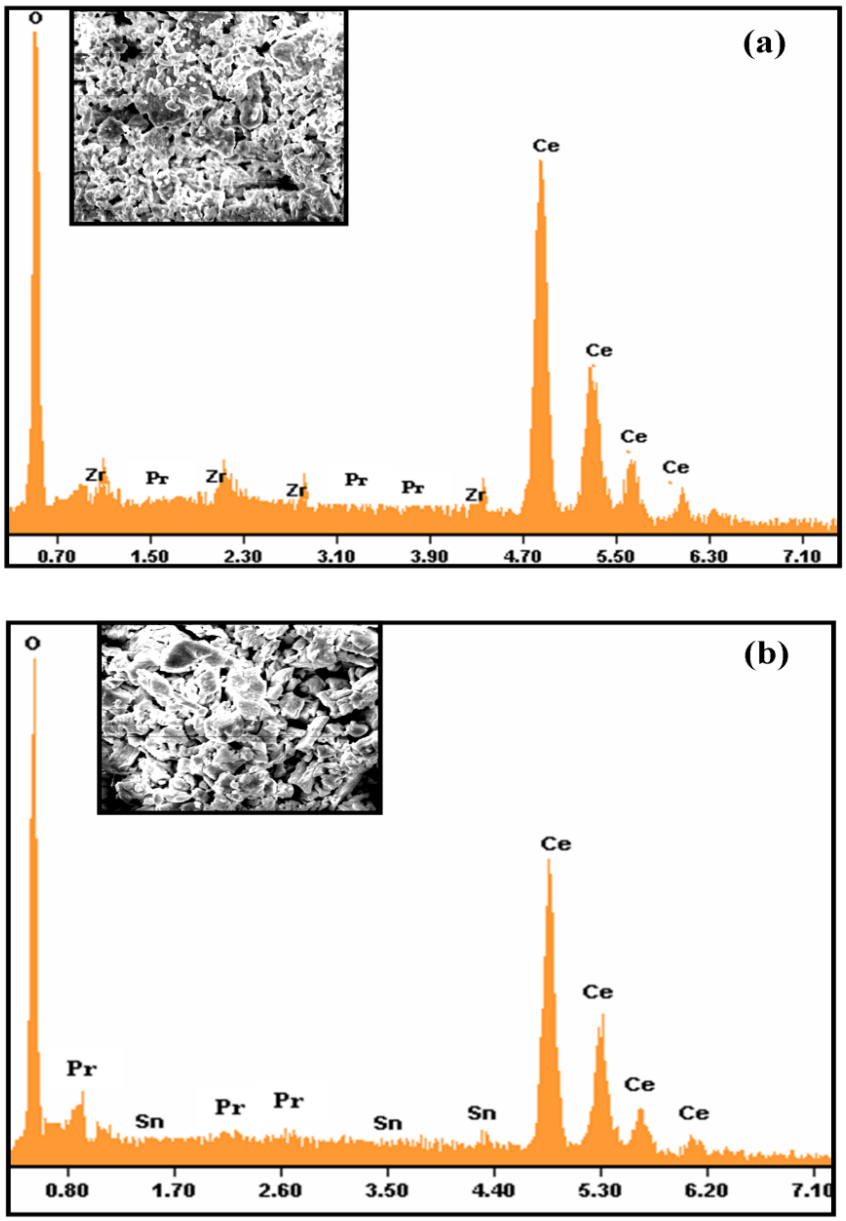

Fig. 2.7. EDS analysis of (a) $Ce_{0.95}Zr_{0.02}Pr_{0.03}O_2$ and (b) $Ce_{0.95}Sn_{0.02}Pr_{0.03}O_2$ pigments.

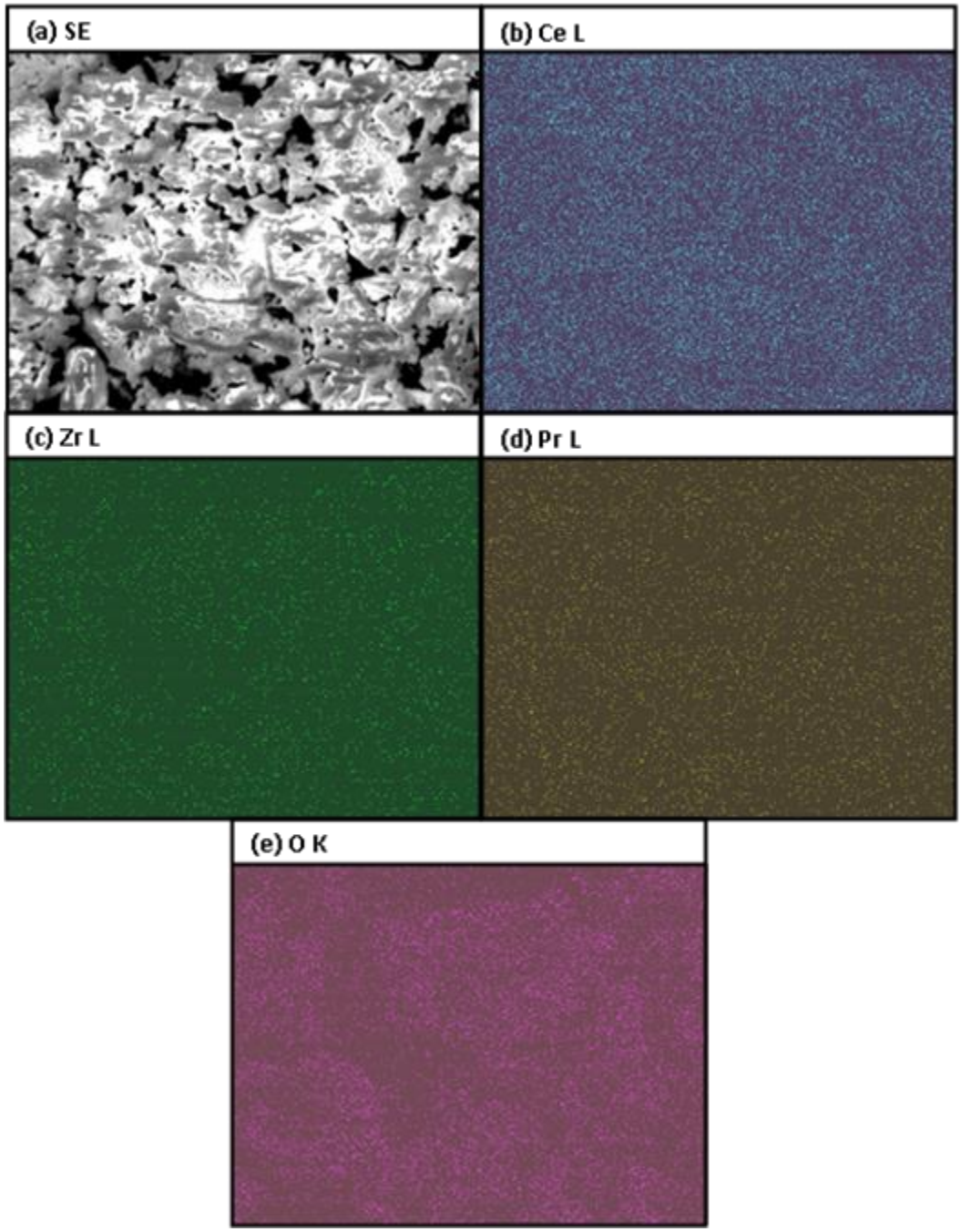

Fig. 2.8. X-ray dot mapping analysis of $Ce_{0.95}Zr_{0.02}Pr_{0.03}O_2$ pigment: (a) SEM micrograph and distribution of elements in particles (b) cerium (c) zirconium (d) praseodymium and (e) oxygen.

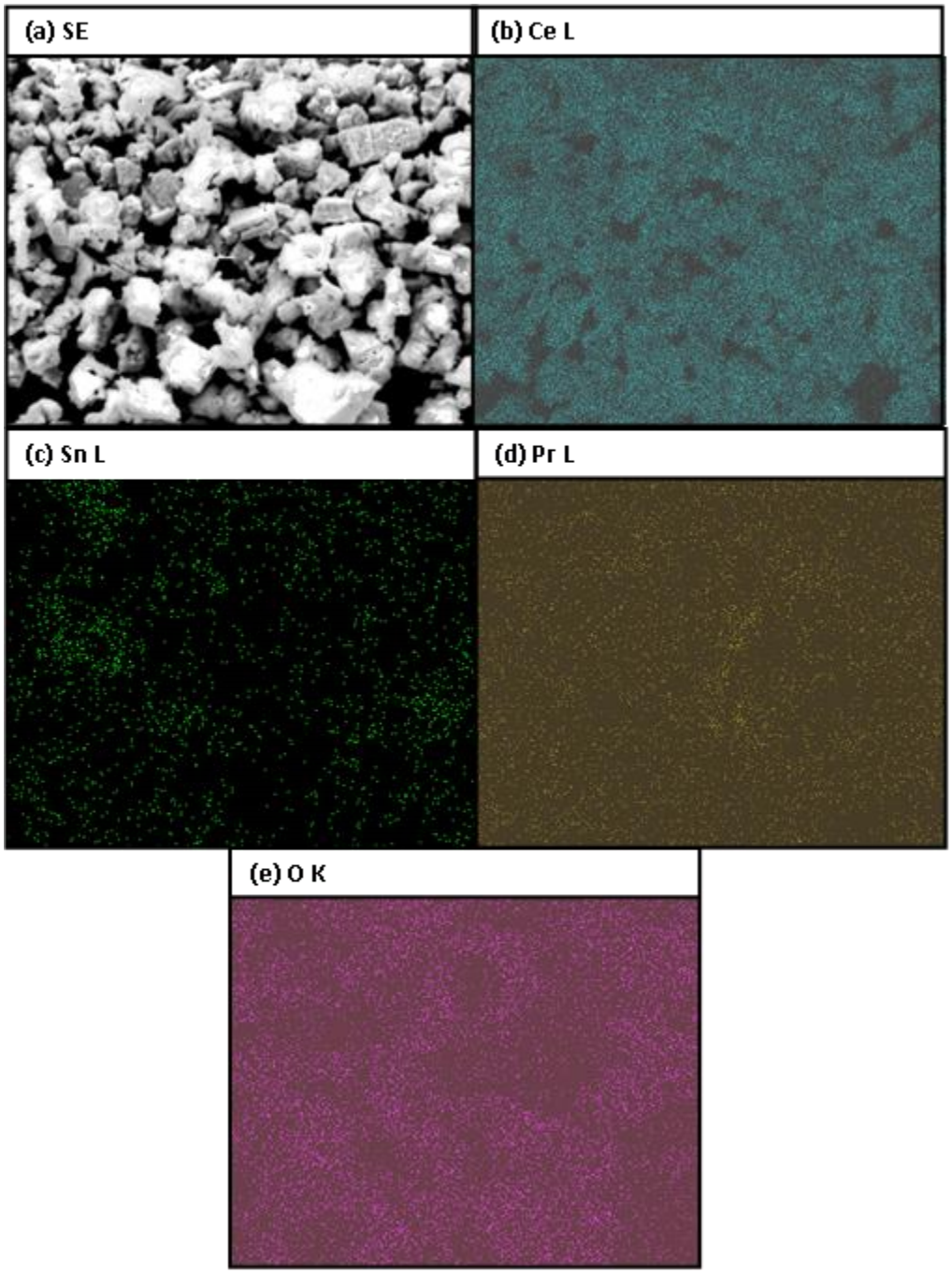

Fig. 2.9. X-ray dot mapping analysis of $Ce_{0.95}Sn_{0.02}Pr_{0.03}O_2$ pigment: (a) SEM micrograph and distribution of elements in particles (b) cerium (c) tin (d) praseodymium and (e) oxygen.

Typical SEM photographs recorded for $Ce_{0.95}Mn_xPr_{0.05-x}O_2$ and $Ce_{0.95}Si_xPr_{0.05-x}O_2$ (x = 0.02 and 0.03) pigment powders are given in Fig. 2.10. The uniform particle size of the samples can be noticed from the SEM photographs. Particle size of Mn substituted pigments is found to be in the range of 2-5 µm and that of Si based pigments in the range of 0.5-1 µm. Si^{4+} co-substituted Pr^{4+}–CeO_2 exhibits smaller particles compared to the Mn^{4+} co-substitute ceria pigments.

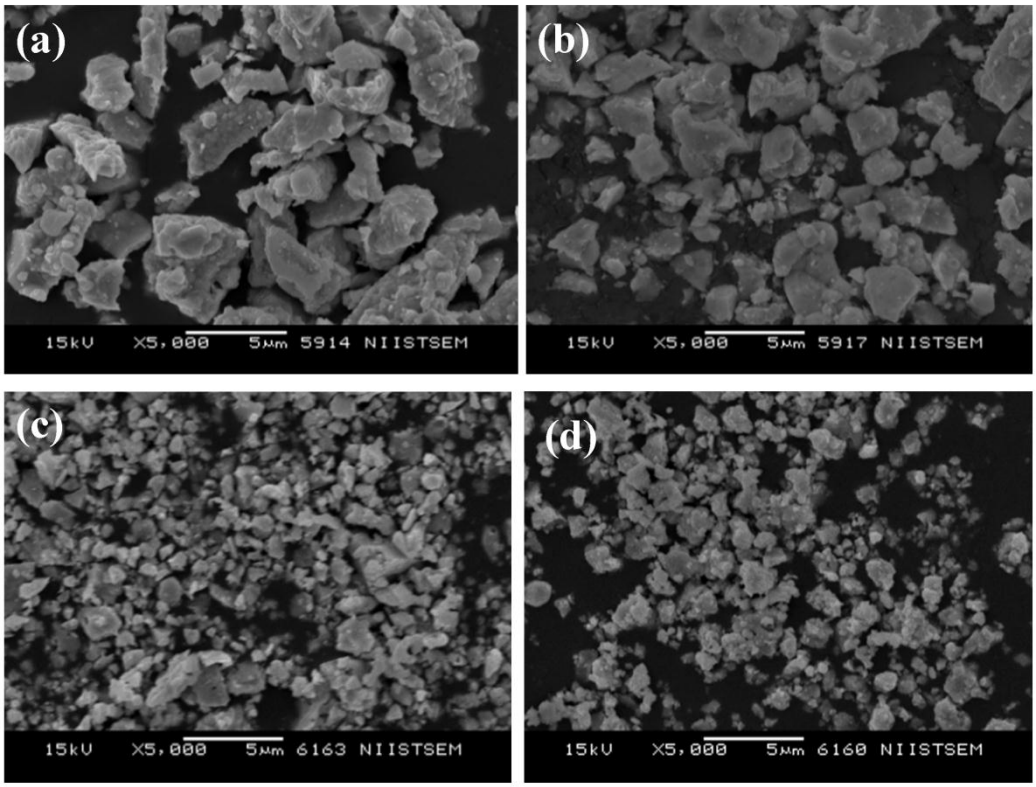

Fig. 2.10. SEM Micrographs of (a) $Ce_{0.95}Mn_{0.02}Pr_{0.03}O_2$, (b) $Ce_{0.95}Mn_{0.03}Pr_{0.02}O_2$, (c) $Ce_{0.95}Si_{0.02}Pr_{0.03}O_2$ and (d) $Ce_{0.95}Si_{0.03}Pr_{0.02}O_2$ pigments.

The effective solid solution formation of $Ce_{0.95}M_xPr_{0.05-x}O_2$ (M= Mn and Si) pigments were checked by energy dispersive spectrophotometer (EDS) analysis attached with TEM. Fig. 2.11 (a) and (b) show EDS analysis of selected samples,

$Ce_{0.95}Mn_{0.02}Pr_{0.03}O_2$ and $Ce_{0.95}Si_{0.02}Pr_{0.03}O_2$ and identifies the presence of all the expected elements.

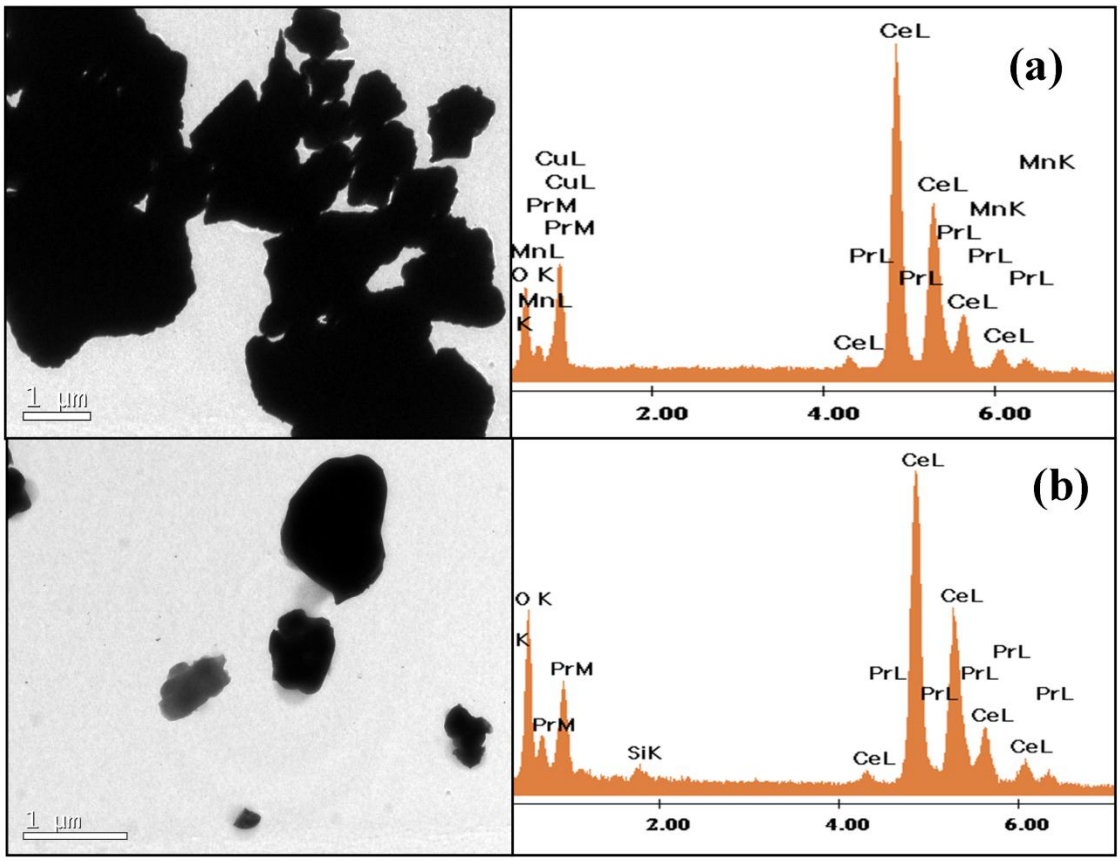

Fig. 2.11. EDS analysis of (a) $Ce_{0.95}Mn_{0.02}Pr_{0.03}O_2$ and (b) $Ce_{0.95}Si_{0.02}Pr_{0.03}O_2$ pigments.

2.3.3 Diffuse reflectance studies of CeO_2 and Pr^{4+}-CeO_2.

Fig. 2.12 shows the visible absorption spectra of the investigating oxides. Cerium oxide shows strong absorption below 400 nm originated from the O_{2p}-Ce_{4f} charge transfer transitions and no visible absorption is detected. The absorption spectra of Pr_2O_3 shows peaks at 448, 475, 488, 591 and 605 nm, which can be assigned to Pr(III) transitions. The bands in the region 440–490 (blue) and 590–625nm (red), can be assigned based on the

energy levels $^3H_4 \rightarrow {}^3P_2$, $^3H_4 \rightarrow {}^3P_1$, $^3H_4 \rightarrow {}^3P_0$, $^3H_4 \rightarrow {}^3D_2$ (upper) and $^3H_4 \rightarrow {}^3D_2$ (lower) respectively (George *et al.* 2005; Sivakumar and Varadaraju 2005). The absorption edge of iron oxide is near 550 nm due to charge transfer between O_{2p} and Fe_{3d}. Pr_6O_{11} and MnO_2 show strong absorption in the entire visible region. ZrO_2 and SnO_2 hardly absorb in the visible region. However, the absorption bands corresponding to the Pr(III) state are absent in the absorption spectra of $Ce_{0.95}Pr_{0.05}O_2$ (Fig. 2.13). It is assumed that Pr(IV) state exists in CeO_2 lattice and also in agreement with other published results (Aruna *et al.* 2001).

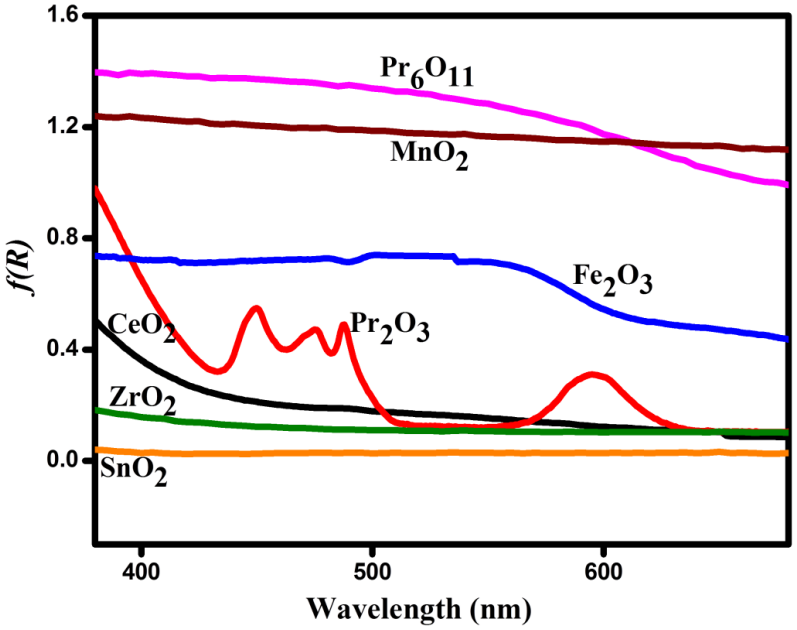

Fig. 2.12. Absorption spectra of investigating oxides.

According to Jørgensen and Rittershaus (Jørgensen and Rittershaus 1967) the red color of the Pr-doped ceria is assigned to a charge transfer from the ligand orbitals to the praseodymium cation. According to the band structure model proposed by Koelling et al. (Koelling *et al.* 1983) for CeO_2 and PrO_2 , the electronic spectra arise due to the electron transfer from the ligand orbitals to the localized $4f^1$ level of Pr. The position of the

absorption edge depends critically on the praseodymium content. It is red shifted with increasing Pr content. The slope of the electronic spectra decreases with increasing praseodymium content. This evolution is consistent with the observed charge transfer spectra of tetravalent lanthanide ions in oxides (Hoefdraad 1975) and confirms the substitution of Pr for Ce in the fluorite ceria crystal.

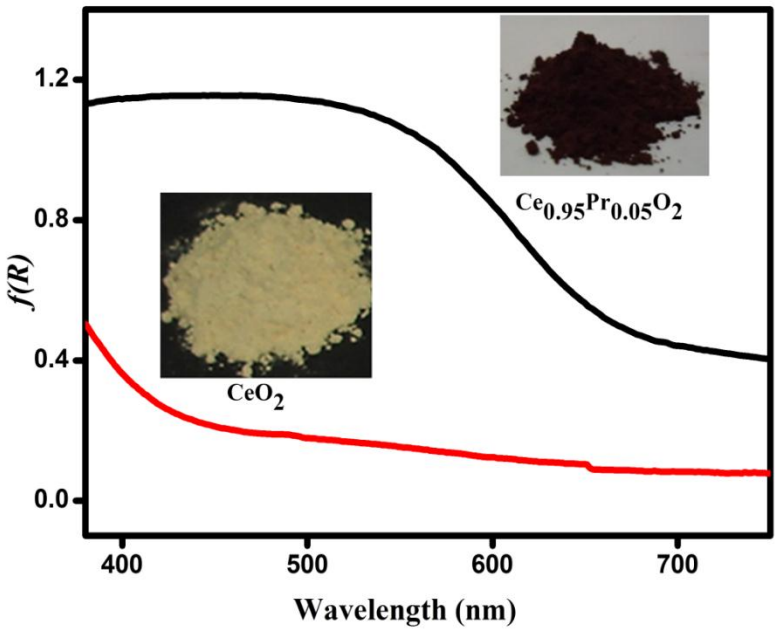

Fig. 2.13. Absorbance spectra of CeO_2 and $Ce_{0.95}Pr_{0.05}O_2$.

2.3.4 Diffuse reflectance studies and chromatic properties of Iron (Fe^{3+}) co-substituted Pr^{4+}-CeO_2.

The visual color of $Ce_{0.9}Fe_xPr_{0.1-x}O_{2-\delta}$ (x = 0.02, 0.04, 0.06, 0.08 and 0.095) and $Ce_{0.8}Fe_xPr_{0.2-x}O_{2-\delta}$ (x = 0.04, 0.08, 0.12, 0.16 and 0.19) pigment powders varies from brick red to dark brown (Fig. 2.14) with the variation of iron content. The effect of co-substitution of iron in Pr-CeO_2 was analyzed from the diffuse reflectance spectra shown in Fig. 2.15. The color co-ordinate data are given in Table 2.1 and 2.2. High reflectance

occurs in the region 600-800 nm in both set of compositions. The reflectance spectra show a greater absorption in the blue and green region with an increasing number of chromophore ions. This causes the color of the pigment to vary from brick red to dark brown (Fig. 2.14).

Fig. 2.14. Photographs of (a) $Ce_{0.9}Fe_xPr_{0.1-x}O_{2-\delta}$ (x = 0.02, 0.04, 0.06, 0.08 and 0.095) and (b) $Ce_{0.8}Fe_xPr_{0.2-x}O_{2-\delta}$ (x = 0.04, 0.08, 0.12, 0.16 and 0.19) pigments.

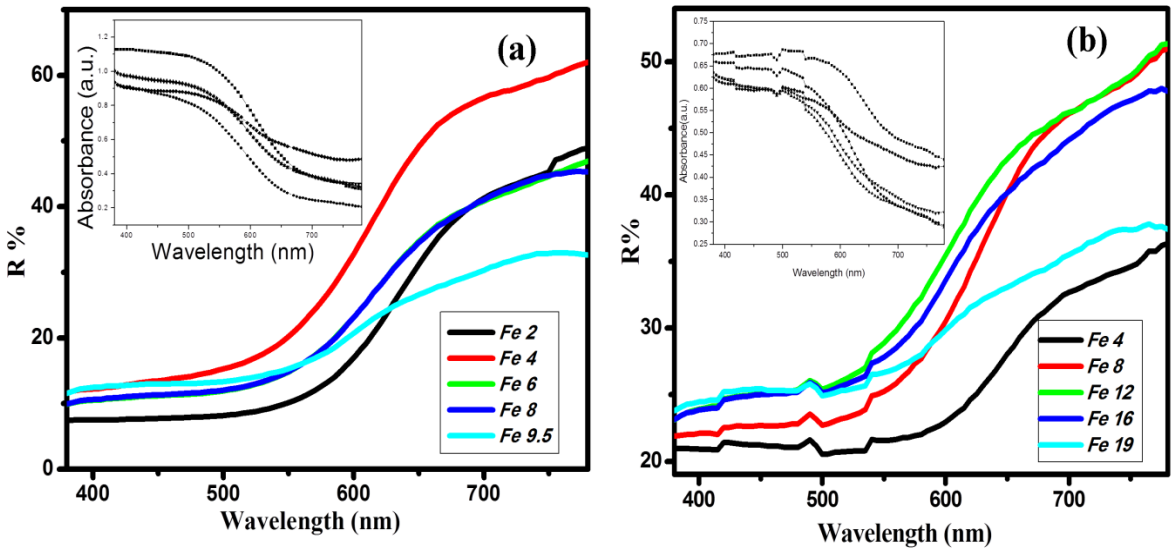

Fig. 2.15. Reflectance spectra of (a) $Ce_{0.9}Fe_xPr_{0.1-x}O_{2-\delta}$ $_{-\delta}$ (x = 0.02, 0.04, 0.06, 0.08 and 0.095) and (b) $Ce_{0.8}Fe_xPr_{0.2-x}O_{2-\delta}$ (x = 0.04, 0.08, 0.12, 0.16 and 0.19) pigments.

In the Fe rich stoichiometric compositions, $Ce_{0.8}Fe_xPr_{0.2-x}O_{2-\delta}$ (x = 0.04, 0.08, 0.12, 0.16 and 0.19), two intense absorption bands in the visible range can be attributed

without any doubt to two charge transfers, O_{2p}-Ce_{4f} and O_{2p}-Fe_{3d}. The intensity of the absorption bands increases with the richness of iron in the solid solutions because the O_{2p}-Ce_{4f} charge transfer (CT) is coupled with the dominating Laporte allowed O_{2p}-Fe_{3d} CT. Incorporation of Fe^{3+} in to Pr-substituted CeO_2 shifts the absorption edge towards the higher energy side. The position of the absorption edge depends critically on iron content.

Table 2.1. Color co-ordinates, band gap and cell parameter of $Ce_{0.9}Fe_xPr_{0.1-x}O_{2-\delta}$ (x = 0.02, 0.04, 0.06, 0.08 and 0.095) pigments.

Sample	Color Co-ordinates					E_g	*a*
	*L**	*a**	*b**	*C**	*h°*	*(eV)*	*(nm)*
CP	44.25	18.35	15.49	24.01	40.16	1.88	0.54083(3)
Fe 2	40.98	18.46	14.28	23.33	37.72	1.88	0.54022(5)
Fe 4	55.49	18.30	21.55	28.27	49.66	1.91	0.54021(3)
Fe 6	47.08	16.01	15.33	22.16	43.75	1.92	0.54013(9)
Fe 8	48.11	15.91	15.21	20.55	39.27	1.92	0.53988(6)
Fe 9.5	46.28	12.63	13.01	51.1	86.90	1.97	0.53943(7)

The color measurements performed on all powders showed changes in the CIE-*L*a*b** 1976 color scales directly correlated with the variation of iron in the system. The *L**, *a** and *b** parameters of $Ce_{0.9}Fe_xPr_{0.1-x}O_{2-\delta}$ and $Ce_{0.8}Fe_xPr_{0.2-x}O_{2-\delta}$ pigment samples are listed in Table 2.1 and 2.2 respectively. The parameter lightness (*L**) shows no systematic change, but the color parameters *a** (green-red parameter) and *b** (blue-yellow parameter) increases as the iron content increases up to certain concentration and thereafter decreases in both set of compositions. This is also reflected in its chroma value

(*C**) which gets enhanced from 17.23 to 28.27 (Table 2.2). A further increase in substituent concentration of the chromophore ion brings about a slow decrease in the red hue and the outcome is a change in color from brick red to reddish brown. The increase of iron content than a critical level would have induced a darkening of the samples and in fact, an opposite trend in *a** and *b** values.

Table 2.2. Color co-ordinates, band gap and cell parameter of $Ce_{0.8}Fe_xPr_{0.2-x}O_{2-\delta}$ (x = 0.04, 0.08, 0.12, 0.16 and 0.19) pigments.

Sample	Color Co-ordinates					E_g	*a*
	*L**	*a**	*b**	*C**	*h°*	*(eV)*	*(nm)*
CP	44.25	18.35	15.49	24.01	40.16	1.88	0.54083(3)
Fe 04	31.68	12.34	5.58	25.52	42.98	1.81	0.53998(6)
Fe 08	43.14	18.67	17.40	28.27	49.66	1.87	0.53974(8)
Fe 12	50.65	15.39	18.18	23.81	49.75	1.95	0.53954(6)
Fe 16	49.45	14.39	14.41	20.36	45.03	1.96	0.53944(7)
Fe 19	44.79	9.77	7.94	12.58	39.10	1.97	0.53938(1)

The compositions, $Ce_{0.9}Fe_{0.04}Pr_{0.06}O_{1.95}$ and $Ce_{0.8}Fe_{0.08}Pr_{0.12}O_{1.9}$ exhibits better *L**, *a** and *b** values (55.49, 18.30, 21.55) and (43.14, 18.67, 17.40) respectively. It clearly shows that the small additions of iron to the CeO_2–Pr_6O_{11} solid solutions significantly improves the color parameters (*a**and *b**) and enhances the red hue. The present values are significantly better than recently reported Pr-CeO_2 pigments (5% Pr-substituted CeO_2: *L** = 66; *a** = 12; *b** = 9.5) synthesized by microwave assisted hydrothermal route (Bondioli *et al.* 2005). However, Zhen-Feng et al. (Zhu Zhen-Feng *et al.* 2006) have reported some better values of color co-ordinates for the same composition (5%

praseodymium substituted CeO_2: L^* = 59.37; a^* = 24.28; b^* = 22.15) synthesized by low temperature combustion assisted hydrothermal route. Nahum et al. (Nahum *et al.* 2003) have reported similar color properties as found in the present study with Pr^{4+} substituted ceria pigments calcined at 1400–1500 °C. Further, it is also clear from this study that the solid solutions of these pigments can be prepared at lower calcination temperatures by the addition of iron as compared to the previously reported CeO_2–Pr_6O_{11} solid solution.

2.3.5 Diffuse reflectance studies and chromatic properties of Zirconium/Tin (Zr^{4+}/Sn^{4+}) co-substituted Pr^{4+}-CeO_2.

Color of $Ce_{0.95}Zr_xPr_{0.05-x}O_2$ and $Ce_{0.95}Sn_xPr_{0.05-x}O_2$ (x = 0, 0.01, 0.02, 0.03, 0.04 and 0.05) pigments varies from dark brown via brick red to bright cream with the variation of zirconium/tin content in the system (Fig. 2.16). The effect of co-substitution of Zr and Sn in Pr-CeO_2 was analyzed from the Kubelka – Munk absorption spectra as shown in Fig. 2.17. As it is evident from the spectra of the pigments, the charge transfer band of $Ce_{0.95}Pr_{0.05}O_2$ at 650 nm is shifted to shorter wavelengths (600 nm) with the substitution of Zr^{4+}/Sn^{4+} chromophore ions. The pigment samples without praseodymium ($Ce_{0.95}Zr_{0.05}O_2$ and $Ce_{0.95}Sn_{0.05}O_2$) show major absorption below 400 nm like that of CeO_2 but with high intensity and hence appear bright cream.

Fig. 2.16. Photographs of (a) $Ce_{0.95}Zr_xPr_{0.05-x}O_2$ and (b) $Ce_{0.95}Sn_xPr_{0.05-x}O_2$ (x = 0, 0.01, 0.02, 0.03, 0.04 and 0.05) pigments.

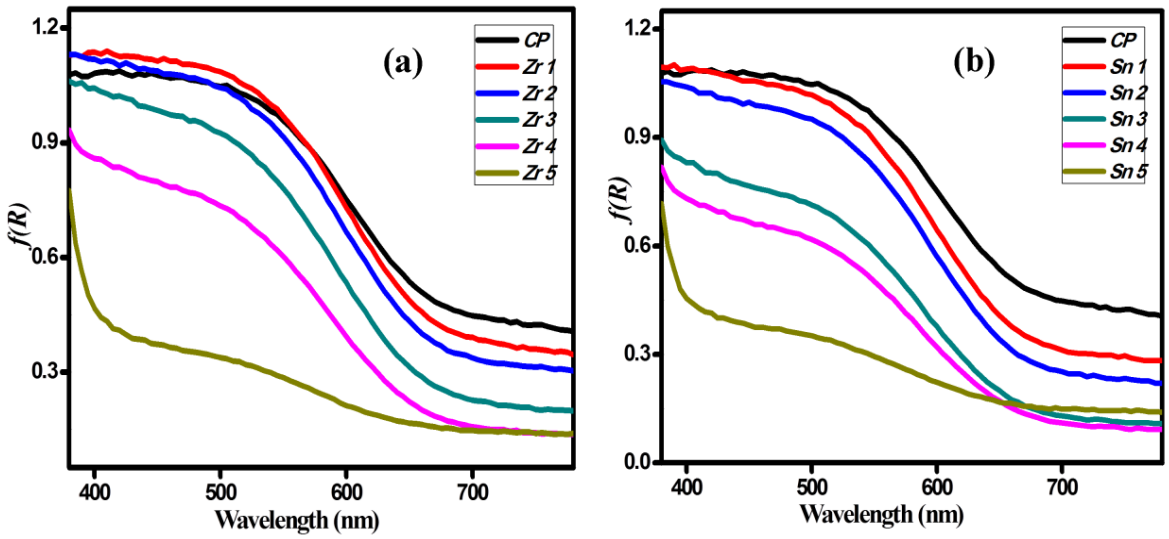

Fig. 2.17. Absorption spectra of (a) $Ce_{0.95}Zr_xPr_{0.05-x}O_2$ and (b) $Ce_{0.95}Sn_xPr_{0.05-x}O_2$ (x = 0, 0.01, 0.02, 0.03, 0.04 and 0.05) pigments.

Table 2.3. Color co-ordinates, band gap and cell parameter of $Ce_{0.95}Zr_xPr_{0.05-x}O_2$ (x = 0, 0.01, 0.02, 0.03, 0.04 and 0.05) pigments.

Sample	Color Co-ordinates					E_g	*a*
	*L**	*a**	*b**	*C**	*h°*	*(eV)*	*(nm)*
CP	44.25	18.35	15.49	24.01	40.16	1.88	0.54083(3)
Zr 1	45.22	20.77	18.22	27.62	41.25	1.90	0.54051(9)
Zr 2	47.63	22.60	22.08	31.59	44.33	1.91	0.54009(4)
Zr 3	51.48	22.19	24.03	32.70	47.27	1.92	0.53991(7)
Zr 4	59.23	20.87	25.89	33.25	51.12	1.96	0.53988(1)
Zr 5	83.01	6.17	14.26	15.53	66.60	3.06	0.53952(6)

Table 2.4. Color co-ordinates, band gap and cell parameter of $Ce_{0.95}Sn_xPr_{0.05-x}O_2$ (x = 0, 0.01, 0.02, 0.03, 0.04 and 0.05) pigments.

Sample	Color Co-ordinates					E_g	*a*
	*L**	*a**	*b**	*C**	*h°*	*(eV)*	*(nm)*
CP	44.25	18.35	15.49	24.01	40.16	1.88	0.54083(3)
Sn 1	50.46	22.77	22.33	31.89	44.44	1.92	0.54012(8)
Sn 2	54.65	22.35	23.26	32.25	46.14	1.93	0.53995(0)
Sn 3	59.71	20.42	23.62	31.22	49.15	1.95	0.53988(2)
Sn 4	63.99	18.56	23.02	29.57	51.12	2.00	0.53968(7)
Sn 5	82.44	7.35	13.77	15.60	61.90	3.07	0.53902(0)

The *L**, *a** and *b** parameters of the Zr/Sn co-substituted pigment samples are listed in Tables 2.3 and 2.4. An evaluation of the color of pigment samples using chromaticity coordinates, and its relation with the component concentrations is described here. The change in substituent concentration gives a nonlinear variation of the color coordinate *a**. Lightness (*L**) and *b** increases as the zirconium and tin content increases in both the set of compositions. The compositions $Ce_{0.95}Zr_{0.02}Pr_{0.03}O_2$ and $Ce_{0.95}Sn_{0.02}Pr_{0.03}O_2$ exhibit better *L**, *a** and *b** values (47.63, 22.60 and 22.08) and (54.65, 22.35 and 23.26) respectively. The present *L**, *a** and *b** values are also comparable with that of commercially available red pigment (Zinc–Iron–Chromite: *L** = 39.92; *a** = 20.5; *b** = 19.63) marketed by Kawamura chemicals, Japan. As in the case of Fe co-substituted ceria red pigments, it is clear that red pigments can be prepared at lower calcinations temperature by the addition of zirconium/tin as compared to CeO_2–Pr_6O_{11} solid solutions reported elsewhere in literature (Nahum *et al.* 2003). The increase

of Zr/Sn content in $Ce_{0.95}Zr_xPr_{0.05-x}O_2$ and $Ce_{0.95}Sn_xPr_{0.05-x}O_2$ increases the lightness of the pigment from 44.25 to 83.01 and from 44.25 to 82.44 respectively. On the other hand, *a** and *b** values decrease considerably for sample without praseodymium, which is responsible for the change of the color of pigment from dark brown via brick red to bright cream.

2.3.6 Diffuse reflectance studies and chromatic properties of Manganese/Silicon (Mn^{4+}/Si^{4+}) co-substituted Pr^{4+}-CeO_2.

Si^{4+}substitution in Pr – substituted ceria exhibits bright reddish brown color whereas Mn^{4+} substitution shows dark brown hue (Fig. 2.18). Absorbance spectra of CeO_2–PrO_2 system co-substituted with Mn and Si are shown in Fig. 2.19. As far as the effect of counter ions is concerned, Si co-substituted pigments give practically the same spectra with a blue shift in the absorption edge resulting in bright reddish brown hue. A gradual shift of CT band can be actually appreciated along with the increase in concentration of Si in Pr-CeO_2. Mn co-substituted pigments show increased absorbance and results in dark brown hue.

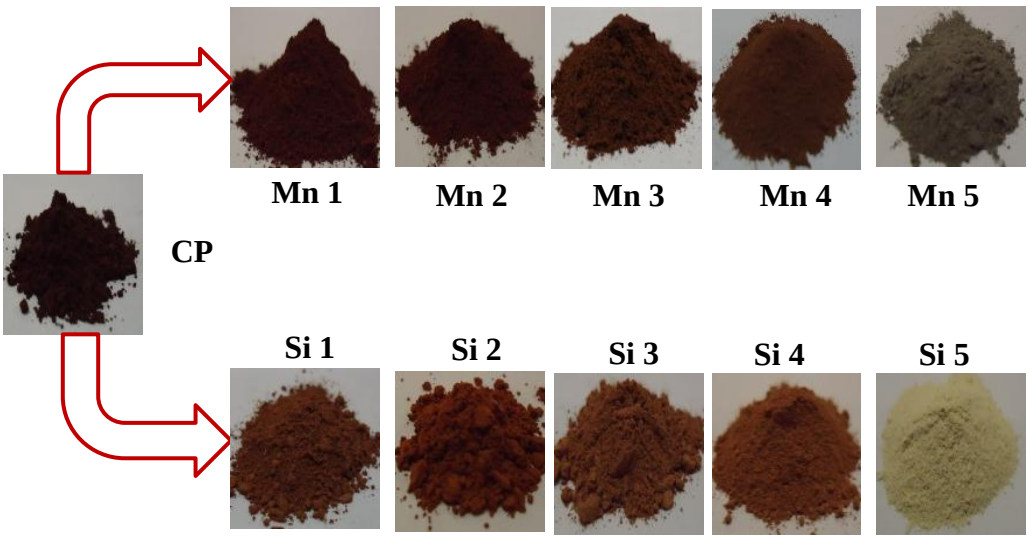

Fig. 2.18. Photographs of $Ce_{0.95}M_xPr_{0.05-x}O_2$ ($M=Mn^{4+}/Si^{4+}$; x = 0, 0.01, 0.02, 0.03, 0.04 and 0.05) pigments.

The width of the band gap is determined by the extent of overlap of the valence orbitals and the difference between the electronegativities of the cations and anions involved (Jansen and Letschert 2000; Jorgensen 1969; Philips 1973). As Si has higher electronegativity than Mn and Ce, the difference in electronegativity between the cations and oxygen decreases and more shift in absorption edge is expected for Si co-substituted samples than that of Mn containing compounds. The change in color of CP with increasing content of substituted elements accounts for the shift in absorption edge which is caused by the change in chemical bonding nature by incorporating higher electronegative metal ion into the praseodymium-cerium matrix.

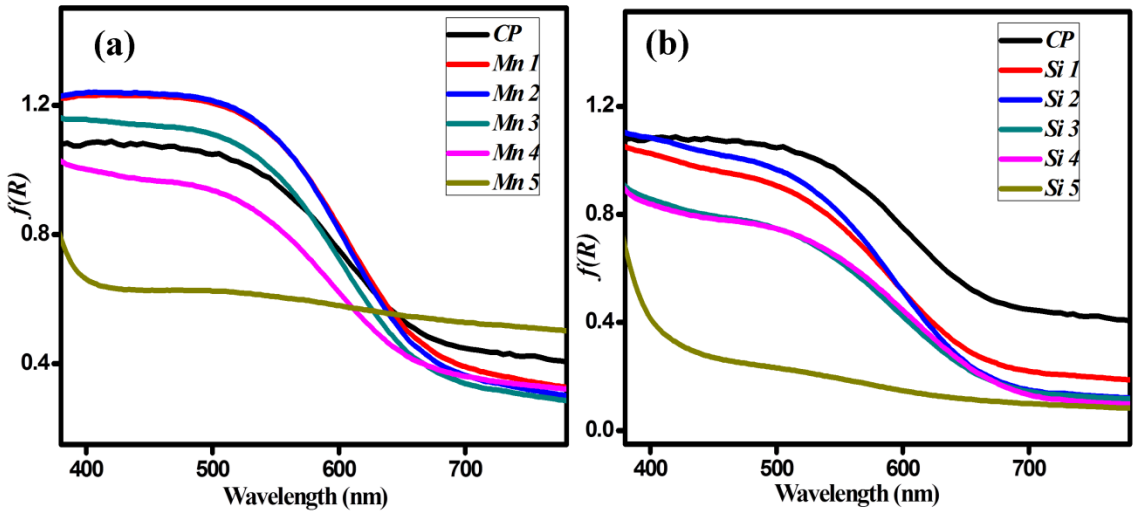

Fig. 2.19. Absorbance spectra of (a) $Ce_{0.95}Mn_xPr_{0.05-x}O_2$ and (b) $Ce_{0.95}Si_xPr_{0.05-x}O_2$ (x = 0, 0.01, 0.02, 0.03, 0.04 and 0.05) pigments.

Color of the synthesized pigments is numerically expressed in terms of the color co-ordinates as given in Table 2.5 and 2.6. The lightness (L^*) increases as the concentration of co-substituents increase in both set of compositions. Si co-substituted Pr^{4+}-CeO_2 exhibits increased lightness compared to Mn^{4+} co-substituted ceria due to smaller particles as evident from the SEM micrographs (Fig. 2.10). The redness (a^*) of compounds increases with increase in concentration of Mn, with low b^* values and hence

the samples exhibit more dark brown color. For Si co-substituted $Ce_{0.95}Pr_{0.05}O_2$ compounds both *a** and *b** are almost same and exhibit bright reddish brown hue. The parameters, *a** and *b** decrease considerably for samples without praseodymium, which is responsible for the change of the color of the pigment from dark brown via bright reddish brown to bright cream for Si co-substituted Pr-ceria and ash color for Mn substituted ceria (Fig. 2.18). The hue angle values reveal that the $Mn^{4+}$and Si^{4+} co-substituted $Ce_{0.95}Pr_{0.05}O_2$ pigments lie in the brick red to dark-brown region of the cylindrical color space (h°= 0-35 for red and 35-70 for orange). It is interesting to note that the chromatic properties of $Ce_{0.95}M_xPr_{0.05-x}O_2$ (M = Mn and Si) pigments summarized in Table 2.5 and 2.6 are significantly higher than recently reported praseodymium substituted ceria powders (5% Pr doped CeO_2 : *L** = 66; *a** = 12; *b** = 9.5), synthesized by microwave-assisted hydrothermal route (Bondioli *et al.* 2005).

Table 2.5. Color co-ordinates, band gap and cell parameter of $Ce_{0.95}Mn_xPr_{0.05-x}O_2$ (x = 0, 0.01, 0.02, 0.03, 0.04 and 0.05) pigments.

Sample	Color Co-ordinates					E_g	*a*
	*L**	*a**	*b**	*C**	*h°*	*(eV)*	*(nm)*
CP	44.25	18.35	15.49	24.01	40.16	1.88	0.54083(3)
Mn 1	37.64	20.75	15.11	25.67	36.06	1.86	0.54104(4)
Mn 2	38.33	21.96	16.19	27.29	36.39	1.88	0.54036(9)
Mn 3	41.89	21.41	17.17	27.44	38.72	1.87	0.54012(1)
Mn 4	47.88	17.61	16.11	23.86	42.45	1.90	0.5403(2)
Mn 5	56.85	2.61	2.60	3.69	44.81	2.78	0.5404(6)

Table 2.6. Color co-ordinates, band gap and cell parameter of $Ce_{0.95}Si_xPr_{0.05-x}O_2$ (x = 0, 0.01, 0.02, 0.03, 0.04 and 0.05) pigments.

Sample	Color Co-ordinates					E_g (eV)	*a* (nm)
	*L**	*a**	*b**	*C**	*h°*		
CP	44.25	18.35	15.49	24.01	40.16	1.88	0.54083(0)
Si 1	51.55	22.07	22.23	31.32	45.20	1.89	0.54052(5)
Si 2	50.70	25.85	24.73	35.78	43.72	1.87	0.54038(8)
Si 3	57.07	20.34	20.14	28.62	44.70	1.86	0.54177(9)
Si 4	55.88	20.03	18.32	27.14	42.44	1.84	0.54113(8)
Si 5	84.31	4.25	12.83	13.51	71.66	2.90	0.53985(9)

2.3.7 Band gap Engineering

$Ce_{0.9}Fe_xPr_{0.1-x}O_{2-\delta}$ (x = 0.02, 0.04, 0.06, 0.08 and 0.095) and $Ce_{0.8}Fe_xPr_{0.2-x}O_{2-\delta}$ (x = 0.04, 0.08, 0.12, 0.16 and 0.19) solid solutions were found to shift their absorption edge towards the higher energy side as the substitution of iron increases for Pr with band gap changing from 1.88 eV to 1.97 eV. This is originated from the O_{2p}–Ce_{4f} and O_{2p}–Fe_{3d} double charge transfer transitions. But one may doubt for the presence of *d*-*d* intra-atomic transitions which can occur with a d^5 configuration in octahedral coordination. Charge transfer such as O^{2-}-Fe^{3+} has a high probability to occur in visible range (1.5-3 eV) compared to intra-atomic *d*-*d* transitions (Pailhe *et al.* 2008). The blue shift in the absorption edge of Pr-CeO_2 by the co-substitution of Fe^{3+} is due to the coupled CT from O_{2p}–Ce_{4f} and O_{2p}-Fe_{3d}. The acceptor like substitution of Fe^{3+} for Pr^{4+} creates oxygen vacancies in the cerium oxide lattice and reduces the lattice parameter (Table 2.1 and

2.2). Also, the ionic radius of Fe^{3+} is (0.78 Å) smaller than Ce^{4+} (0.97 Å). The cell parameter decreases with the progressive substitution of Fe^{3+} for Ce^{4+}. It is known that the band gap of a material is engineered by control of the crystallite size that leads to tunable absorption edge (Suzuki and Kijima 2005). It is found that the band gap energy (E_g) of the $Ce_{0.9}Fe_xPr_{0.1-x}O_{2-\delta}$ and $Ce_{0.8}Fe_xPr_{0.2-x}O_{2-\delta}$ solid solutions varies as a function of substituent concentration. The co-substitution of Fe^{3+} with Pr^{4+} for Ce^{4+} altered significantly the absorption properties of CeO_2 in CeO_2-Pr_6O_{11}-Fe_2O_3 solid solutions. The brilliance and purity of a semiconductor's color is determined by the steepness of the absorption edge. The band structure of $Ce_{0.9}Fe_xPr_{0.1-x}O_{2-\delta}$ and $Ce_{0.8}Fe_xPr_{0.2-x}O_{2-\delta}$ solid solutions can be considered as conduction band formed of Ce_{4f} and Fe_{3d} and valence band of $O_{2p.}$ The partially filled Pr 4*f* orbital lies above the valence band of O_{2p}. Since localized 4*f* orbitals of Ce constitute the conduction band of CeO_2, substitution of Fe^{3+} to the CeO_2 lattice influence the conduction band by admixing Fe_{3d} orbitals. As the concentration of Fe^{3+} chromophore ion increases, the width of conduction band increases and simultaneously the width of partially filled Pr 4*f* band decreases as the Pr concentration decreases in the same composition. But as the concentration of the substituted Fe^{3+} ions are less compared to that of Pr^{4+} ions in CeO_2, the manipulation effect on conduction band is minimal and thus systematic increase in the band gap occurs with an increasing concentration of Fe in Pr-CeO_2 lattice.

$Ce_{0.95}Zr_xPr_{0.05-x}O_2$ and $Ce_{0.95}Sn_xPr_{0.05-x}O_2$ (x = 0, 0.01, 0.02, 0.03, 0.04 and 0.05) solid solutions were found to shift their absorption edge towards the higher energy side as the substitution of zirconium/tin increases with band gap changing from 1.88 - 3.06 eV and 1.88 - 3.07 eV respectively. It was found that various concentrations of the components change the intensity of the reflectance spectra, whereas the band positions exhibits only small deviations from the pure compound. It can be found that the band gap energy of $Ce_{0.95}Zr_xPr_{0.05-x}O_2$ and $Ce_{0.95}Sn_xPr_{0.05-x}O_2$ compositions varies as a function of Zr and Sn concentration respectively. The electronegativities of the metals only vary in

small steps and the substitution of one metal by the other usually produces small shifts in elctronegativity difference and hence small change in band gap is expected on co-substitution of Zr or Sn with Pr in the cerianite lattice.

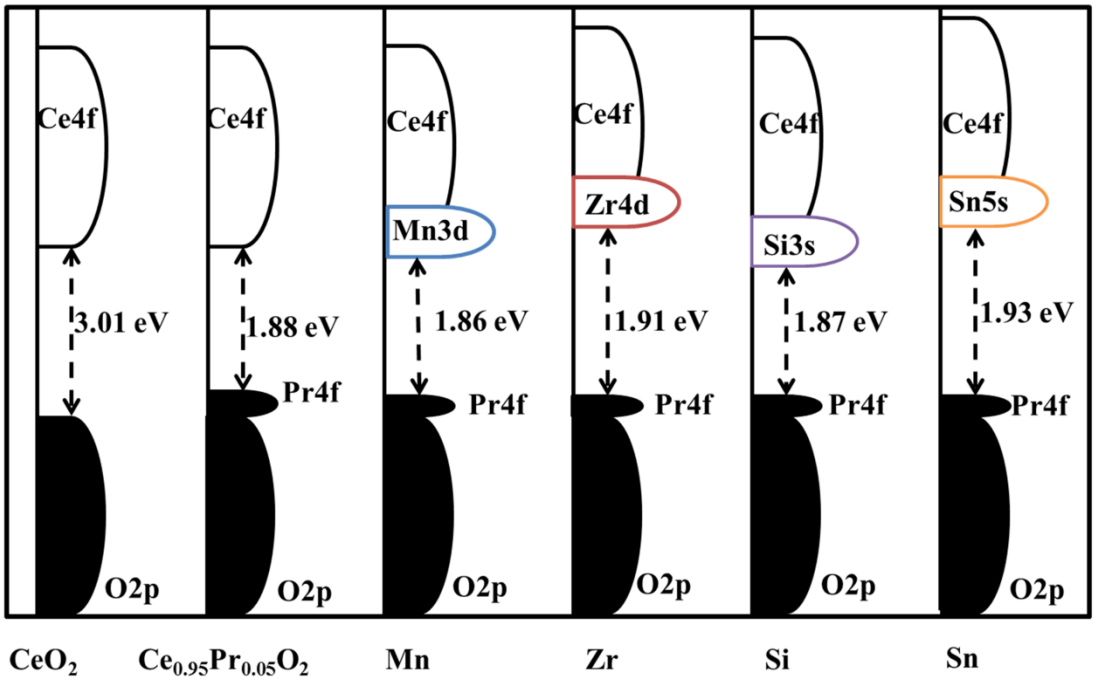

Fig. 2.20. Schematic representation of band structures of CeO_2, $Ce_{0.95}Pr_{0.05}O_2$ and M^{4+}-co-substituted $Ce_{0.95}Pr_{0.05}O_2$ (M = Mn, Zr, Si and Sn) pigments.

The band gap energy (E_g) (Table 2.5 and 2.6) calculations reveal a substantial reduction in the band gap of $Ce_{0.95}M_xPr_{0.05-x}O_2$ (M= Mn and Si) when compared to CeO_2. Substitution of Mn^{4+}/Si^{4+} into Pr-CeO_2 lattice induces formation of intermediate energy levels on either side of fermi level that cause a change in the band gap. The formation of mixed oxide alters the optical characteristics of the resultant material due to the contribution of Mn_{3d} and Si_{3s} to the conduction band. In the case of solid solution containing Mn^{4+}/Si^{4+} and Ce^{4+}, the conduction band is formed by Ce_{4f} and Mn_{3d}/Si_{3s} resulting in the band gap widening (2.78/2.90 eV).

Fig. 2.20 shows the schematic representation of the band structures of CeO_2, $Ce_{0.95}Pr_{0.05}O_2$ and M^{4+}-co-substituted $Ce_{0.95}Pr_{0.05}O_2$ (M = Mn, Zr, Si and Sn) pigments. The partially filled Pr 4*f* orbital lies above the valence band of O_{2p}. The band gap energy of $Ce_{0.95}Pr_{0.05}O_2$ was found to be 1.88 eV from the absorption edge. This narrowing of band gap from 3.01 eV (in the case of CeO_2) is due to the additional electronic energy level produced by Pr^{4+}. For M^{4+}-co-substituted $Ce_{0.95}Pr_{0.05}O_2$ (M=Mn, Zr, Si and Sn), the band structure would be more complex than that of $Ce_{0.95}Pr_{0.05}O_2$. For 1 mol % Mn co-doped $Ce_{0.95}Pr_{0.05}O_2$, the band gap slightly decreased (1.86 eV) due to the contribution of Mn_{3d} to the conduction band. In the case of $Ce_{0.95}Zr_{0.02}Pr0_{.03}O_2$, the band gap is slightly increased (1.91 eV) than the praseodymium substituted ceria, which resulted from the contribution of Zr_{4d} to the conduction band. The similar is obvious in the case of $Ce_{0.95}Sn_{0.02}Pr0_{.03}O_2$, where Sn_{5s} contributes to the conduction band. The band gap reduction of 2 mol % Si co-substituted $Ce_{0.95}Pr_{0.05}O_2$ arises from the contribution of Si_{3p} to the conduction band. In the case of solid solution containing Zr^{4+}/ $Sn^{4+}Mn^{4+}/Si^{4+}$ and Ce^{4+} the conduction band is formed by Ce_{4f} and vacant orbital of the respective co-substituents resulting in the band gap widening.

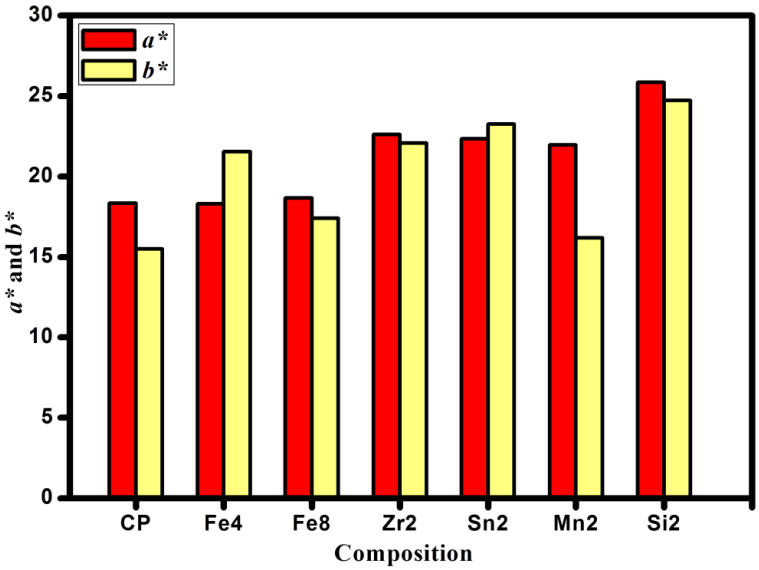

Fig. 2.21. Variation of the color co-ordinates (*a** and *b**) of pigments with composition.

Fig. 2.21 represents the variation of the redness (a^*) and yellowness (b^*) with different composition of the $M^{3+/4+}$ ion co-substituted Pr-CeO_2 pigments. Co-substitution of metal ions in ceria matrix helps to improve the redness and yellowness of the ceria red pigments.

2.3.8 Acid/Alkali resistance studies of the pigments

The acid/alkali resistance of the pigments was carried out in 10% HNO_3 and NaOH. A pre–weighed amount of the pigment was treated with acid/alkali and soaked for half an hour with constant stirring using a magnetic stirrer. The pigment powder was then filtered, washed with water, dried and weighed. Negligible weight loss of pigment was noticed. Among the series of colorants synthesized, typically Fe 4, Fe 08, Zr 2, Sn 2, Mn 2 and Si 2 were tested for its acid and alkali resistance. The color co-ordinates of the resultant tested samples were measured and compared with the untreated samples. The total color difference ΔE^*_{ab} was calculated and is summarized in Table 2.7.

Table 2.7. The color co-ordinates (±0.1) of the powder pigments after acid/alkali resistance tests.

Sample	HNO_3				NaOH			
	ΔL^*	Δa^*	Δb^*	ΔE^*_{ab}	ΔL^*	Δa^*	Δb^*	ΔE^*_{ab}
Fe 4	0.4	0.3	0.5	0.7	0.5	0.4	0.3	0.7
Fe 08	0.5	0.6	0.4	0.8	0.5	0.5	0.4	0.8
Zr 2	0.2	0	0.4	0.5	0.6	0.5	0.4	0.9
Sn 2	0.1	0.1	0.3	0.3	0.4	0.5	0.3	0.7
Mn 2	0.3	0.1	0.1	0.4	0.5	0.2	0.3	0.6
Si 2	0.3	0.5	0.2	0.6	0.4	0.5	0.5	0.8

$$\Delta E^*_{ab} = [(\Delta L^*)^2+(\Delta a^*)^2+(\Delta b^*)^2]^{1/2}$$

The negligible values of ΔE^*_{ab} reveal that the pigments are chemically stable towards the acid/alkali tested. The industrially acceptable limits of ΔE^*_{ab} are as follows: when $\Delta E^*_{ab} \leq 1$ unit indicate that the color change is almost indistinguishable from the original color, whereas, $\Delta E^*_{ab} \leq 5$ units are considered to be good. It is apparent that the color co-ordinate values of the pigment samples after acid and alkali test is nearly same as that of the pigment sample. This specifies that the investigated pigments are chemically stable.

2.3.9 Coloration of Plastics

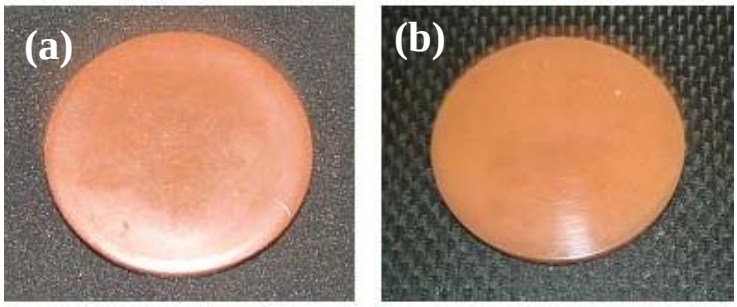

Fig. 2.22. Photographs of pigmented polymers with 8 wt% pigments (a) $Ce_{0.9}Fe_{0.04}Pr_{0.06}O_{2-\delta}$ and (b) $Ce_{0.8}Fe_{0.08}Pr_{0.12}O_{2-\delta}$.

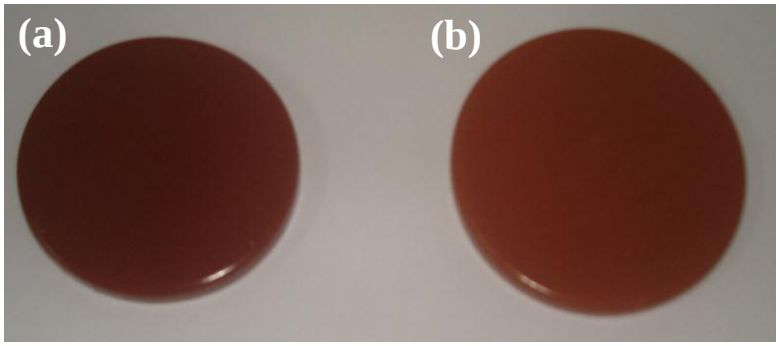

Fig. 2.23. Photographs of (a) $Ce_{0.95}Zr_{0.02}Pr_{0.03}O_2$ (10%) + PMMA and (b) $Ce_{0.95}Sn_{0.02}Pr_{0.03}O_2$ (10%) + PMMA.

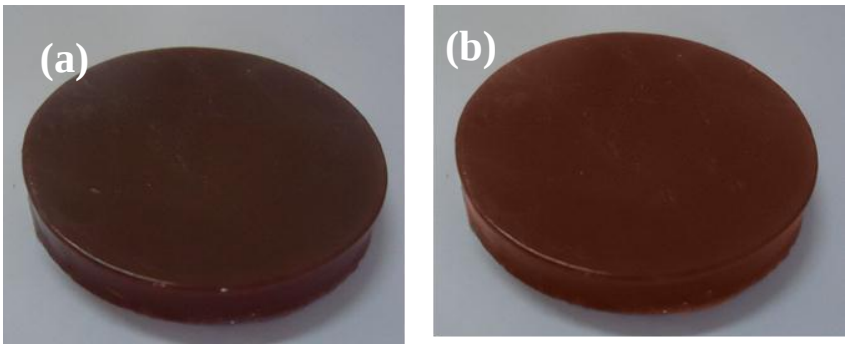

Fig. 2.24. Photographs of (a) $Ce_{0.95}Mn_{0.02}Pr_{0.03}O_2$ (10%) + PMMA, and (b) $Ce_{0.95}Si_{0.02}Pr_{0.03}O_2$ (10%) + PMMA.

Table 2.8 Color co-ordinates (±0.1) of the $M^{3+/4+}$ co-substituted Pr-CeO_2 pigment powders after applying in polymer.

Sample	Color Co-ordinates		
	*L**	*a**	*b**
Fe 4 (8 %)	52.05	17.48	20.12
Fe 08 (8 %)	36.53	15.25	12.85
Zr 2 (10%)	38.32	16.62	13.10
Sn 2 (10 %)	43.97	18.90	16.12
Mn 2 (10 %)	33.90	19.66	14.32
Si 2 (10 %)	46.06	21.75	20.47

In order to test the capacity of pigment samples to produce a red hue, pigment compositions with the best chromatic property from each system was chosen. Poly (methyl methacrylate) (PMMA) was used as the polymer matrix for fabricating the pigmented compact. Color co-ordinates of the pigmented polymer compacts are given in

Table 2.8. The red hue is achieved by dispersing 8 wt. % of the pigments, (Fe 4 and Fe 08) in poly (methyl methacrylate) (PMMA) polymer. The red color remained, when the polymer was compacted into discs (Fig. 2.22). The light resistance of the typical pigmented polymer (Fig. 2.23) (Zr 2 and Sn 2) was tested by exposing it to sun light at various time intervals and measured the color coordinates. The L^* a^* b^* values of tested polymer compacts (Table 2.8) were found to be nearly same as that of the unexposed sample which indicates that the pigmented polymer is resistant to light. The color co-ordinates of the test pieces, Mn 2 and Si 2 were measured at different locations (Fig. 2.24). The L^* a^* b^* values obtained were more or less the same indicating the uniform distribution of pigment particles in the polymer matrix. Thus, the developed pigments may find potential application in the coloring of various plastic materials.

2.4 Conclusions

Inorganic pigments having the general formula $Ce_{0.95}M_xPr_{0.05-x}O_2$, (M = Zr, Sn, Mn and Si, x = 0, 0.01, 0.02, 0.03, 0.04 and 0.5), $Ce_{0.9}Fe_xPr_{0.1-x}O_{2-\delta}$ (x = 0.02, 0.04, 0.06, 0.08 and 0.095) and $Ce_{0.8}Fe_xPr_{0.2-x}O_{2-\delta}$ (x = 0.04, 0.8, 0.12, 0.16 and 0.19) displaying wide range of colors from bright cream to brick red and dark brown, have been developed by traditional solid state route and well characterized. The prepared solid solutions absorb the visible blue and green below 600 nm efficiently, which is originated from the shift of charge transfer band of CeO_2 by co-substitution of transition metal and praseodymium for cerium. The optical absorption edge of these pigments depends on the Pr and transition metal (Fe, Zr Mn, Si and Sn) content. It was found that small substitutions of transition metals into $Ce_{0.95}Pr_{0.05}O_2$ system shift their absorption edge towards the higher energy side as the co-substitution of metal ion increases with change in band gap. It is interesting to note that the co-substitution of Fe^{3+} and Pr^{4+} for Ce^{4+} in ceria gently red shifted the absorption edge due to O_{2p}–Ce_{4f} and O_{2p}–Fe_{3d} double charge transfer transitions. The small substitutions of Zr and Sn in $Ce_{0.95}Pr_{0.05}O_2$ system offers fine

optical band gap tuning from 1.88 eV to 3.06 eV with significant improvement in the color characteristics such as lightness (L^*) and redness (a^*) of the pigments. The incorporation of Mn^{4+}/Si^{4+} into the CeO_2–PrO_2 system slightly shifted the color to dark brown and bright reddish brown. The present investigations establish that various color hues can be achieved by the incorporation of suitable chromophore metal ions in CeO_2 host lattice by tuning of the band gaps. Furthermore, the synthesized pigments commercial significance is in their thermal, chemical and light stability. In addition, they can be considered as comparatively less toxic inorganic pigments, because they are composed of non-toxic and safe elements. The color properties of the present pigments suggest that they have a potential to be applied as satisfactory pigments for the coloration of plastics.

CHAPTER 3

Synthesis and Characterization of Pr - Substituted $TiCeO_4$ Pigments

New inorganic pigments having the general formula $TiCe_{1-x}Pr_xO_4$ (x = 0, 0.05, 0.1, 0.3, 0.5 and 0.7) displaying colors ranging from white to brick red have been synthesized by a traditional solid state route, as viable alternatives to toxic red inorganic colorants. The products were characterized for their structure, morphology and optical properties. The coloring mechanism is based on the strong absorptions of the pigments in the visible region below 650 nm, which could originate from the introduction of an additional energy level between O_{2p} valence band and the Ce_{4f} conduction band from the $4f^1$ electron of praseodymium. The presence of titanium in Pr^{4+} - substituted ceria matrix helps to improve the lightness and opacity of the synthesized pigments. The designed red pigments consist of non–toxic elements and found to be thermally and chemically stable. The utility of the designed pigment for surface coating applications is also evaluated.

Sandhya Kumari et al. ***Dyes Pigm.*** *77* (2008) 427-431.

3.1 Introduction

The development of red ceramic pigments with high temperature stability is of great importance to the ceramic industry (Buxhaum 1993; Eppler 1998.; Smith 2002). The classical red pigments used hitherto in the ceramic industry are of two types: iron oxide or cadmium sulfoselenide encapsulated in zircon matrixes and lead oxide in tin oxide matrix (Aruna *et al.* 2001; Bondioli *et al.* 1998; Nahum *et al.* 2003). However, some of these pigments are toxic and unstable above 900°C. These materials can be easily replaced by rare earth metal oxides, which are generally having a low toxicity rating (Arvela 1979; Haley 1965). Lanthanide ions have attracted considerable attention due to their unique optical properties and specific functions make them useful in a wide range of industrial applications that includes tunable lasers, amplifiers for optical communications, organic light–emitting diodes and inorganic pigments (Bunzli and Piguet 2005; Buxbaum and Pfaff 2005; Hiroshi *et al.* 1995; Kido and Okamoto 2002). The intense coloration of rare earth based materials can arise from mostly charge transfer interactions between a donor and an acceptor with the metal ions playing generally the role of an acceptor. Dopants based on rare earth elements in mixed oxide systems offer an opportunity to tune the color response through the manipulation of energy gaps and delocalization phenomena in conduction and valence bands. This phenomenon offers wide scope for designing of colorants for specific applications. Hence in the recent past a large number of rare earth based pigments have been proposed as alternatives to traditional toxic inorganic pigments (Dohnalova *et al.* 2009; Fernandez-Gonzalez *et al.* 2011; Martos *et al.* 2008). Jansen and Letschert have reported that the colors of the solid solutions $Ca_{1-x}La_xTaO_{2-x}N_{1+x}$ of the perovskite type pigments could be tuned from yellow through orange to deep red by simple composition adjustments. Further, they demonstrated that any color in the range from light yellow to deep red can be tailored by proper adjustment of the O/N ratio in the solid solution. Though these pigments are non–toxic and show excellent color hue, the synthesis procedure of these materials utilizes

toxic and inflammable ammonia gas for longer periods. Rare earth sulphides and related compounds have also been proposed as promising candidates for various surface coating applications (Busnot and Macaudiere 2002; Gauthier *et al.* 2003; Perrin and Wimmer 1996; Zhukov *et al.* 1997). The chromatic properties of cerium sulphides arise from the fact that the optical absorption associated with the $4f \rightarrow 5d$ electronic transition of their Ce^{3+} ions range from ~1.9 eV to 2.1 eV (Perrin and Wimmer 1996). The synthesis of sulphide based pigments uses toxic hydrogen sulphide gas. $ZrSiO_4:Fe^{3+}$ is a well-known commercial red pigment which has been widely used in the industry for coloring of ceramics (Blonski 1994; Hill *et al.* 2000).

TiO_2 based pigments are widely employed in industrial applications due to their color range, which depends on the chromophore ions (Borgarello *et al.* 1982; Cavalcante *et al.* 2009; Matteucci *et al.* 2007) or counter ions (Coster *et al.* 2005) added to the matrix. These pigments can also act as opacifying agents (Stengl *et al.* 2009). The addition of ceria to the TiO_2 matrix results in a yellow pigment that can be employed in the fabrication of dental prostheses (Santos *et al.* 2007), with the possibility of obtaining a color similar to that of commercial dentine. The doping of titanium oxide with vanadium and zirconium oxides produces a bright yellow shade whose colorimetric parameters are very similar to those of industrial ceramic pigments (Dondi *et al.* 2007). TiO_2–CeO_2 mixed oxides have attracted much interest for catalytic applications because of their improved properties. Many studies on TiO_2–CeO_2 mixtures have shown improvements regarding redox, (Koebrugge *et al.* 1993) textural and structural properties (Lopez *et al.* 2004). These improvements have been attributed to modification of the structure, electronic properties, or thermal stability by Ti–Ce interaction and control of the structure. Replacing cerium ions in the CeO_2 crystalline structure (cerianite) by cations of different size or charge and which modify ion mobility inside the lattice (Byong K 1991; Connell and Morris 2000) results in the formation of a defect fluorite structure (Rynkowski *et al.* 2000). Such modifications confer new properties to the

material such as better resistance to sintering at high temperatures and high catalytic activity for various reactions (Pijolat *et al.* 1995). Scarce literature exists about the use of this mixed oxide as a matrix for luminescent materials. Recently, new insights on the structural and optical properties of Ce–Ti mixed oxide nanoparticles doped with praseodymium was reported (Fernandez-Gonzalez *et al.* 2011). Interestingly these pigments exhibited yellow coloration and red coloration depending on the calcination temperature. The rare earth doped TiO_2– CeO_2 system offers an opportunity to study and tune the color of the material through the manipulation of energy gaps and delocalization phenomena in conduction and valence bands (Rao and Reddy 2007). This phenomenon offers wide scope for the designing of optical materials for specific applications. These factors have prompted to study the optical properties of the typical pigments $TiCe_{1-x}Pr_xO_4$ (x = 0, 0.05, 0.1, 0.3, 0.5 and 0.7). The thermal and chemical stability of the pigments have also been evaluated. The coloring performance of the pigments in the plastics is also evaluated.

3.2 Experimental Section

3.2.1 Materials and Methodology

Solid solutions in different stoichiometric compositions: $TiCe_{1-x}Pr_xO_4$ (x = 0, 0.05, 0.1, 0.3, 0.5 and 0.7) were synthesized by a solid state reaction, using precursor oxides, CeO_2, TiO_2 and Pr_6O_{11} (Sigma Aldrich, 99.99%) as the starting materials. $TiCe_{1-x}Pr_xO_4$ (x = 0, 0.05, 0.1, 0.3, 0.5 and 0.7) are designated as TC, TCP_5, TCP_{10}, TCP_{30}, TCP_{50} and TCP_{70} respectively. The raw materials were weighed according to the stoichiometry of the samples and then mixed thoroughly in an agate mortar and homogenized by wet milling in acetone media. Residual acetone was removed by evaporation. Then, the mixture was dried in an air oven at 100 °C for 1 h. This procedure of mixing and subsequent drying was repeated thrice to get a homogeneous mixture. The resultant powders were calcined in platinum crucibles in an high temperature electric furnace at an

optimized temperature of 1250 ^{o}C for 3 hours in air atmosphere, followed by auto–cooling in the furnace. The heating of the furnace was programmed to increase the temperature initially at 10 °C/min up to 1000 °C and afterwards the heating rate was decreased to 5 °C/min up to 1250 ^{o}C. The pigment compositions thus obtained were ground in an agate mortar in order to refine and homogenize the particle size. The phase purity and chromatic properties were not satisfactory below 1250 °C.

3.2.2 Characterization Techniques

The crystalline nature and phase purity of the samples were investigated using powder X-ray diffraction analysis with Ni-filtered Cu-Kα ($K\alpha_1$ = 1.54060 Å, $K\alpha_2$ = 1.54443 Å) , radiation using a PANalytical Philips X'pert Pro diffractometer. Data were collected by scanning over a 2θ range from 10° to 90°. The morphology of the synthesized samples was recorded on a scanning electron microscope JEOL JSM–5600 model, with an acceleration voltage of 15 kV. The particle size distribution of the typical pigment sample $TiCe_{0.5}Pr_{0.5}O_4$ was investigated in water medium using the Laser Scattering Particle Size Distribution Analyzer (CILAS 930 Liquid). The samples were ultrasonically homogenized for 180 s during measurement and the signal was evaluated on the basis of Fraunhofer bending.

The diffuse reflectance of the powdered pigment samples were measured (200 – 780 nm) with a UV–vis Spectrophotometer (Shimadzu UV–2450 with an integrating sphere attachment, ISR–2200) using barium sulphate as the reference. The band gap values were calculated from the corresponding absorbance spectra by straight forward extrapolation method using the formula $E(eV) = hc/\lambda$ (where λ represents the wavelength in nm). The color coordinates were determined by coupling analytical software (UVPC Color Analysis Personal Spectroscopy Software V3, Shimadzu) to the UV–2450 spectrophotometer. The CIE 1976 $L^*a^*b^*$ colorimetric method was used, as recommended by the Commission Internationale de l'Eclairage (CIE).

Thermo gravimetric (TG) and differential thermal analyses (DTA) were performed in a Pyris Diamond TG/DTA Perkin Elmer make. All the experiments were run in a platinum crucible from 50–1000 °C with a heating rate of 20 °C/min in nitrogen atmosphere.

Among the pigment compositions prepared, the typical pigment sample $TiCe_{0.9}Pr_{0.1}O_4$ (5 or 10 wt%) was dispersed in polymer matrix like PMMA to test their coloring performance. The pigment $TiCe_{0.9}Pr_{0.1}O_4$ (5 and 10 wt%) was ultrasonicated in an alcohol-water (1:4) mixture for 10 min to ensure complete dispersion of the pigment particles. A viscous solution of PMMA (95 and 90 wt%) was made using a conventional electrical coil heater. The pigment dispersion was slowly added with stirring and converted to a thick paste. The paste after 2 h curing was compressed uniaxially into a form of cylindrical disk using a hydraulic press at a pressure of 25 MPa. Both sides of the pigmented polymer were lapped using a fine grade emery sheet for obtaining a polished surface. The color coordinates of the pigmented compacts were examined to assess the coloration.

3.3 Results and Discussion

3.3.1 Powder X–ray diffraction studies

The XRD patterns of the pigments $TiCe_{1-x}Pr_xO_4$ (x = 0, 0.05, 0.1 and 0.3) are shown in Fig. 3.1 which represent the characteristic reflections of the cubic fluorite structure of CeO_2 and also in good agreement with the JCPDS No. 34-394. The minor peaks can be assigned to rutile TiO_2 (PDF No. 21-1276) (Baidya *et al.* 2006). On the other hand, with the increase of Pr content in $TiCeO_4$ (x = 0.5 and 0.7), structural transformation from cubic fluorite to pyrochlore can be noticed from the XRD patterns of the pigments $TiCe_{1-x}Pr_xO_4$ as given in Fig. 3.2. When x = 0.5, both the fluorite and pyrochlore phases have been observed. Further, it is also clear from the XRD pattern of the pigment that when x = 0.7 only pyrochlore phase $Ti_2Pr_2O_7$ (PDF No. 35- 267) has

been formed. The intense and sharp peaks found in the diffraction patterns reveal the crystalline nature of the products.

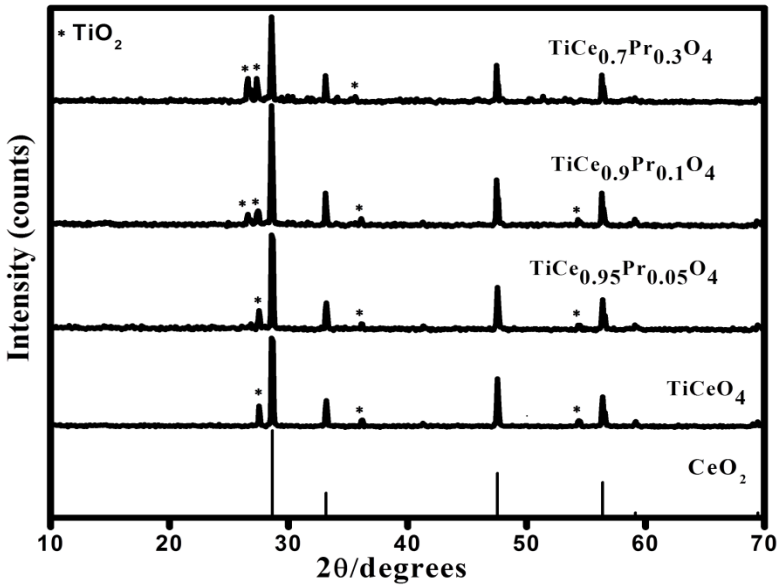

Fig. 3.1. Powder XRD patterns of $TiCe_{1-x}Pr_xO_4$ pigments (x = 0, 0.05, 0.1 and 0.3).

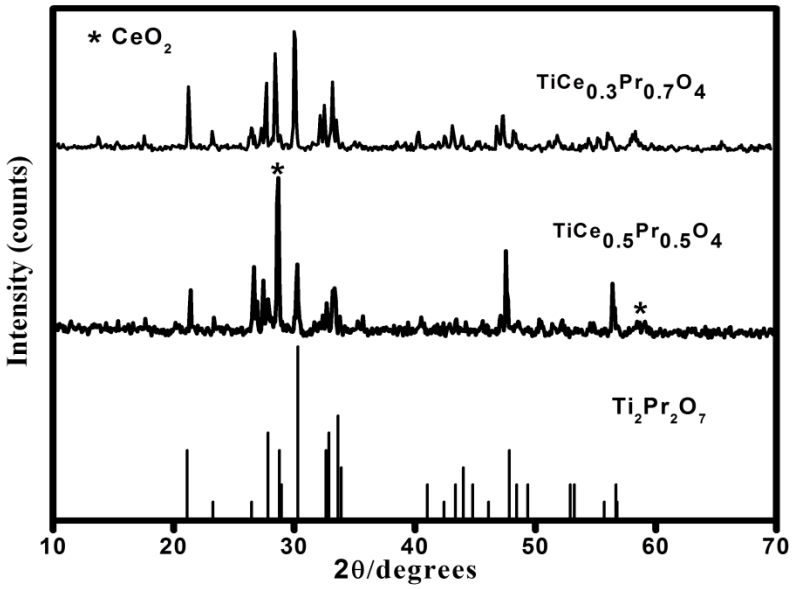

Fig. 3.2. Powder XRD patterns of $TiCe_{1-x}Pr_xO_4$ pigments (x = 0.5 and 0.7).

3.3.2 Morphological and Particle size Studies

The homogeneous and crystalline natures of the samples have also been noticed from the SEM photographs (Fig. 3.3) of $TiCe_{1-x}Pr_xO_4$ pigments. The particle size distribution of the typical pigment, $TiCe_{0.5}Pr_{0.5}O_4$ investigated shows a distribution with 90% of the particles being smaller than 44.13 mm, 50% smaller than 16.03 mm and 10% smaller than 4.51 mm. The mean particle diameter of the pigment sample was found to be 20.87 mm.

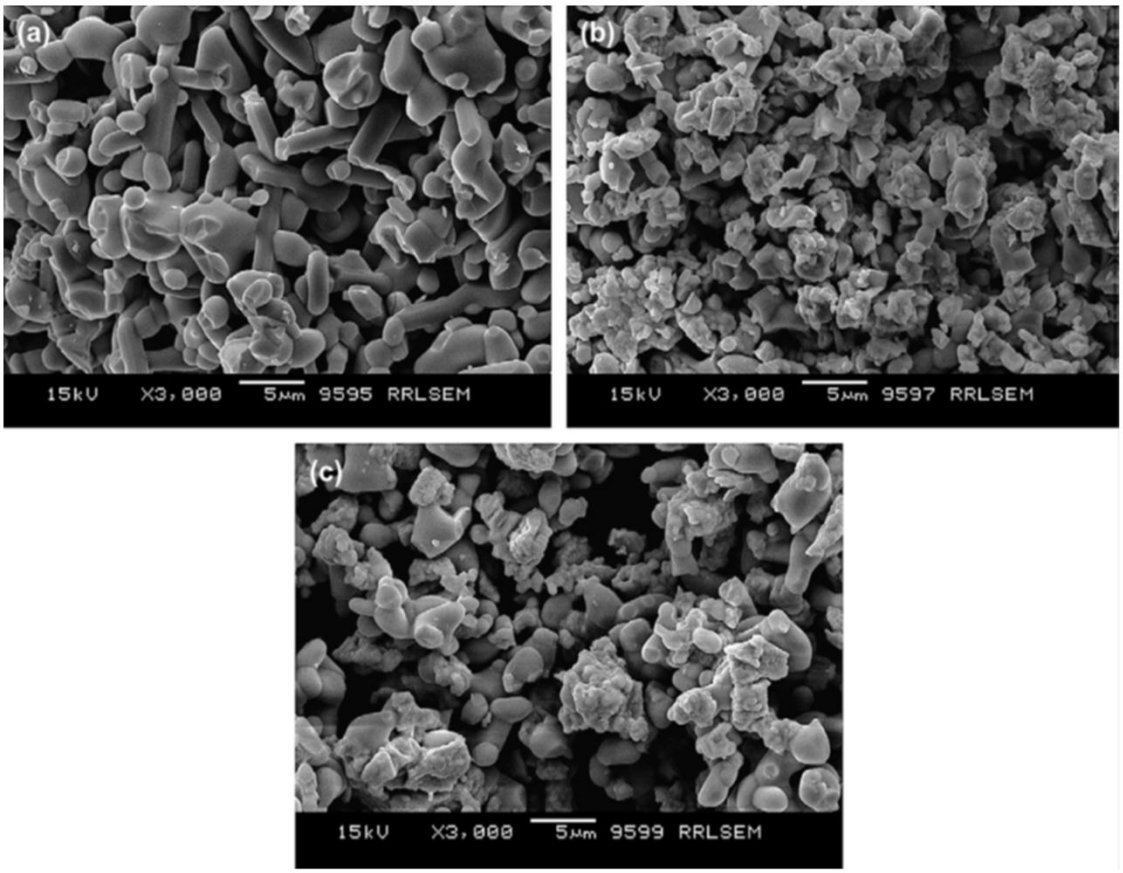

Fig. 3.3. SEM micrographs of (a) TC (b) TCP_{50} and (c) TCP_{70}.

3.3.3 Diffuse reflectance studies and chromatic properties of $TiCe_{1-x}Pr_xO_4$

$TiCe_{1-x}Pr_xO_4$ exhibits colors varying from white to brick red as the concentration of Pr^{4+} ion increases from zero to 70 mol % (Fig. 3.4). Fig. 3.5 depicts the diffused reflectance spectra obtained for the $TiCe_{1-x}Pr_xO_4$ pigments. The absorption curve of the pure TiO_2-CeO_2 is dominated by an absorption band located below 420 nm which is red shifted compared to pure CeO_2 (3.01 eV) and pure TiO_2 (3.0 eV). The spectrum proportioned a band gap value of 418 nm (2.96 eV), associated with the characteristic charge transfer between the O^{2-} valence and the Ce^{4+} conduction bands which is overlapped with the charge transfer between the O^{2-} valence and the Ti^{4+} conduction bands. The absorption band is red shifted in Pr^{4+} substituted samples in comparison to pure CeO_2–TiO_2 materials.

Fig. 3.4. Photograph of $TiCe_{1-x}Pr_xO_4$ (x= 0, 0.05, 0.1, 0.3 0.5 and 0.7) pigments.

In the UV-vis spectra of the $TiCe_{1-x}Pr_xO_4$ samples, the absorption is shifted towards the visible region. The band gap is now around 677 nm (1.83 eV) for TCP_{70}. The red shift is a consequence of the introduction of additional energy levels ($4f^1$ electrons) from the Pr ion which is more efficiently incorporated into the CeO_2 network. The reflectance spectra show a greater absorption in the visible region with increasing number of chromophore ions because the gap between the valence and conduction bands narrows.

This causes the color of the pigment to vary from white to brick red (Fig. 3.4). The position of the absorption edge critically depends on the Pr content and is red shifted (Fig. 3.5). This evaluation is consistent with the observed charge transfer spectra of tetravalent lanthanide ions in oxides (Hoefdraad 1975). By substituting $TiCeO_4$ with Pr^{4+} ions, the $4f^1$ electron of the praseodymium valence shell introduces an additional electronic level between the O^{2-} valence and the Ce^{4+} conduction band, and reduces the band gap from 2.96 to 1.83 eV (Table 3.1).

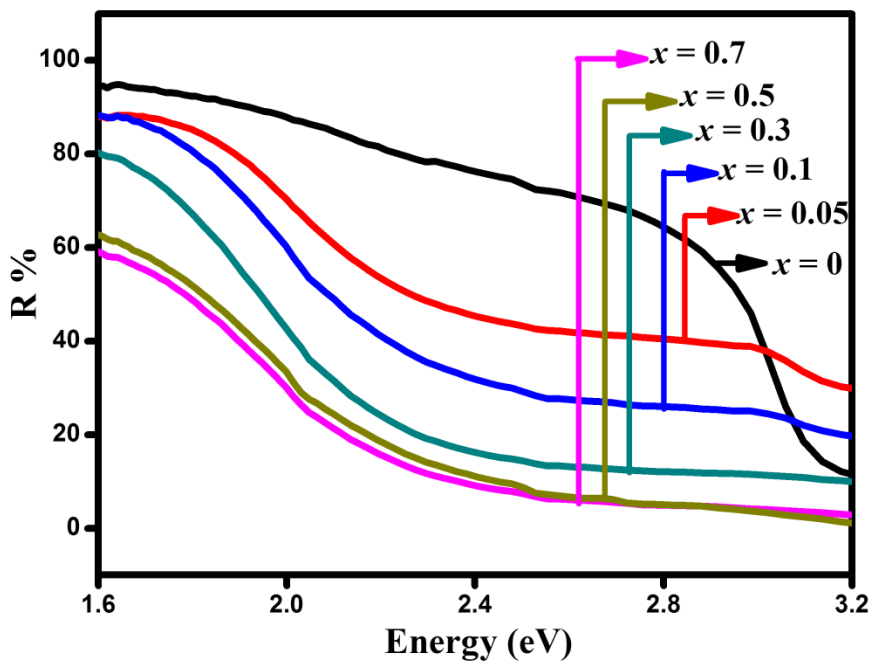

Fig. 3.5. Diffuse reflectance spectra of $TiCe_{1-x}Pr_xO_4$ (x= 0, 0.05, 0.1, 0.3 0.5 and 0.7) pigments.

Table 3.1 summarizes the color co-ordinates and band gap of $TiCe_{1-x}Pr_xO_4$ (x =0 to 0.7). The substitution of 5 mol % of Pr^{4+} for Ce^{4+} in $TiCeO_4$ drastically increases the red component (a*) from 0.02 to 17.92, and increases the yellow component (b*) from 9.46 to 21.47 as compared to the praseodymium free sample. In addition to the above, the chroma (C*) of the pigment has been significantly enhanced from 9.46 to 27.96. It is

clear from the $L^*a^*b^*$ values of the $TiCe_{1-x}Pr_xO_4$ pigments (Table 3.1) that the present values are significantly higher than recently reported praseodymium doped ceria powders (5% Pr-doped CeO_2: $L^* = 66$; $a^* = 12$; $b^* = 9.5$), synthesized by microwave-assisted hydrothermal route (Bondioli *et al.* 2005). It implies from the present study that ceria based red pigments can be prepared at lower calcination temperature by the addition of titanium as compared to the previously reported CeO_2-Pr_6O_{11} solid solutions (Nahum *et al.* 2003; Sulcova and Trojan 2001). The increase of praseodymium content in $TiCeO_4$ decreases the lightness of the pigment from 90.51 to 57.82. The L^* values of Pr^{4+}-$TiCeO_4$ is found to be higher than those obtained for CeO_2-PrO_2 red pigments. The presence of Ti has considerably increased the lightness of the pigments leading to good bright brick red hue. Similarly, a^* and b^* values considerably increase which is responsible for the change of color from white to brick red of the pigment.

Table 3.1 Color co-ordinates and band gap of $TiCe_{1-x}Pr_xO_4$ (x= 0, 0.05, 0.1, 0.3 0.5 and 0.7).

Sample	Color Co-ordinates					E_g
	*L**	*a**	*b**	*C**	*h°*	*(eV)*
TC	90.51	0.023	9.46	9.46	89.86	2.96
TCP_5	64.50	14.11	20.60	24.96	55.59	1.91
TCP_{10}	54.53	17.92	21.47	27.96	50.14	1.89
TCP_{30}	61.73	16.18	25.14	29.89	57.23	1.87
TCP_{50}	53.36	16.57	25.83	30.68	57.31	1.84
TCP_{70}	57.82	13.48	25.52	28.86	62.15	1.83

3.3.4 Thermal and chemical stability studies of the pigments

The thermal stability (TG/DTA analysis) of the typical synthesized pigment sample $TiCe_{0.5}Pr_{0.5}O_4$ was examined in the temperature range of 50–1000 °C and the results are depicted in Fig. 3.6. The results clearly indicate that there is no loss of weight and phase transformation in the temperature range 50-1000 °C.

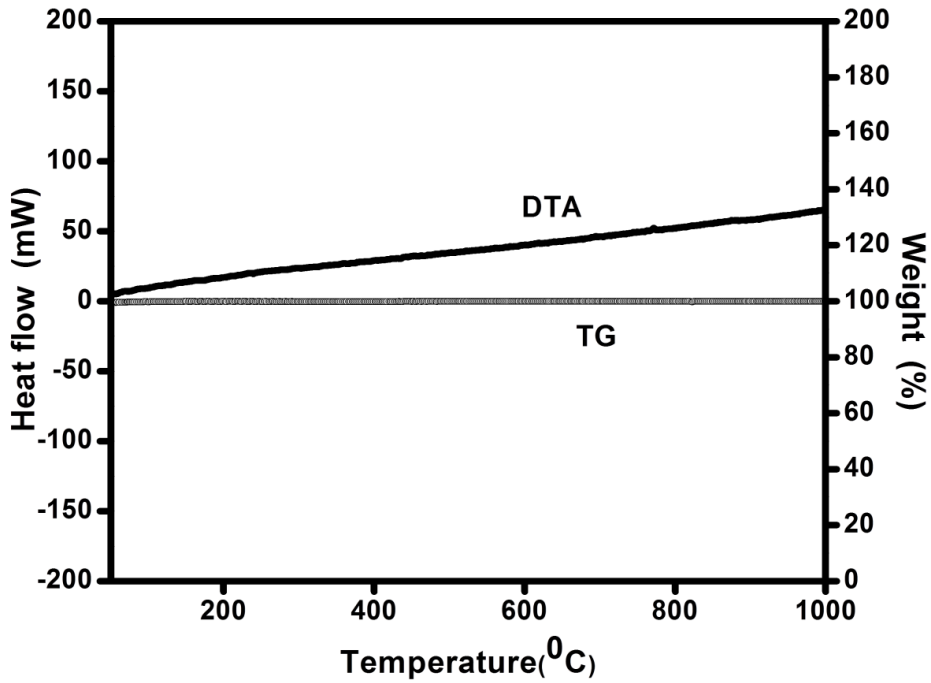

Fig. 3.6. The TG/DTA of $TiCe_{0.5}Pr_{0.5}O_4$ pigment.

Among the series of colorants prepared, typically $TiCe_{0.5}Pr_{0.5}O_4$ was tested for its acid resistance and alkali resistance. A small quantity of weighed pigment sample is mixed with 10% $HCl/H_2SO_4/HNO_3$ and 10 % NaOH, and soaked for half an hour with constant stirring using a magnetic stirrer. Then, the pigment was filtered, washed with water, dried and weighed. Negligible weight loss was noticed for all the acids and alkali tested. The color co-ordinates of the typical pigments were measured after acid/alkali treatment and the total color difference, ΔE^*_{ab} of all the pigments are found to be

negligible (Table 3.2). This indicates that the pigment samples are chemically and thermally stable.

Table 3.2. The color coordinates (±0.1) of $TiCe_{0.5}Pr_{0.5}O_4$ powder pigment after chemical resistance tests.

10 % Acid/Alkali	$TiCe_{0.5}Pr_{0.5}O_4$			
	L*	***a****	***b****	ΔE^*_{ab}
HCl	57.9	13.6	25.8	0.3
HNO_3	56.9	14.3	25.2	1.3
H_2SO_4	58.1	14.5	26.1	0.5
NaOH	56.0	14.0	24.0	1.2

$\Delta E^*_{ab} = [(\Delta L^*)^2+(\Delta a^*)^2+(\Delta b^*)^2]^{½}$

3.3.5 Coloration of plastics

The coloring performance of the typically synthesized pigment, $TiCe_{0.9}Pr_{0.1}O_4$ (TCP_{10}) was tested for its coloring application in a substrate material like PMMA. Typically 5 or 10 wt% pigment sample was dispersed in PMMA and compressed to a cylindrical disc (Fig. 3.7). The color coordinates of the test pieces were measured and depicted in Table 3.3. These test pieces exhibit very fine and uniform brick red hue. Thus the developed pigments may find potential applications in coloring of various plastic materials.

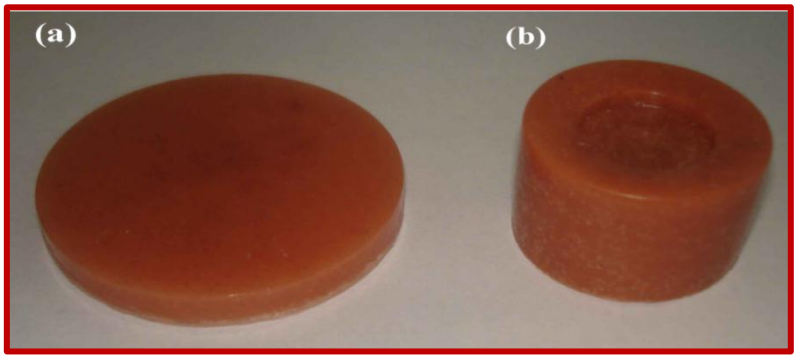

Fig. 3.7. Photographs of (a) TCP_{10} (5%) + PMMA and (b) TCP_{10} (10%) + PMMA.

Table 3.3. The color coordinates (±0.1) of the $TiCe_{0.9}Pr_{0.1}O_4$ pigment powder after applying in polymer.

Sample	Color Co-ordinates		
	*L**	*a**	*b**
TCP_{10}	54.53	17.92	21.47
TCP_{10} (5%) + PMMA	46.17	20.01	22.60
TCP_{10}(10%) + PMMA	52.05	18.48	20.12

3.4 Conclusions

Novel inorganic pigments, $TiCe_{1-x}Pr_xO_4$ (x= 0, 0.05, 0.1, 0.3 0.5 and 0.7) have been successfully synthesized having colors ranging from white to brick red. By incorporation of chromophore metal ion, Pr^{4+} for Ce^{4+}, in the host compound $TiCeO_4$, the absorption edge (418 nm) has been greatly shifted to the higher wavelengths (677 nm).

Further, the position of the absorption edge critically depends on the concentration of Pr^{4+}. The coloring mechanism of Pr^{4+} doped $TiCeO_4$ pigments is based on the introduction of an additional electronic level of energy in cerianite forbidden band, arising from unpaired $4f^1$ electrons of praseodymium ions. Presence of Ti in the Pr^{4+}-CeO_2 enhanced the lightness of the pigments. The developed pigments are found to be thermally and chemically stable and also do not contain toxic metals. The designed pigments are also found to be useful for coloration of plastic materials. Thus, the present pigments may find potential alternative to the classical toxic inorganic red pigments for coloring plastics and paints.

CHAPTER 4

RE-Substituted Bi_2MoO_6 (RE = Y, Pr, Nd, Sm, Tb and Yb) Yellow and Greenish Yellow Pigments for Coloration of Plastics

A new class of yellow and greenish yellow inorganic pigments having the general formula $BiREMoO_6$ (RE = Y, Pr, Nd, Sm, Tb and Yb) have been synthesized by solid state route and characterized by various spectroscopic techniques. The substitution of different rare earths for Bi^{3+} in Bi_2MoO_6 gently red shifted the absorption edge to low energy side and consequently the designed compounds exhibit different shades of yellow color for Sm, Y, Tb and Yb compounds; greenish yellow color for Pr and light green color for Nd compounds. The coloring mechanism is based on the charge transfer transitions from O_{2p} valence band to conduction band made of primary Mo_{4d} and secondary Bi_{6p}. The substitution of RE^{3+} introduces partially occupied 4*f* electronic level in between the band gap and the position of 4*f* level depend on the number of *f* electrons. Energy level of RE 4*f* bands continuously lowers with increasing the number of 4*f* electrons and thereby increasing the band gap. The developed pigments demonstrated good coloration to plastics and are chemically stable.

Sandhya Kumari et al. ***J. Am. Ceram. Soc.***, 94 [2] (2011) 320-323.

4.1 Introduction

The inorganic pigments in yellow, orange, red and maroon colors are always insufficiently represented for coloring of plastics, paints and ceramics. Compounds that contain metal ions with variable oxidation states sometimes exhibit unusual charge transfer and conductivity properties that may be of theoretical interest and technological importance. In particular, interesting properties arise in mixed-metal oxides containing both rare-earth and transition metal ion in which the chemical potential of the RE ion is energetically close to the Fermi level of the bands formed from the transition metal d states. In situ charge transfer can occur and, depending on its time scale, can result in intermediate valent or heavy fermion behavior (Bornick and Stacy 1994). Although $PbCrO_4$, $PbMoO_4$, $Pb_2Sb_2O_7$ and CdS have been widely employed as conventional yellow inorganic pigments, the use of these pigments has been restricted because they contain toxic elements (Badenes *et al.* 2002). Driven by national laws and regulations in the ecological and toxicological area, "sustainable development" and substitution pressures have resulted in the replacement of formerly well-known and highly recommended inorganic pigments, by more "environmentally friendly" or less toxic substances. Rare earth based yellow inorganic pigments form an important class of environmentally benign inorganic pigments (Gauthier *et al.* 2003; George *et al.* 2008; Jansen and Letschert 2000).

Oxo salts of bismuth (III) exhibit interesting properties as ionic conductors, yellow pigments and selective oxidation catalyst (Abraham *et al.* 1988; Sleight 1980; Takahashi and Iwahara 1978). Pigments on the base of Bi_2O_3 seem to be interesting, because they provide interesting color hues from yellow to orange (Prabhakar Rao and Reddy 2004). Intense colors of these pigments are based on the incorporation of doped Ln ions into the host lattice of Bi_2O_3 (Mizoguchi *et al.* 1999; Prabhakar Rao and Reddy 2004; Sulcova and Prokleskova 2008; Sulcova *et al.* 2010a; Sulcova and Trojan 2006) and the Bi_2O_3 itself is a light yellow powder. Bi_2O_3 easily forms solid solutions with

many other metal oxides. These doped systems exhibit a complex array of structures and properties dependent on the type of dopant, the dopant concentration and the thermal history of the sample. The most widely studied systems are those involving rare earth metal oxides, Ln_2O_3, including yttria, Y_2O_3 (Bosacka *et al.* 2005). Recent investigations reveal that the toxic yellow pigments can be replaced by solid solutions of $(Bi_2O_3)_{1-x}(R_2O_3)_x$, R: Nd, Sm and Dy (Gonzalvo *et al.* 2001), $Bi_{2-x}Y_{x/2}Zr_{3x/8}O_3$ (Sulcova and Trojan 2008c), CeO_2-SiO_2-Bi_2O_3 (Imanaka *et al.* 2008) and CeO_2-ZrO_2-Bi_2O_3 (Masui *et al.* 2006). Rare earth metal cations are generally very stable, have similar chemical properties to one another and are similar in size to Bi^{3+}, which has a radius of 1.03 Å (Shannon 1976), making them all excellent dopants. Bismuth oxide is an important metal oxide semiconductor with a direct band gap of 2.8 eV (Krishna Reddy *et al.* 2009; Reddy *et al.* 2008; Zhang *et al.* 2006). $BiVO_4$ pigments are relatively new pigment class that has gained importance over the last few decades. The pigments exhibit brilliant greenish yellow to reddish yellow shades with compositions ranging from $BiVO_4$ to the mixed pigment $4BiVO_4$ x $3Bi_2MoO_6$ (Erkens 1999). $BiVO_4$ based pigments are nontoxic inorganic pigments used in coating industry to manufacture brilliant yellow, orange, red and green shades with good gloss and hiding power.

Bismuth molybdates have been studied extensively as a model catalyst system both for selective oxidation and ammoxidation of propene to acrolein and acrylonitrile, and the oxidative dehydrogenation (ODH) of butene to butadiene (Li *et al.* 2009). Recently, bismuth molybdates have also been demonstrated to exhibit visible-light driven photocatalytic activity (Shimodaira *et al.* 2006b; Yu and Kudo 2005). Bismuth mixed oxides with the Aurivillius structure are represented by $(Bi_2O_2)^{2+}$ $(A_{n-1}B_nO_{3n+1})^{2-}$ (A = Ba, Bi, Pb; B= Ti, Nb, W, Mo). The γ-Bi_2MoO_6 with the Aurivillius structure has been found to possess unique layered structure in which perovskite slabs of corner-sharing, distorted MoO_6 octahedra are sandwiched between $(Bi_2O_2)^{2+}$ layers (Shimodaira *et al.* 2006b). Compared with Bi_2WO_6, Bi_2MoO_6 with a narrower band gap (2.77 eV for Bi_2WO_6 and

2.63 eV for Bi_2MoO_6) has the ability to harness more sunlight (Zhou *et al.* 2010). A low band gap material like Bi_2MoO_6 offers wide scope of tuning the band gap by substituting different metal ions to produce various shades. In the rare earth compounds, the strongly localized *f* shell that is considered usually as a core-like shell determines the similar chemical and physical properties of the lanthanides. The variation of their properties across the lanthanides often has a monotonic character (Tung *et al.* 1999). In the present study, the new pigments in $BiREMoO_6$ (RE = Y, Pr, Sm, Nd, Yb and Tb) system have been prepared. Their color properties, as possible potential ecological inorganic pigments have been investigated for coloration of plastics.

4.2 Experimental Section

4.2.1 Materials and Methodology

Compositions based on $BiREMoO_6$ (RE = Y, Pr, Sm, Nd, Tb and Yb) were prepared from the corresponding oxides: Bi_2O_3, Y_2O_3, Pr_6O_{11}, Sm_2O_3, Nd_2O_3, Tb_4O_7, Yb_2O_3, and MoO_3 (99.9%) supplied by M/s Sigma Aldrich. Among the synthesized compounds Y and Pr substituted Bi_2MoO_6 were systematically studied by varying the concentration of rare earth as 0, 0.2, 0.4, 0.6, 0.8 and 1.0. Y substituted samples are named as $BY_{0.2}M$, $BY_{0.4}M$, $BY_{0.6}M$, $BY_{0.8}M$ and BYM, and Pr substituted compounds as $BP_{0.2}M$, $BP_{0.4}M$, $BP_{0.6}M$, $BP_{0.8}M$ and BPM with reference to mole percentage of doping. Unsubstituted Bi_2MoO_6 is named as BM. (This nomenclature is followed hereinafter for ease of understanding). Stoichiometric proportions of the chemicals were weighed and were thoroughly wet mixed in an agate mortar with acetone as the wetting medium for 1 h and dried in an air oven. This process of mixing and drying was repeated thrice to obtain a homogeneous mixture. $Bi_{2-x}Y_xMoO_6$ (x= 0, 0.2, 0.4, 0.6, 0.8 and 1.0) were then calcined at 1100 °C for 6 h, $Bi_{2-x}Pr_xMoO_6$ (x= 0, 0.2, 0.4, 0.6, 0.8 and 1.0) were calcined at 950 °C for 9 h and $BiREMoO_6$ (RE = Nd, Tb and Yb) were calcined at 1000 °C in air. The calcination process was repeated thrice for the same sample. To refine and

homogenize the particle size after calcinations, the resulting products were ground in an agate mortar.

4.2.2 Characterization Techniques

The crystalline nature and phase purity of the samples were investigated using powder X-ray diffractometer with Ni-filtered Cu-Kα ($K\alpha_1$ = 1.54060 Å , $K\alpha_2$ = 1.54443 Å) , radiation using a PANalytical Philips X'pert Pro diffractometer. Data were collected over a 2θ range from 10° to 90°. The morphology of the synthesized samples was recorded on a scanning electron microscope JEOL JSM–5600 model, with an acceleration voltage of 15 kV.

The diffuse reflectance of the powdered pigment samples were measured (200 – 780 nm) with a UV–vis Spectrophotometer (Shimadzu UV–2450 with an integrating sphere attachment, ISR–2200) using barium sulphate as the reference. The color coordinates were determined by coupling analytical software (UVPC Color Analysis Personal Spectroscopy Software V3, Shimadzu) to the UV–2450 spectrophotometer. The CIE 1976 *L*a*b** colorimetric method was used, as recommended by the Commission Internationale de l'Eclairage (CIE).

Among the pigment compositions prepared, the typical pigment sample $BiYMoO_6$ and $BiTbMoO_6$ were dispersed in polymer matrix like PMMA to test their coloring performance. The pigments, $BiYMoO_6$ and $BiTbMoO_6$ (10 wt%) were ultrasonicated in an alcohol-water (1:4) mixture for 10 min to ensure complete dispersion of the pigment particles. A viscous solution of PMMA (90 wt%) was made using a conventional electrical coil heater. The pigment dispersion was slowly added with stirring and converted to a thick paste. The paste after 2 h curing was compressed uniaxially into a form of cylindrical disk using a hydraulic press at a pressure of 25 MPa. Both sides of the pigmented polymer were lapped using a fine grade emery sheet for obtaining a polished

surface. The color coordinates of the pigmented compacts were examined to assess the coloration.

4.3 Results and Discussion

4.3.1 Powder X–ray diffraction studies

The powder XRD patterns of $BiREMoO_6$ (RE = Y, Pr, Nd, Sm, Tb and Yb) are presented in Fig. 4.1. All of the diffraction peaks could be attributed to a monoclinic $BiREMoO_6$ type structure with different space groups depending on the rare earth element. Crystallographic analysis reveals that the $BiYMoO_6$, $BiTbMoO_6$ and $BiYbMoO_6$ compounds belong to the monoclinic system with space group P2/c. Both $BiPrMoO_6$ and $BiNdMoO_6$ crystallize with monoclinic crystal lattice (space group C2/c). The formation of monoclinic $BiSmMoO_6$ (space group C2) can be judged from the diffraction patterns.

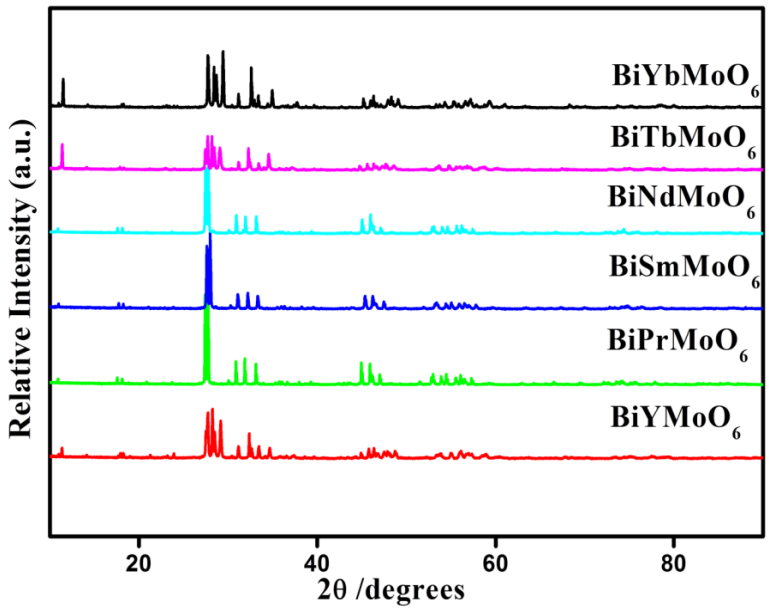

Fig. 4.1. Powder X-ray diffraction patterns of $BiREMoO_6$ (RE = Y, Pr, Nd, Sm, Tb and Yb) pigments.

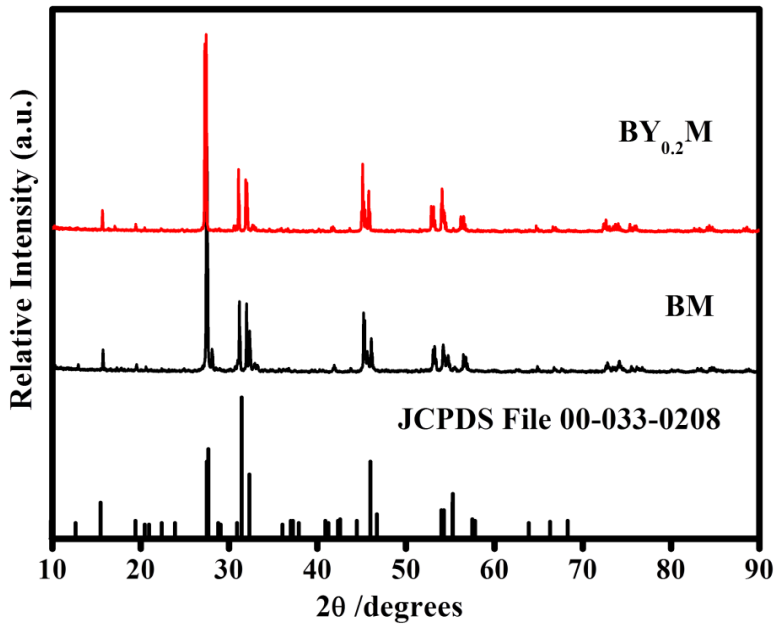

Fig. 4.2. Powder X-ray diffraction patterns of $Bi_{2-x}Y_xMoO_6$ (x = 0 and 0.2) pigments.

The powder XRD patterns of $Bi_{2-x}Y_xMoO_6$ (x = 0 and 0.2) are shown in Fig. 4.2. The intense and sharp peaks found in the diffraction patterns reveal the crystalline nature of the powders. The two compounds BM and $BY_{0.2}M$ crystallize with a monoclinic phase with the space group P21/c and all the reflections are indexed as per the JCPDS database number 00-033-0208. The powder XRD patterns of $Bi_{2-x}Y_xMoO_6$ (x = 0.4, 0.6, 0.8 and 1.0) are shown in Fig. 4.3. The compositions with x>0.2 form the monoclinic phase which can be indexed as per the JCPDS card number 00-042-0360 with the space group P2/c. The crystallite size was calculated from Debye Scherrer formula $D = 0.9\lambda/\beta\cos\theta$, where D is the crystallite size, λ is the wavelength of X – ray used, β is the full width at half maximum of X – ray diffraction lines and θ is half of 2θ. Crystallite size of the compounds: BM and $BY_{0.2}M$ is found to be in the range 108-141nm. For Y substitution with x = 0.4, 0.6, 0.8 and 1.0 it is in the range 75-112 nm.

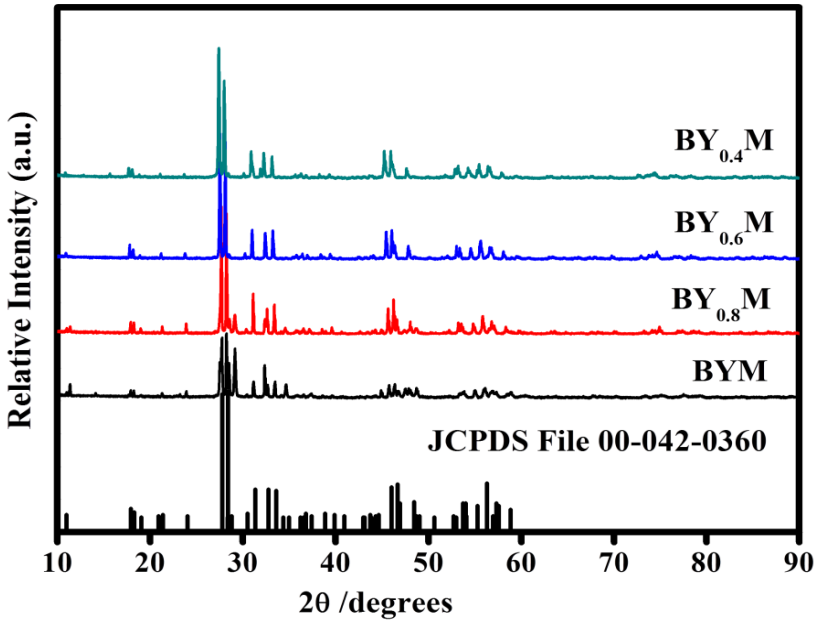

Fig. 4.3. Powder X-ray diffraction patterns of $Bi_{2-x}Y_xMoO_6$ (x = 0.4, 0.6, 0.8 and 1.0) pigments.

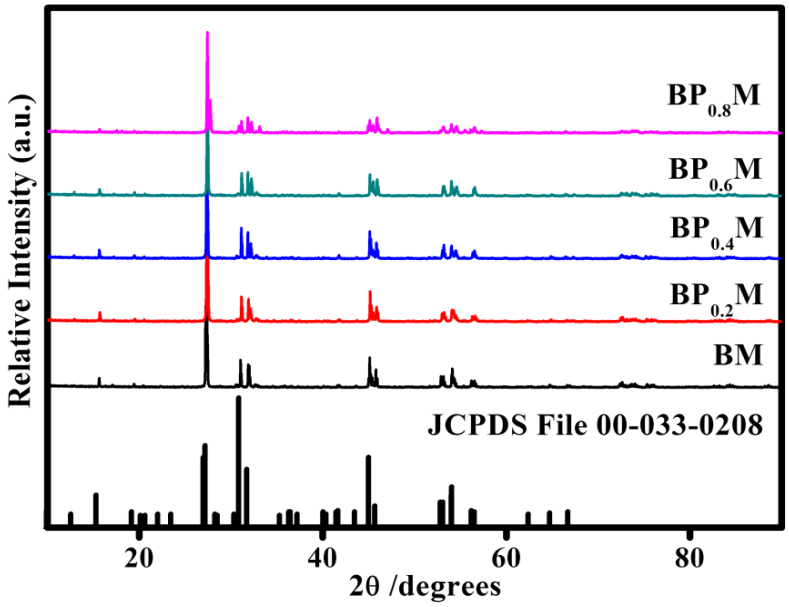

Fig. 4.4. Powder X-ray diffraction patterns of $Bi_{2-x}Pr_xMoO_6$ (x = 0.2, 0.4, 0.6 and 0.8) pigments.

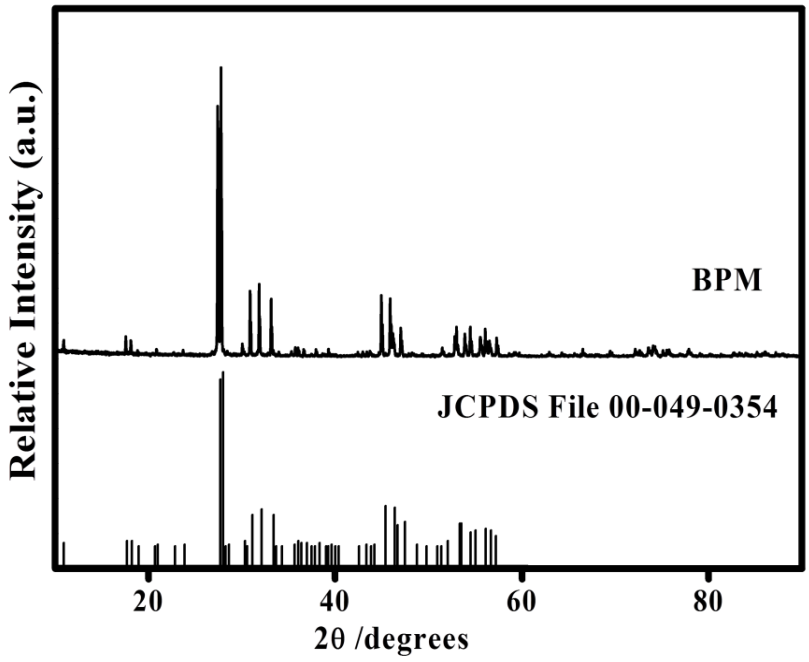

Fig. 4.5. Powder X-ray diffraction pattern of $BiPrMoO_6$ pigment.

The powder XRD patterns of $Bi_{2-x}Pr_xMoO_6$ (x = 0, 0.2, 0.4, 0.6 and 0.8) are shown in Fig. 4.4. The intense and sharp peaks found in the diffraction patterns reveal the crystalline nature of the powders. The compositions with x<1.0 crystallize with a monoclinic phase with the space group P21/c and all the reflections are indexed as per the JCPDS database number 00-033-0208. Fig. 4.5 summarizes the XRD pattern of $BiPrMoO_6$ which form the monoclinic phase and can be indexed as per the JCPDS card number 00-049-0354 with the space group C2/c. The crystallite size calculated from Debye Scherrer equation was found to be 97 nm for $BiPrMoO_6$.

4.3.2 Morphological analysis

SEM analysis (Fig 4.6) of $BiREMoO_6$ (RE = Y, Pr, Nd, Sm, Tb and Yb) reveals that substitution of different rare earth metal ions in Bi_2MoO_6 changes the morphology of the particles from long rod type particles to small irregular shaped particles. Rare earth substitution in Bi_2MoO_6 is found to decreases the particle size.

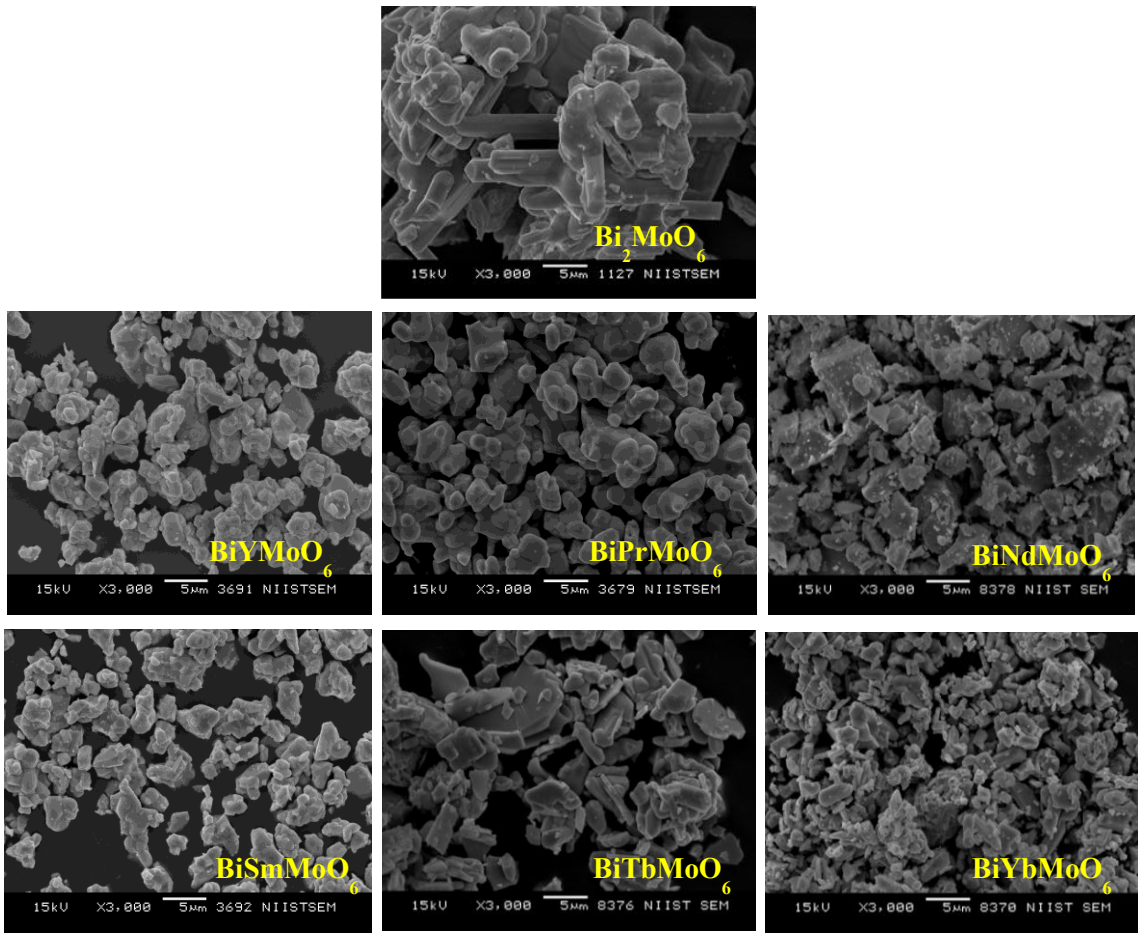

Fig. 4.6. SEM photographs of Bi_2MoO_6 and $BiREMoO_6$ (RE = Y, Pr, Nd, Sm, Tb and Yb).

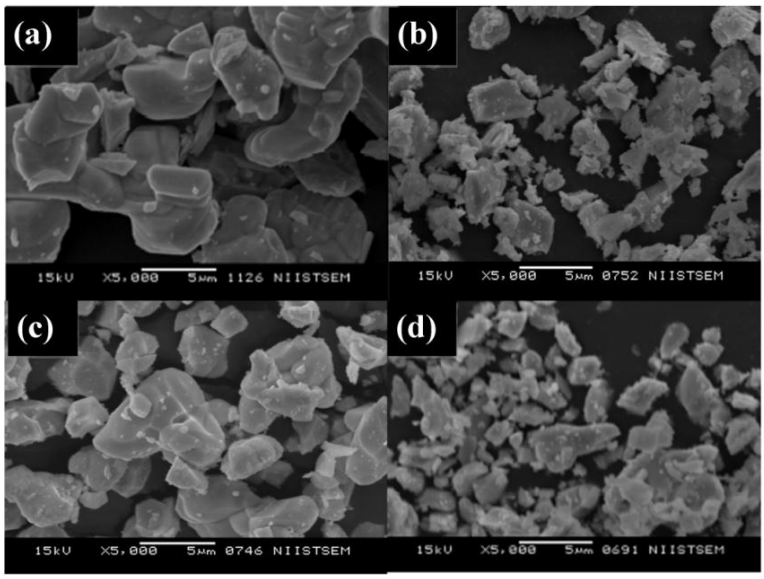

Fig. 4.7. SEM photographs of $Bi_{2-x}Y_xMoO_6$: (a) x=0.2, (b) x=0.4, (c) x=0.6 and (d) x= 1.

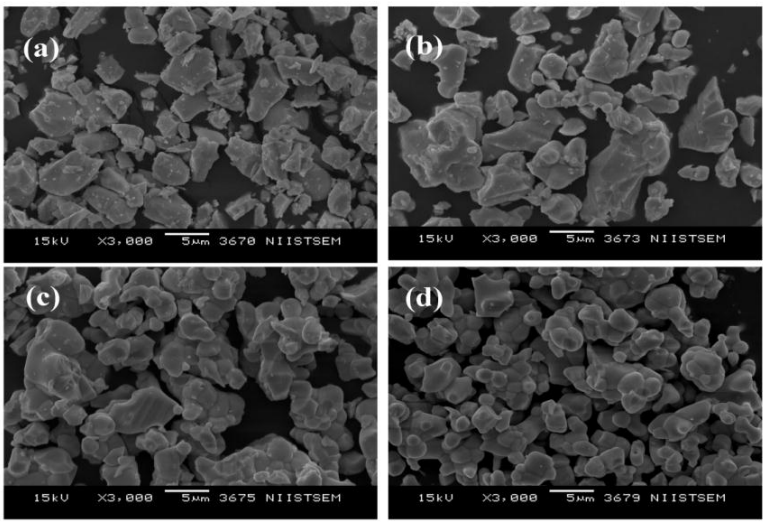

Fig. 4.8. SEM photographs of $Bi_{2-x}Pr_xMoO_6$: (a) x=0.4, (b) x=0.6, (c) x=0.8 and (d) x= 1.

Typical SEM photographs recorded for $Bi_{2-x}Y_xMoO_6$ (x = 0.2, 0.4, 0.6 and 1.0) and $Bi_{2-x}Pr_xMoO_6$ (x=0.4, 0.6, 0.8 and 1.0) pigment powders are shown in Fig. 4.7 and 4.8 respectively. All the samples show particles in 3-8 μm size range. Some aggregation of particles is seen in the SEM micrographs which are essentially clusters of particles. As

the concentration of rare earths increases, the grains are more homogenous and show uniform size.

4.3.3 Diffuse reflectance and chromatic properties of rare earth (RE^{3+}) substituted Bi_2MoO_6

The colors of Bi_2MoO_6 and $BiREMoO_6$ are presented in Fig. 4.9. Y, Tb and Yb substitution leads to yellow color whereas Pr substitution produces greenish yellow color. Light green and light yellow colors were obtained for Nd and Sm substituted Bi_2MoO_6 respectively. Fig 4.10 shows the combined absorption spectra of $BiREMoO_6$ (RE = Y, Pr, Nd, Sm, Tb and Yb). For oxides containing RE^{3+}, there is strong optical absorption in the near-UV region based on O_{2p} – Mo_{4d} charge transfer transition. The absorption edge typically extends far enough into the visible to give a yellow color with different rare earths. The optical absorption edge critically depends on the rare earth element (RE^{3+}) present in the pigment samples. Bi_2MoO_6 absorbs below 400 nm with a sharp edge at ~ 400 nm. Rare earth substitution significantly shifts the absorption edge to low energy side. $BiSmMoO_6$ and $BiNdMoO_6$ show a sharp absorption edge at around 450 nm, with characteristic absorption bands at about 523, 587, 682 and 750 for $BiNdMoO_6$. The spectra of $BiPrMoO_6$ show several well-resolved bands attributed to the *f-f* transitions of the Pr^{3+} ions. $BiPrMoO_6$ displays greenish yellow hue as it absorbs in blue and red region of the visible spectrum. More red shift was observed for $BiYbMoO_6$ and $BiTbMoO_6$ with steep absorption edge at ~500 nm. Y, Tb and Yb - substituted bismuth molybdates absorb blue light efficiently and the compounds exhibit yellow hue. The band gap energy is decreased with the substitution of RE^{3+} in Bi_2MoO_6 from 2.99 to 2.19 eV (Table 4.1).

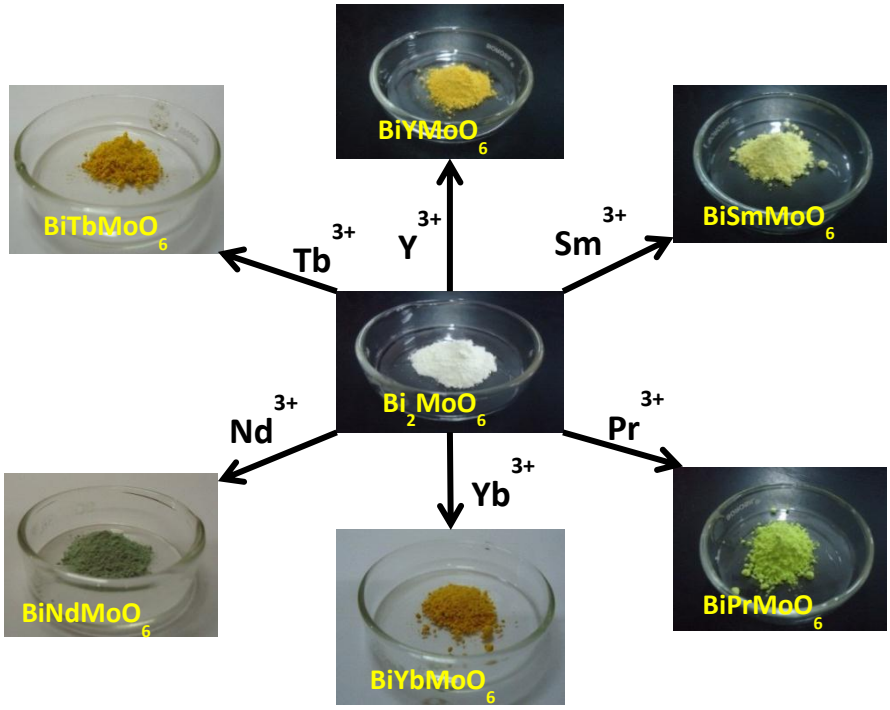

Fig. 4.9. Photographs of Bi_2MoO_6 and $BiREMoO_6$ (RE = Y, Pr, Nd, Sm, Tb and Yb) pigments.

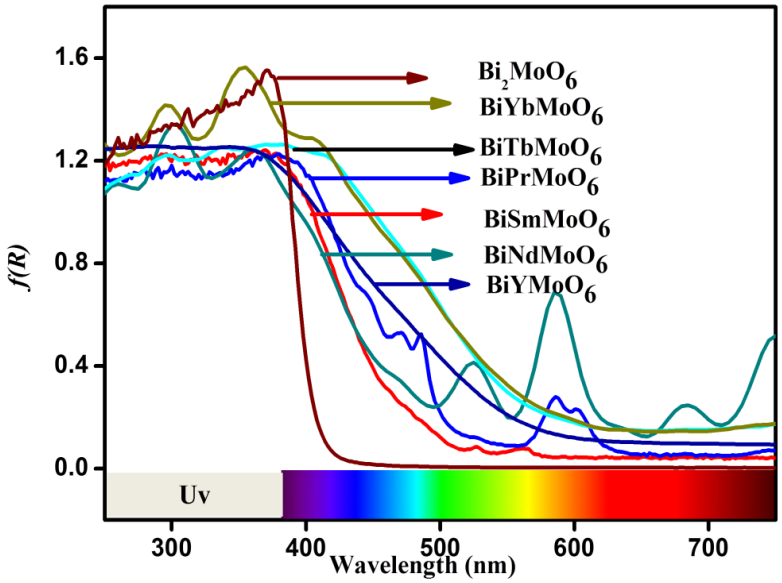

Fig. 4.10. Absorbance spectra of Bi_2MoO_6 and $BiREMoO_6$ (RE = Y, Pr, Nd, Sm, Tb and Yb) pigments.

Table 4.1. Color co-ordinates and band gap of Bi_2MoO_6 and $BiREMoO_6$ (RE = Y, Pr, Nd, Sm, Tb and Yb).

Sample	Color Co-ordinates					E_g
	*L**	*a**	*b**	*C**	*h°*	
Bi_2MoO_6	93.4	-4.3	11.5	12.2	69.4	2.99
$BiYMoO_6$	81.8	2.7	51.1	51.1	86.9	2.33
$BiPrMoO_6$	84.3	-12.6	49.1	50.7	104.4	2.47
$BiNdMoO_6$	74.2	4.7	8.25	9.49	60.3	2.51
$BiSmMoO_6$	91.2	-7.4	39.5	40.2	100.6	2.54
$BiTbMoO_6$	79.1	16.0	61.6	63.3	75.4	2.19
$BiYbMoO_6$	78.3	17.7	58.8	61.4	73.4	2.20

The CIE 1976 color co-ordinates of the powdered pigments are summarized in Table 4.1. The brightness *L** is slightly lowered with the introduction of rare earth but *a** value is found to escalate. The *b** value corresponding to yellow chromaticity depends on the RE^{3+} element. From Tables 4.1, it follows that the *b** coordinate has the wide interval of values ranging from 11.5 to 61.6. This is also reflected in its chroma value (C*) which gets enhanced from 12.2 to 63.6. The richest yellow hue was obtained for $BiTbMoO_6$ and $BiYbMoO_6$ pigment. The color shade is shifting from off white for Bi_2MoO_6 to light yellow color for $BiSmMoO_6$, greenish yellow for $BiPrMoO_6$ and bright yellow color for Y, Tb and Yb containing bismuth molybdate. The hue angle values of the pigments lie in the yellow region of the cylindrical color space (h° = 70–105 for yellow) (Sulcova and Trojan 2007). The color coordinates of the yellow pigments $BiYMoO_6$, BiTbMoO6 and

$BiYbMoO_6$ sample are found to be higher than that of the powder $BiVO_4$ (L^* = 68.0, a^* = 16.5, b^* = 42.35) reported elsewhere in the literature (Neves *et al.* 2003).

4.3.4 Diffuse reflectance and chromatic properties of Yttrium (Y^{3+}) substituted Bi_2MoO_6

Fig. 4.11 depicts the photographs of off-white Bi_2MoO_6 and yellow $BiYMoO_6$. The Kubelka-Munk absorption spectra of the pigment samples are shown in Fig. 4.12. The most important and widely used quantity derived from the Kubelka–Munk theory is the reflectance of an opaque (infinitely thick) film that is described by a very simple equation: $K/S = (1 - R)^2/2R$ where K is the absorption coefficient, S is the scattering coefficient and R is reflectance. From this expression (Kubelka–Munk function) it follows that, within the range of validity of the theory, R depends only on the ratio of the absorption coefficient (K) to the scattering coefficient (S), and not on their individual values. All spectra exhibited similar features, irrespective of the Y content. $Bi_{2-x}Y_xMoO_6$ solid solutions possessed steep edges, indicating that the visible light response of $Bi_{2-x}Y_xMoO_6$ solid solutions is caused by a direct energy band gap from the valence band to the conduction band. Bi_2MoO_6 shows some absorption in the visible region up to 415 nm. For $BiYMoO_6$, the absorption edge became steeper, suggesting that as prepared samples have a direct band gap and absorb visible light due to the band to band transition. The absorption spectra demonstrated that the Y^{3+} shifted the absorption edge to the long wavelength side by substituting Bi^{3+} ions in Bi_2MoO_6 and the hue turned to yellow. Y substitution in the Bi_2MoO_6 matrix decreases the band gap from 2.99 to 2.33 eV when x increased from 0 to 1 (Table 4.2). The absorption edge varies with Bi:Y ratio accompanying with the changes of the width or the position of the valence bands and conduction bands, which is one of the reasons for the narrowing of the optical gap. As a result, the yellow hue of the pigments depends on the composition.

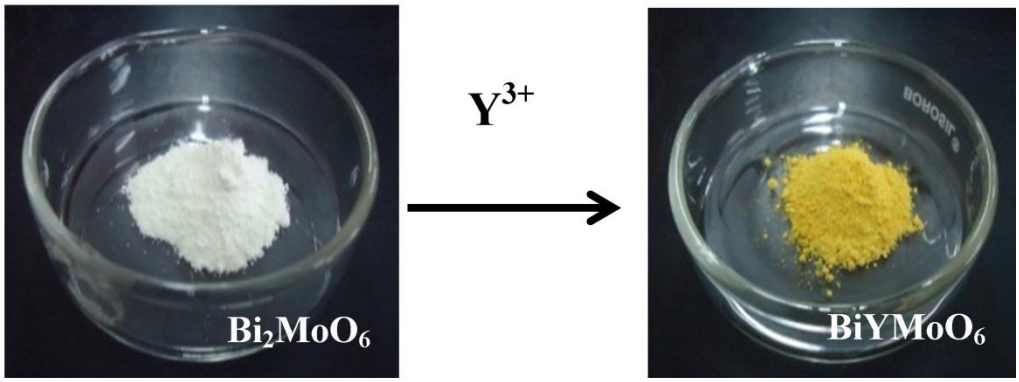

Fig. 4.11. Photographs of Bi_2MoO_6 and $BiYMoO_6$ pigments.

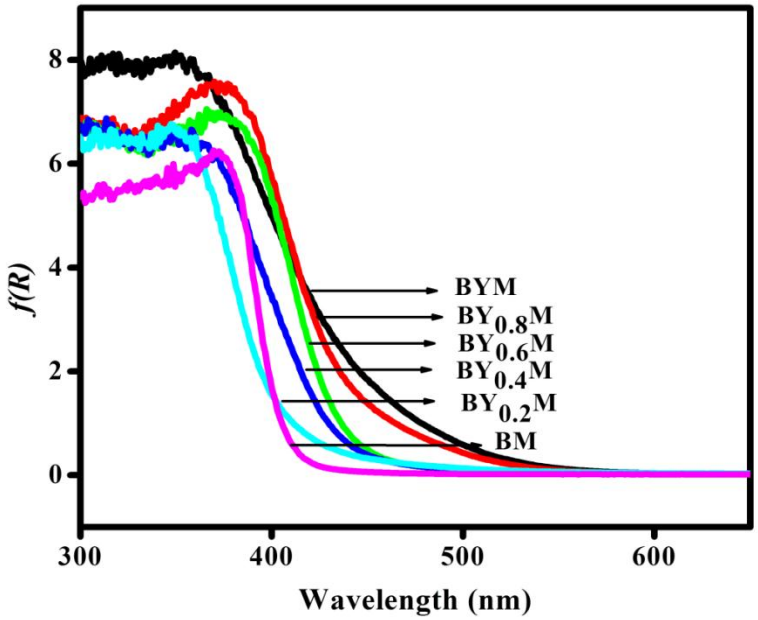

Fig. 4.12. Absorbance spectra of the $Bi_{2-x}Y_xMoO_6$ (x= 0, 0.2, 0.4, 0.6, 0.8 and 1.0) pigments.

The optical absorption edge of these pigments depends on the composition, but all $Bi_{2-x}Y_xMoO_6$ pigments can absorb blue light efficiently. Visible light absorption of Bi_2MoO_6 was revealed to be due to the transition from the valence band consisting of the

O 2p orbitals to the conduction band derived from the primary Mo 4d orbitals in MoO_6 octahedra and the secondary Bi 6p orbitals (Shimodaira *et al.* 2006a). The width of the band gap is determined by the extent of overlap of the valence orbitals and by the difference between the electronegativities of the cations and anions involved (Jansen and Letschert 2000).

Table 4.2. Color co-ordinates and band gap of $Bi_{2-x}Y_xMoO_6$ (x= 0, 0.2, 0.4, 0.6, 0.8 and 1.0).

Sample	Color Co-ordinates					E_g (eV)
	*L**	*a**	*b**	*C**	*h°*	
BM	93.4	-4.3	11.5	12.2	69.4	2.99
$BY_{0.2}M$	86.7	-3.0	22.4	22.6	82.3	2.93
$BY_{0.4}M$	88.1	-5.3	28.4	28.8	79.4	2.77
$BY_{0.6}M$	89.0	-7.5	33.3	34.1	77.3	2.56
$BY_{0.8}M$	83.9	-0.3	48.2	48.2	89.6	2.42
BYM	81.8	2.7	51.1	51.1	86.9	2.33

$Bi_{2-x}Y_xMoO_6$ pigments exhibit yellow shades as indicated by the $L^*a^*b^*$ parameters measured on the powder samples, shown in Table 4.2, in which an increase of +ve b^* can be observed as increasing the Y content that resulted in a color change from off-white to yellow. A difference in color is observed, when yttrium is added to the structure, substituting bismuth ions, a^* values vary from -4.3 to +2.7, while b^* values vary from +11.5 to +51.1. At higher yttrium amounts, higher +b^* values are observed, leading to a high purity yellow color (C^* = 51.1 for $BY_{0.8}M$). Compared to $BiVO_4$, the

*L**, *a** and *b** values of the synthesized pigments were improved significantly in the solid solutions of $Bi_{2-x}Y_xMoO_6$ (Table 4.2). The hue angles (*h*°) of the present pigments were found to be in the yellow region of the cylindrical color space.

4.3.5 Diffuse reflectance and chromatic properties of Praseodymium (Pr^{3+}) substituted Bi_2MoO_6

Praseodymium substitution in Bi_2MoO_6 produces greenish yellow pigments (Fig. 4.13). In the absorption spectra (Fig. 4.14) of the $Bi_{2-x}Pr_xMoO_6$ (*x*= 0, 0.2, 0.4, 0.6, 0.8 and 1.0) colorants, several bands in the visible region have been observed and can be assigned to the electronic transition between $4f^{\,2} \rightarrow 4f^{\,1}\,5d^{\,1}$ states. A similar result with overlapping absorption bands has also been reported in the Bi_2RENbO_7 system (Zou *et al.* 2001). There are bands in the region 440-490 and 590-625 nm, which can be assigned based on the energy levels $^3H_4 \rightarrow {}^3P_2$, $^3H_4 \rightarrow {}^3P_1$, $^3H_4 \rightarrow {}^3P_0$, $^3H_4 \rightarrow {}^3D_2$ (upper) and $^3H_4 \rightarrow {}^3D_2$ (lower) respectively (Connell and Morris 2000; Sivakumar and Varadaraju 2005). $Bi_{2-x}Pr_xMoO_6$ colorants exhibit some greenish yellow color as they absorb red (complementary to green) and blue (complementary to yellow) light. The absorption edge is red shifted (~85 nm) with the Bi:Pr ratio. Pr^{3+} substitution in the Bi_2MoO_6 matrix decreases the band gap from 2.99 to 2.47 eV when *x* increased from 0 to 1 (Table 4.3). The more red shift observed in the case of $Bi_{2-x}Pr_xMoO_6$ solid solutions than $Bi_{2-x}Y_xMoO_6$ may due to the more absorption in the visible region due to the electronic transition between $4f^{\,2} \rightarrow 4f^1\,5d^1$ states in Pr^{3+}. For Pr, the energy of 4*f*-5*d* transition is lower than for the rest of the lanthanides. It is the transition that determines the absorption edge E_g of these oxides (4*f*-band lies above valence band) (Prokofiev *et al.* 1996). A gradual shift of CT band can be observed along with the increase in concentration of Pr^{3+} in Bi_2MoO_6.

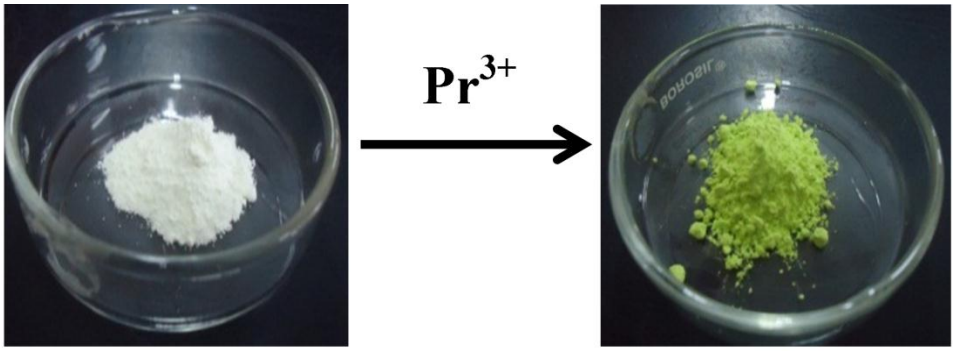

Fig. 4.13. Photographs of Bi_2MoO_6 and $BiPrMoO_6$ pigments.

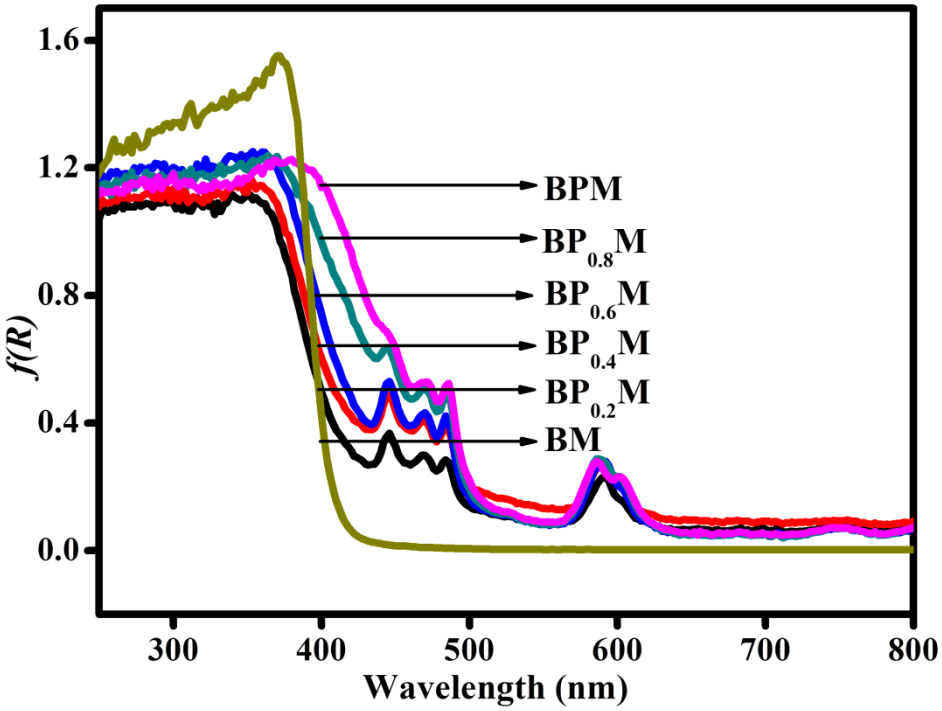

Fig. 4.14. Absorbance spectra of the $Bi_{2-x}Pr_xMoO_6$ (x= 0, 0.2, 0.4, 0.6, 0.8 and 1.0) pigments.

The chromatic properties of the synthesized $Bi_{2-x}Pr_xMoO_6$ (x= 0, 0.2, 0.4, 0.6, 0.8 and 1.0) powder pigments can be assessed from their CIE 1976 color coordinate values depicted in Table 4.3. The partial substitution of Pr^{3+} for Bi^{3+} in the Bi_2MoO_6 lattice enhances the yellow and green hue of the pigment which is expressed by the higher value of the color coordinate, +b* and –a*. Replacing 50 mol % of Pr^{3+} for Bi^{3+} in Bi_2MoO_6 increases the green component (-a*) significantly from –4.3 to -12.6 and yellow component (b*) from 11.5 to 49.1. This is also revealed in its chroma value (C*) which gets enhanced from 12.2 to 50.7.

Table 4.3. Color coordinates and band gap of $Bi_{2-x}Pr_xMoO_6$ (x= 0, 0.2, 0.4, 0.6, 0.8 and 1.0).

Sample	Color Co-ordinates					E_g (eV)
	*L**	*a**	*b**	*C**	*h°*	
BM	93.4	-4.3	11.5	12.2	69.4	2.99
$BP_{0.2}M$	87.8	-6.2	20.2	21.1	107.1	2.83
$BP_{0.4}M$	83.1	-5.9	26.7	27.3	102.4	2.79
$BP_{0.6}M$	86.3	-9.4	31.2	32.6	106.7	2.74
$BP_{0.8}M$	84.9	-12.6	44.3	46.1	105.9	2.50
BPM	84.3	-12.6	49.1	50.7	104.4	2.47

4.3.6 Band gap engineering in $BiREMoO_6$ (RE = Y, Pr, Nd, Sm, Tb and Yb)

The band gap energy of $BiREMoO_6$ calculated from UV-vis absorption spectra (Fig 4.10) indicates a sudden decrease in band gap with red shift in the absorption edge of Bi_2MoO_6. Pure Bi_2MoO_6 showed a clear absorption edge at around 400 nm, and the

corresponding band gap energy is 2.99 eV. This can be explained by the reported band structure of the AS- Bi_2MoO_6, where O_{2p} forms the valence band and the conduction band is derived from the Mo_{4d} orbitals and the Bi_{6p} orbitals (Shimodaira *et al.* 2006b). The contribution of each orbital is not equivalent, although the LUMO consisted of hybrid orbitals of Mo_{4d} and Bi_{6p} orbitals. The Mo_{4d} orbitals mainly contributed to the LUMO rather than the Bi_{6p} orbital. Visible light absorption of AS-Bi_2MoO_6 was revealed to be due to the transition from the valence band consisting of the O_{2p} orbitals to the conduction band derived from the primary Mo_{4d} orbitals in MoO_6 octahedra and the secondary Bi_{6p} orbitals. The band structure model of $BiREMoO_6$ (RE = Y, Pr, Nd, Sm, Tb and Yb) can be illustrated schematically as shown in Figure 4.15. As shown in the schematic diagram, the band gap is therefore the difference between the top of the O_{2p} band and the bottom of the Mo_{4d} band for Bi_2MoO_6. Red shifted absorption edge observed for RE substituted bismuth molybdate depends on the partly filled RE 4*f* shell.

Shift of optical absorption edge towards lower energy side is continued from Sm to Pr compounds, suggesting that the filled 4*f* levels are positioned between the O_{2p} valence band and Mo_{4d} + Bi_{6s} conduction band. The variation of E_g can be explained by the energy of filled RE 4*f* levels that become lowered with an increase of 4f electrons. Prokofiev and co-workers have studied periodicity in the optical band gap variation of Ln sesquioxides (Prokofiev *et al.* 1996). According to their recent report (Prokofiev *et al.* 1996), the occupied 4*f* band in Ce_2O_3, Pr_2O_3, and Nd_2O_3 lies above the O_{2p} band, and thus, 4*f*-5*d* transition may determine the band-gap energy. The RE 4*f* level gradually becomes lowered with an increase of their atomic number, finally lying in the valence band, which results in a monotonic increase of band gap energy from Ce_2O_3 to Sm_2O_3. Considering this, we can assume the band structure of $BiSmMoO_6$ to be composed of valence band consisting of the O_{2p} orbitals and the conduction band derived from the primary Mo_{4d} orbitals in MoO_6 octahedra and the secondary Bi_{6p} orbitals along with occupied Sm $4f^5$ lying overlapped with the valence band. Correspondingly the band gap

is reduced to 2.54 eV from 2.99 eV with the substitution of Sm^{3+}. But the Nd $4f^3$ and Pr $4f^2$ filled levels are still raised in energy due to the lower no. of 4*f* electrons. For $BiNdMoO_6$ the band gap is still lowered to 2.51 eV as Nd $4f^3$ level lies just above the O_{2p} valence band. Similar band structure with partially filled Pr $4f^2$ orbital located within the band gap above the valence band can be assumed for $BiPrMoO_6$. Thus the highest occupied level is formed by Sm 4*f* overlapped with O_{2p} for $BiSmMoO_6$ or by filled Pr 4*f* lying above the O_{2p} bands for $BiPrMoO_6$.

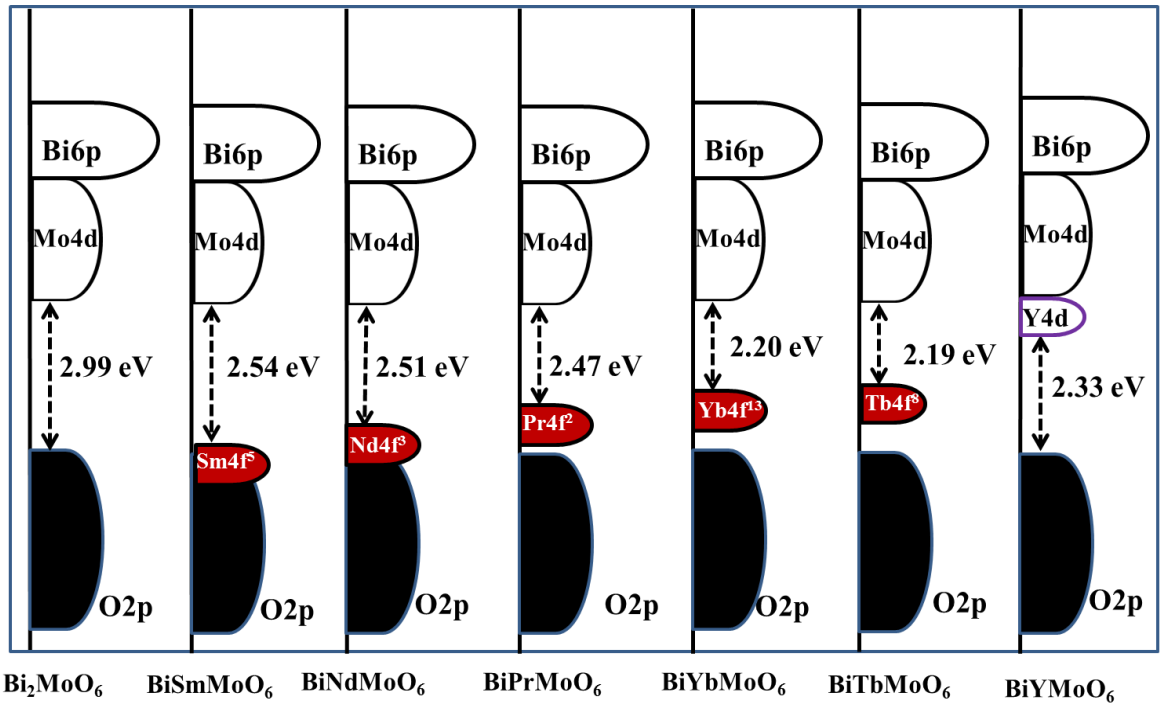

Fig. 4.15. Band structure models of $BiREMoO_6$ (RE = Y, Pr, Nd, Sm, Tb and Yb).

In contrast to the increased no. of 4*f* electrons in Tb and Yb compounds, they show minimum band gap values compared to other rare earths. For Ce, Pr and Tb the energy of 4*f*-5*d* transition is lower than for the rest of the lanthanides. It is the transition that determines the absorption edge E_g of these oxides (4*f* band lies above valence band)

(Prokofiev *et al.* 1996). This explains the lower E_g values of Tb compound. As soon as the f-band enters into the 2p-band the E_g values become constant. The oxides of Sm, Ho, Er and Tm have the same position of their 4*f* band (within the valence band) as the Gd and Lu oxides. As Yb^{3+} possesses only one unpaired electron, the 4*f*-band in $BiYbMoO_6$ positions much above the valence band and hence reduced band gap of 2.20 eV is observed. Y substitution in Bi_2MoO_6 changes the band structure by modifying the conduction band with Y_{4d} orbitals and the band gap calculated is 2.33 eV. The red shift in absorption edge in $BiYMoO_6$ is attributed to the overlapping of the 4d orbitals of Y^{3+} and Mo^{6+} which lowers the conduction band and also the contribution of Bi_{6s} orbitals to the valence band reduces the band gap in Y-substituted Bi_2MoO_6. This difference in RE 4*f* levels and the corresponding difference in the band gaps lead to different color, as can be seen from Table 4.1.

4.3.7 Acid/Alkali resistance studies of the pigments

The acid/alkali resistance of the pigments was carried out in 10% HNO_3 and NaOH. A pre–weighed amount of the pigment was treated with acid/alkali and soaked for half an hour with constant stirring using a magnetic stirrer. The pigment powder was then filtered, washed with water, dried and weighed. Negligible weight loss of pigment was noticed for all the acids and alkali tested. The color coordinates of the resultant tested samples were measured and compared with the untreated samples. The total color difference ΔE^*_{ab} was calculated and is summarized in Table 4.4. The negligible values of ΔE^*_{ab} reveal that the pigments are chemically stable towards the acid/alkali tested. Among the series of colorants synthesized, typically $BiYMoO_6$, $BiPrMoO_6$, $BiNdMoO_6$, $BiSmMoO_6$, $BiTbMoO_6$ and $BiYbMoO_6$ were tested for its acid and alkali resistance. The typical L^* a^* b^* values after acid and alkali resistance tests are given in Table 4.4. It is apparent that the color co-ordinate values of the pigment samples after acid and alkali test is nearly same as that of the pigment sample. This specifies that the investigated pigments are chemically stable.

Table 4.4 The color coordinates (±0.1) of the powder pigments after acid/alkali resistance tests.

Sample	Acid				Alkali			
	*ΔL**	*Δa**	*Δb**	*ΔE**	*ΔL**	*Δa**	*Δb**	ΔE^*_{ab}
$BiYMoO_6$	0.9	0.2	0.92	1.30	0.84	0.63	0.11	1.05
$BiSmMoO_6$	0.76	0.76	0.88	1.38	0.9	0.15	0.62	1.10
$BiPrMoO_6$	1.0	0.64	0.93	1.50	0.8	0.94	0.28	1.26
$BiNdMoO_6$	0.56	0.33	0.60	0.88	0.71	0.64	0.47	1.06
$BiTbMoO_6$	0.42	0.21	0.24	0.52	0.81	0.53	0.50	1.08
$BiYbMoO_6$	0.67	1.0	0.53	1.31	0.43	0.26	0.21	0.54

$\Delta E^*_{ab} = [(\Delta L^*)^2+(\Delta a^*)^2+(\Delta b^*)^2]^{1/2}$

4.3.8 Coloration of plastics

The coloring performance of the typically synthesized pigments, $BiTbMoO_6$ and $BiYMoO_6$ were tested for its coloring application in a substrate material like PMMA. Typically, 10 wt % pigment samples were dispersed in PMMA and compressed to a cylindrical disc (Fig. 4.16). The color co-ordinates of the test pieces were measured at different locations. The average $L^*a^*b^*$ values (L^* = 80.98, a^* = 13.2, b^* = 63.12 for $BiTbMoO_6$ and L^* = 85.31, a^* = 3.8, b^* = 53.91 for $BiYMoO_6$) obtained were more or less the same indicating the uniform distribution of pigment particles in the polymer matrix. The light resistance of the typical pigmented polymers was tested by exposing it to sun light at various time intervals and measured the color coordinates. The $L^*a^*b^*$ values of pigment composition were found to be nearly same as that of the unexposed

sample which indicates that the pigmented polymer is resistant to light. Thus, the developed pigments may find potential application in the coloring of various plastic materials.

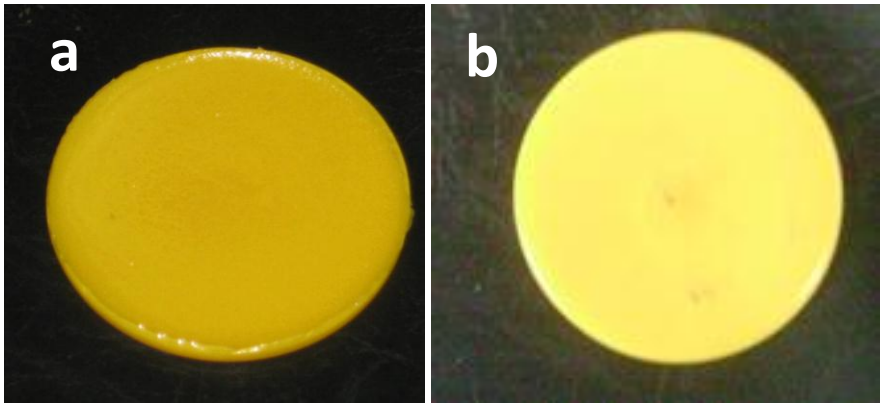

Figure 4.16. Photographs of (a) $BiTbMoO_6$ (10%) + PMMA and (b) $BiYMoO_6$ (10%) + PMMA.

4.4 Conclusions

A series of novel rare earth substituted bismuth molybdate pigments, $BiREMoO_6$ (RE = Y, Pr, Nd, Sm, Tb and Yb) have been synthesized. It is observed that the substitution of rare earth for bismuth in Bi_2MoO_6 red shifted the absorption edge leading to yellow color for Y, Sm, Yb and Tb and greenish yellow color for Pr and light green color for Nd. Rare earth dependence of band gap is governed by the position of energy level of RE 4*f* levels in the band structure, which lowers with increase of *f* electrons in RE^{3+}. The partially occupied 4*f* levels close to the valence band edge decreases the band gap of Bi_2MoO_6 and produces various color shades. The position of 4*f* band depends on the no. of *f* electrons in RE and hence is the band gap. In $BiYMoO_6$ band gap is reduced because the conduction band is formed largely from antibonding orbitals of the molybdate ions, with some Y_{4d} character. The developed pigments demonstrated good coloration to plastics and are chemically stable. The characteristics of the pigments

suggest that these products have potential to be used as interesting alternatives to existing toxic yellow pigments for coloration of plastics.

CHAPTER 5

Near–Infrared Reflecting Inorganic Pigments Based on M^{5+} (M = Nb, Ta and P) Substituted $BiVO_4$: Synthesis, Characterization and Optical Properties

A series of novel near–infrared (NIR) reflecting inorganic pigments based on bismuth vanadate substituted with pentavalent metal ion (Nb^{5+}, Ta^{5+} and P^{5+}) have been synthesized and characterized. The distortion produced by the substitution of M^{5+} in monoclinic $BiVO_4$ and the reduced crystallite size brought about special optical properties. The substitution of M^{5+} for V^{5+} in $BiVO_4$ enhanced the yellow coloration of bismuth vanadate by blue sifting the absorption edge. Most importantly, the pentavalent metal ion substitution in bismuth vanadate enhanced the NIR reflectance of $BiVO_4$ significantly to ~ 90 % in the wavelength range 700–2500 nm. The newly designed yellow pigments with improved yellow coloration exhibits good NIR reflectance, thus rendering them as excellent candidates for use as 'Cool Pigments' to reduce the heat build-up.

5.1 Introduction

Solar radiation control is an effective means to conserve electrical energy used for cooling buildings. Rising energy cost continues to drive advances in new technologies designed to improve energy efficiency across the globe. One such technology is to reflect the invisible heat from the object to minimize heat build–up, when exposed to solar radiation. Ultimately the reflection of solar energy lowers the heat build–up resulting in reduction on the load of the cooling system and therefore energy saving. Recent advances in pigmentation technology have allowed formulators to achieve a greater infrared reflectivity versus traditional pigmentation technologies in functional coatings, while maintaining the appropriate light absorption in the visible spectrum to impart color. Inorganic class of NIR reflectors are mainly metal oxides and are primarily useful in two major applications: (i) visual camouflage and (ii) reducing heat build–up on the surface of building roofing materials (Jeevanandam *et al.* 2007). Most of the literatures on these pigments exist as patents, which again indicate their wide potential applications (Modly 1986; Sliwinsky *et al.* 2002; Swiler and Axtell 2003; Swiler 2002). TiO_2 rutile, a white pigment with a high NIR solar reflectance of about 87.0% (Levinson *et al.* 2005b), is the best pigment used for roofing materials. However, the owners of homes with pitched roofs often prefer non-white roofing products for aesthetic reason (Levinson *et al.* 2007a; Levinson *et al.* 2007b; Synnefa *et al.* 2007). Manganese vanadium oxide pigments show improved NIR reflectance of ~ 82% and thereby reducing the IR – induced heat build-up (Swiler 2002).

Complex inorganic pigments based on mixed metal oxides (eg:– chromium green, cobalt blue, cadmium stannate, lead chromate, cadmium yellow and chrome titanate yellow) which have been widely used in camouflage absorb visible light but reflect the NIR portion of the incident radiation (Levinson *et al.* 2005a; Levinson *et al.* 2005b; Levinson *et al.* 2007b). However many of these pigments encompass toxic metals and hence their use is restricted. Thus there is a strong incentive to develop new colored NIR reflecting pigments to substitute for industrial pigments based on heavy metals hazardous

to health and environment. Recently lanthanide based NIR reflective pigments have been proposed as viable alternates to traditional toxic pigments due to their low toxicity (George *et al.* 2011; Swiler and Axtell 2003; Vishnu and Reddy 2010; Vishnu and Reddy 2011). Corundum hematite solid solutions were found to possess ~85% NIR reflectance and these materials serve as coloring pigments in camouflage paints (Sliwinsky *et al.* 2002). The reported inorganic pigments based on bismuth and vanadium include bismuth manganese oxide pigments that can be used as additives in plastics and paints (Sakoske *et al.* 2001) and manganese vanadium oxide pigments such as $Mn_2V_2O_7$, rare earth manganese oxides etc (Swiler and Axtell 2003; Swiler 2002).

Among transition metals, vanadium, and more particularly in the pentavalent state, is well known for its coloring properties. For example, vanadium pentoxide V_2O_5, whose color is due to the charge transfer band from O_{2p} - V_{3d}, is commonly used as a classic yellow pigment in glazes. The charge transfer energy of the colorless VO_4^{3-} ion is larger than that of the yellow CrO_4^{2-} ion. Consequently, many vanadate salts are white. Numerous A*x*V*y*O*z* colored ternary oxides are described in the literature (Smith 2002). Among the compounds, $BiVO_4$ is particularly notable. $BiVO_4$ has three crystal structures, monoclinic scheelite type $BiVO_4$, tetragonal zircon type $BiVO_4$ and tetragonal scheelite type $BiVO_4$. The phase transition between monoclinic scheelite structure and tetragonal scheelite structure of $BiVO_4$ reversibly occurs at about 255 °C, whereas the irreversible transition from tetragonal zircon structure to monoclinic $BiVO_4$ occurs after heat treatment at 400–500 °C and cooling to room temperature (Kudo *et al.* 1999). The base centered monoclinic crystal structure (space group 15, C^6_{2h}) contains four unique lattice sites: Bi (4e), V (4e), O1 (8f), and O2 (8f) (Sleight *et al.* 1979). The distinct feature is that its basic structural unit is constructed by VO_4 tetrahedron and BiO_8 dodecahedron. The isolated VO_4 tetrahedron is connected with BiO_8 dodecahedron by sharing an apex oxygen atom. So, every BiO_8 dodecahedron is surrounded by eight isolated VO_4 tetrahedra. Another obvious feature is that Bi atoms and V atoms arrange alternately along the crystallographic axis, consequently monoclinic clinobisvanite $BiVO_4$ exhibits

the characteristics of a layered structure. There are four types of Bi–O bond, and two types of V–O bond. This indicates that both VO_4 tetrahedron and BiO_8 dodecahedron are slightly distorted. It is reported that the distortion of BiO_8 dodecahedron can enhance the lone-pair impact of Bi 6s states and can bring about special optical properties.

Furthermore, the visible light absorption of $BiVO_4$ also depends on its crystal structure, and the monoclinic scheelite like $BiVO_4$ is a much more active structure than a tetragonal scheelite or tetragonal zircon structure. $BiVO_4$ with scheelite structure, especially a tetragonal system at high temperature is found to exhibit murky yellow rather than monoclinic scheelite $BiVO_4$ which shows vivid yellow (Tokunaga *et al.* 2001). The monoclinic $BiVO_4$ has a direct band gap of 2.4–2.5 eV and good optical absorption properties (Walsh *et al.* 2009). The coloring mechanism of monoclinic $BiVO_4$, results from the charge transfer transition between 6s valence band of bismuth and 3d conduction band of vanadium. It is expected that the color of the $BiVO_4$ pigment can be tuned by introducing other elements into the $BiVO_4$ lattice to control the lattice size, because the extent of the orbital hybridization in the valence band should depend on the interionic distance between Bi^{3+} and O^{2-}. After examining the effect of various cations doping on the crystal structure of scheelite $BiVO_4$, Hoffart et al. pointed out that highervalent cations doping at B sites can stabilize the BO_4 tetrahedra, whereas highervalent cations doping at A sites may destabilize the rigid BO_4 coordination and reduce the strength of the B-O bonds (Hoffart *et al.* 1994). It is expected that replacing some of the VO_4 in $BiVO_4$ with MO_4 impose lattice strain or distortion in the VO_4 tertahedra and which in turn can bring about slight distortion in the BiO_8 polyhedra (Zhao *et al.* 2011).

Even though $BiVO_4$ has been well explored as inorganic yellow pigment, its NIR reflectance has not been studied yet to the best of our knowledge. In this chapter, a series of NIR reflective yellow colored inorganic pigments of the formula $BiV_{1-x}M_xO_4$ (M = Nb, Ta and P; x = 0, 0.05, 0.10, 0.15 and 0.2) were synthesized and characterized. Main attention was concentrated on bringing about distortion in the monoclinic bismuth

vanadate by substituting pentavalent metal ions Nb^{5+} (r_{Nb5+} =0.48), P^{5+} (r_{P5+} = 0.17 Å) and Ta^{5+} (r_{Ta5+} = 0.64 Å) in place of V^{5+} (r_{V5+} = 0.35 Å) at the B site and study its influence on the optical properties. Particular interest was focused on the effect of pentavalent metal ion substitution in $BiVO_4$ for enhanced optical properties. The NIR reflectance is enhanced significantly by the substitution of Nb, Ta or P into the vanadium sites of $BiVO_4$.

5.2 Experimental Section

5.2.1 Materials and Methodology

Powder samples of the present system, $BiV_{1-x}M_xO_4$ (M = Nb, Ta and P; x = 0, 0.05, 0.10, 0.15 and 0.2) were synthesized by solid state reaction, using precursor oxides Bi_2O_3 (99.9 %), Nb_2O_5 (99.9 %), Ta_2O_5 (99.9%), and $NH_4H_2PO_4$ (99.9%) supplied by M/s. Sigma Aldrich as starting materials. Stoichiometric proportions of the precursors were transferred into an agate mortar and homogenized by wet milling in acetone media. Residual acetone was removed by evaporation and the resultant powders were calcined in platinum crucibles in Okay high temperature electric furnace at an optimized temperature of 800 °C for 9 h in air atmosphere, followed by auto cooling in the furnace. The heating of the furnace was programmed to increase the temperature initially at 10 °C/min up to 500 °C and afterwards the heating rate was decreased to 5 °C/min up to 800 ^{o}C. The pigment compositions thus obtained were ground in an agate mortar in order to refine and homogenize the particle size.

5.2.2 Characterization Techniques

The crystalline nature and phase purity of the synthesized samples were characterized by powder X–ray diffractometer (Philips X'pert Pro) with Ni–filtered Cu K_α (λ = 0.154060 nm) radiation. Data were collected by step scanning over a 2θ range from 10° to 90° with a step size of 0.016°. The FT NIR Raman spectra of the powdered samples were recorded on a Bruker RFS100/S spectrometer using near-infrared laser excitation (Nd: YAG, 1064 nm). A standard Ge detector cooled to liquid nitrogen

temperature was used, and was set to scan over the range 50–1000 cm^{-1}. The resolution of the spectrometer was 4 cm^{-1}. The morphology of the synthesized samples was recorded on a scanning electron microscope (JEOL JSM–5600 model), with an acceleration voltage of 15 kV. High resolution transmission electron microscope images of the samples were taken using transmission electron microscope (TECNAI $30G^2$ S-TWIN). A small amount of finely powdered sample was dispersed in acetone medium by ultrasonication, drop cast on carbon-coated copper grids, and dried.

The diffuse reflectance of the powdered pigment samples were measured (380–780 nm) with a UV–vis Spectrophotometer (Shimadzu UV–2450 with an integrating sphere attachment, ISR–2200) using barium sulphate as the reference. The color coordinates were determined by coupling an analytical software (UVPC Color Analysis Personal Spectroscopy Software V3, Shimadzu) to the UV–2450 spectrophotometer. The CIE 1976 $L^*a^*b^*$ colorimetric method was used, as recommended by the Commission Internationale de l'Eclairage (CIE).

The near–infrared reflectance of the powdered pigment samples was measured with a UV–vis–NIR spectrophotometer (Shimadzu, UV–3600 with an integrating sphere attachment) using poly–tetrafluoroethylene (PTFE) as a reference. Optical measurements were performed in the wavelength range from 700 to 2500 nm.

5.3 Results and Discussion

5.3.1 Powder X–ray diffraction analysis

Powder XRD patterns (Figure 5.1) confirmed that $BiVO_4$ has scheelite monoclinic structure (space group I2/b). The X-ray diffraction patterns obtained for Nb (x = 0, 0.05, 0.10, 0.15 and 0.2) substituted $BiVO_4$ are shown in Fig. 5.1 a. Nb substitution in $BiVO_4$ causes the phase change from monoclinic to tetragonal at x = 0.1. The diffraction peaks corresponding to x = 0, could be indexed on the basis of a monoclinic $BiVO_4$ and those for the rest of the compositions could be indexed on the basis of tetragonal cell of $BiVO_4$. The formation of tetragonal scheelite type structure is

confirmed (Fig. 5.1b) by the absence of a characteristic scheelite monoclinic peak at 15º and unsplit peaks at 18.5º and 35º. (Tokunaga *et al.* 2001). The powder XRD patterns (Fig. 5.2) of the $BiV_{1-x}M_xO_4$ (M = Ta and P; x = 0.05, 0.10, 0.15 and 0.20) powder shows monoclinic $BiVO_4$ phase along with minor impurity peaks originating from monoclinic $BiTaO_4$ and $BiPO_4$.

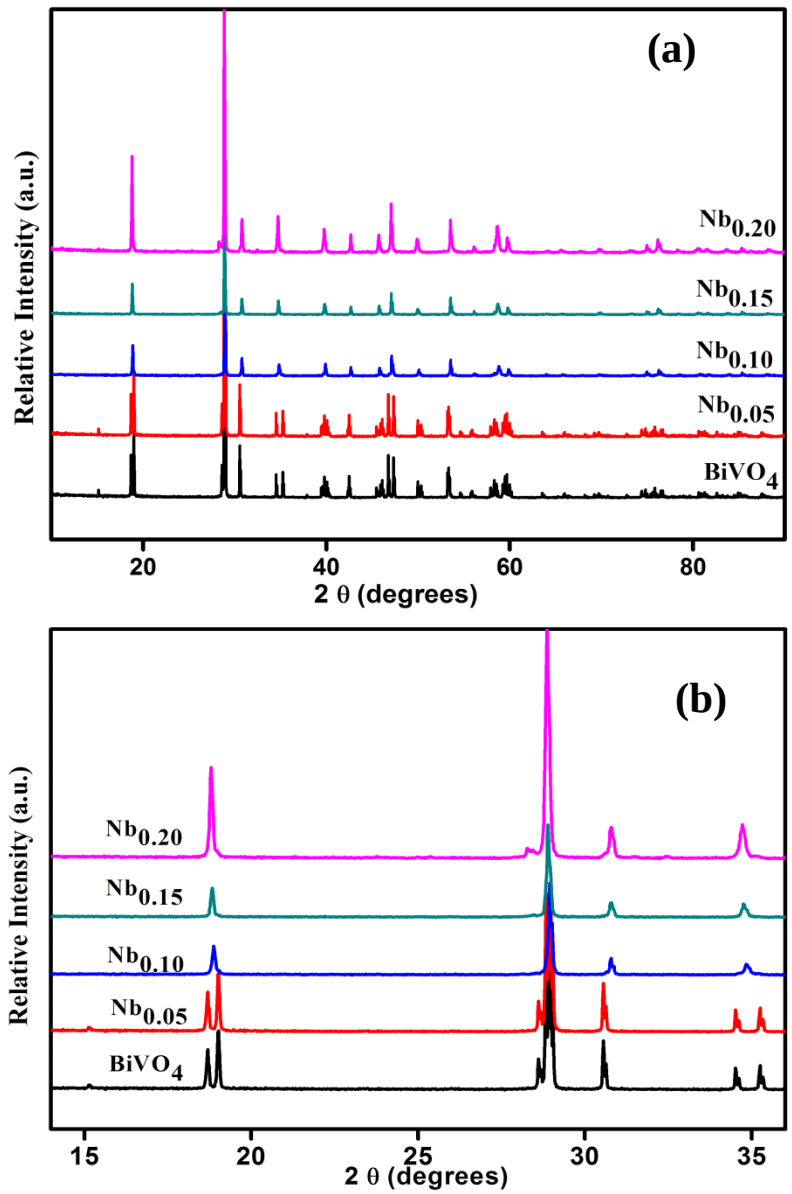

Fig. 5.1. Powder X-ray diffraction patterns of (a) $BiV_{1-x}Nb_xO_4$ (x = 0, 0.05, 0.10, 0.15 and 0.20) and (b) magnified peaks from 15º to 35º.

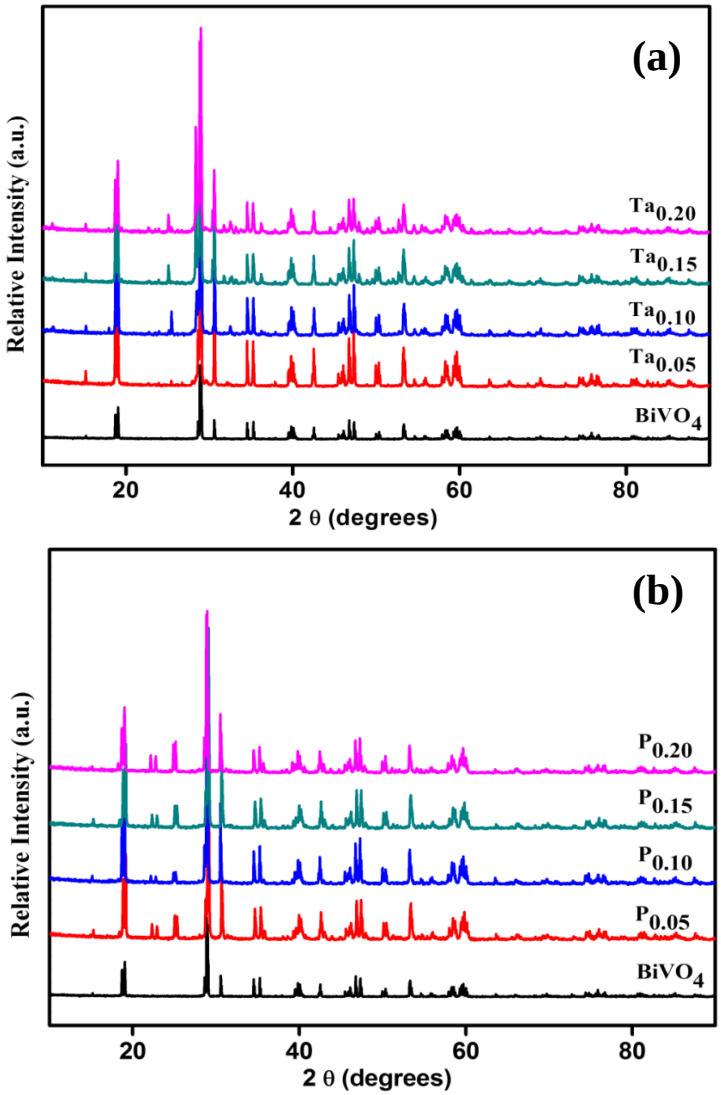

Fig. 5.2. Powder X-ray diffraction patterns of (a) $BiV_{1-x}Ta_xO_4$ and (b) $BiV_{1-x}P_xO_4$ (x = 0.05, 0.10, 0.15 and 0.20).

5.3.2 Raman spectroscopic investigations

Raman spectroscopic investigation has been found to provide the short range structural differences since Raman spectroscopy is primarily sensitive to oxygen-cation vibrations and is an excellent probe for local disorder (Glerup *et al.* 2001). The crystalline samples of $BiV_{1-x}Nb_xO_4$ (x = 0.05, 0.10 and 0.15) were examined by Raman spectroscopy in the frequency range 200-1000 cm^{-1} to look for any structural differences. Fig. 5.3

shows the Fourier-transform Raman spectra of Nb- substituted $BiVO_4$ compounds. Based on the crystal structure and group theory analysis of $BiVO_4$, all modes corresponds to symmetric and antisymmetric stretching and bending motions of V-O bonds. The Raman spectra of crystalline $BiVO_4$ (Fig. 5.3) reflect the structure of one type of VO_4 tetrahedron that consists of two sets of V–O bonds. In accordance with the interpretation of Hardcastle et al. major Raman modes of monoclinic bismuth vanadate such as A_g at ~831 cm^{-1} and ~708 cm^{-1} can be assigned to the symmetric V–O stretching mode of the shorter and longer V–O bond respectively and B_g at ~644 cm^{-1} assigned to asymmetric V–O stretch (Hardcastle and Wachs 1991). The symmetric (A_g) and antisymmetric (B_g) bending modes are at 366 and about 326 cm^{-1}, respectively, and external modes occur at 212 cm^{-1}. During the phase transition process from monoclinic to tetragonal $BiVO_4$ some Raman bands disappear, such as 325 cm^{-1} and 365 cm^{-1}, which are characteristic bands of monoclinic. From Fig. 5.3, it is noticed that the intensity of Raman band of monoclinic at around 828 cm^{-1} is not stronger than that of tetragonal at around 817 cm^{-1}, hence we can assume that the tetragonal bonds may be more sensitive than monoclinic. With the structural transition from monoclinic to tetragonal phase of $BiVO_4$, the Raman bands shift regularly, due to the different bond structure of V–O and Bi–O in monoclinic and tetragonal phases.

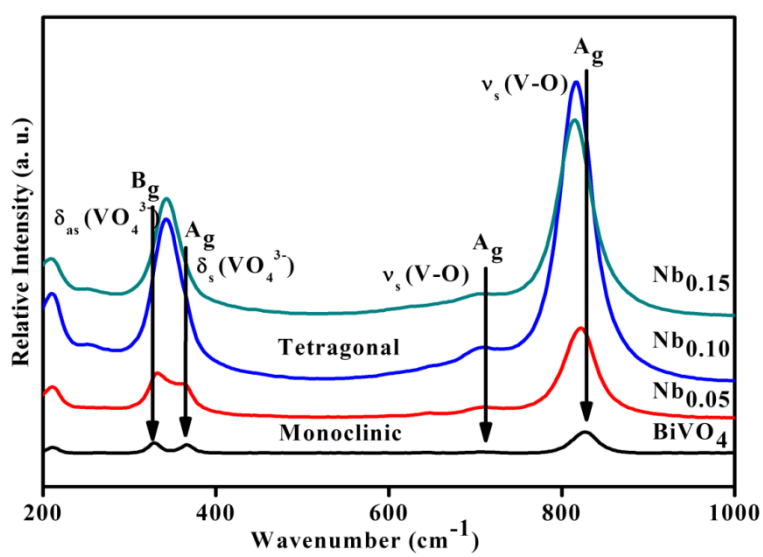

Fig. 5.3. Raman spectra for $BiV_{1-x}Nb_xO_4$ (x = 0.05, 0.10 and 0.15).

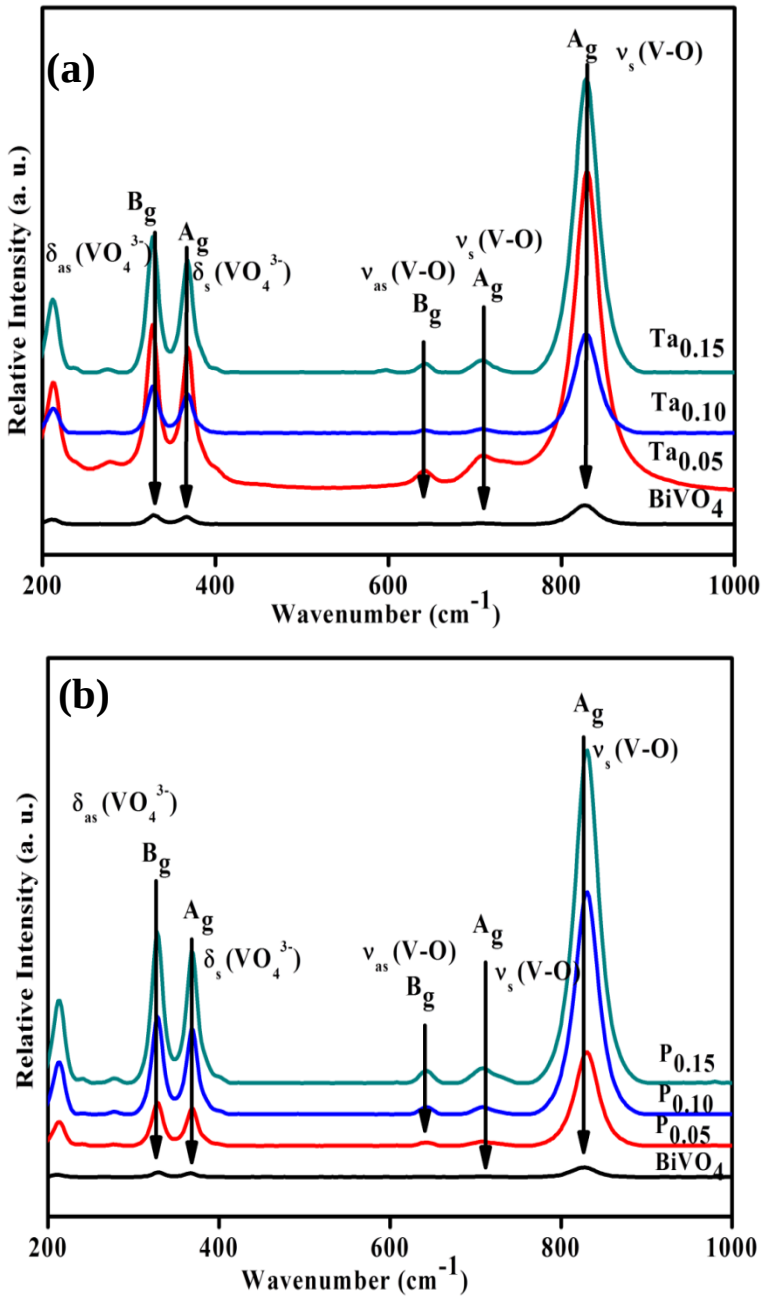

Fig. 5.4. Raman spectra for (a) $BiV_{1-x}Ta_xO_4$ and (b) $BiV_{1-x}P_xO_4$ ((x= 0, 0.05, 0.10 and 0.15).

The Raman spectra (Figure 5.4 a and 5.4 b) of $BiV_{1-x}Ta_xO_4$ and $BiV_{1-x}P_xO_4$ (x= 0, 0.05, 0.10 and 0.15) have major Raman modes of monoclinic bismuth vanadate. It is noteworthy that the symmetrical stretching motions of longer and shorter V-O bonds

slightly shift with the increasing content of M^{5+} ions in the solid solutions, suggesting the change in bond length with the introduction of pentavalent metal ions. A continuous shift of the most intense Raman band at about 828 cm^{-1} to lower wavenumbers, reveals that the average short range symmetry of the VO_4 tetrahedra becomes more regular. A calculation of the V–O bond length for $BiVO_4$ from Raman spectra using the empirical expression suggested by Brown and Wu, and Hardcastle and Wachs (Brown and Wu 1976; Gotic *et al.* 2005; Hardcastle and Wachs 1991) reveals that the shorter and longer V–O bond length decreases with increasing the disparity between the two bond lengths by the substitution of Ta and P.

5.3.3 Morphological Analysis

5.3.3.1 Morphological Analysis (SEM)

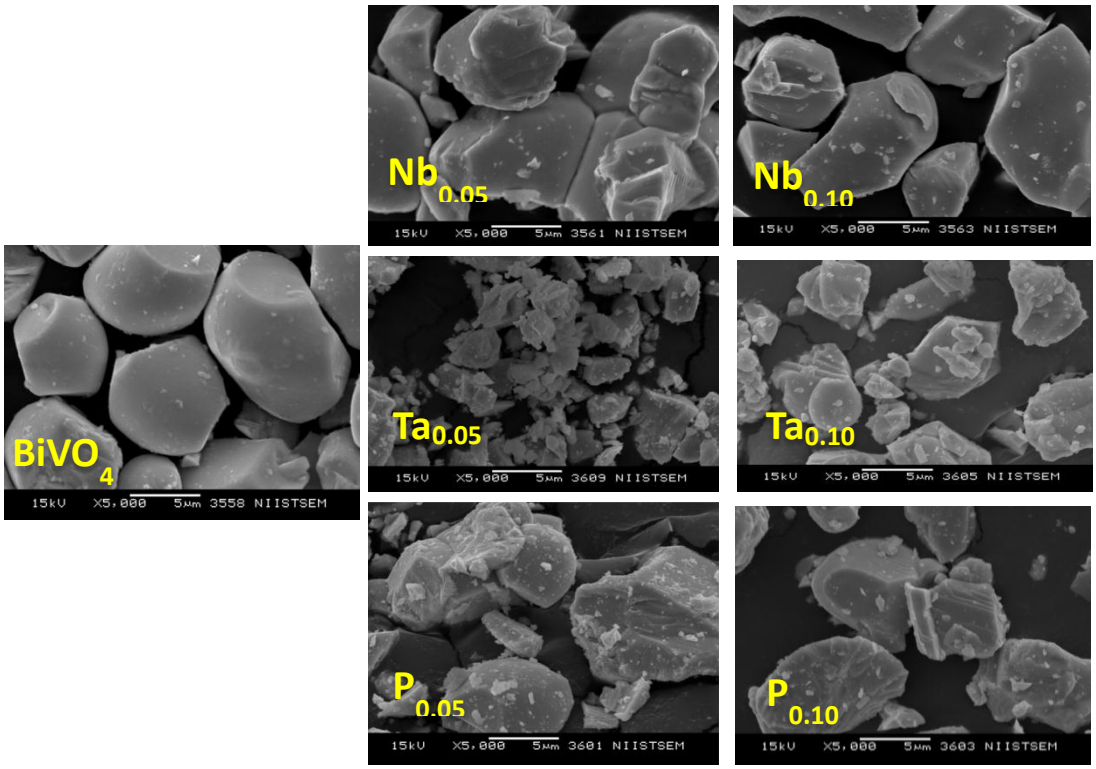

Fig. 5.5. SEM micrographs of $BiVO_4$ and 5 and 10 mol % Nb, Ta and P substituted $BiVO_4$.

The SEM micrographs recorded for $BiVO_4$, $BiV_{1-x}Nb_xO_4$, $BiV_{1-x}Ta_xO_4$ and $BiV_{1-x}P_xO_4$ (x= 0.05 and 0.10) are shown in Fig. 5.5. The primary particles of the pure $BiVO_4$ had a round shape and are well dispersed. The average particle size of the pigment as observed from the SEM images shown in Fig. 5.5 is approximately 5 µm. However, when compared to the round shaped $BiVO_4$, the substituted sample turns to be much more irregular. From Fig. 5.5 it is clear that with the substitution of Ta^{5+}/P^{5+} into bismuth vanadate, rough layer type particles with few clusters are formed instead of the larger dispersive particles with smooth surface. Morphological evolution from smooth round particles ($BiVO_4$) to rough layer type particle (Nb, Ta and P substituted $BiVO_4$) can be noticed. The micrographs of pentavalent metal ion substituted bismuth vanadate reveal a heterogeneous distribution of the particle size, ranging from 5 µm to the sub micro-meter range. In the case of P-substituted pigments (Fig. 5.5) the morphology is remarkably different and shows the growth of certain layers.

5.3.3.2 Morphological Analysis (TEM)

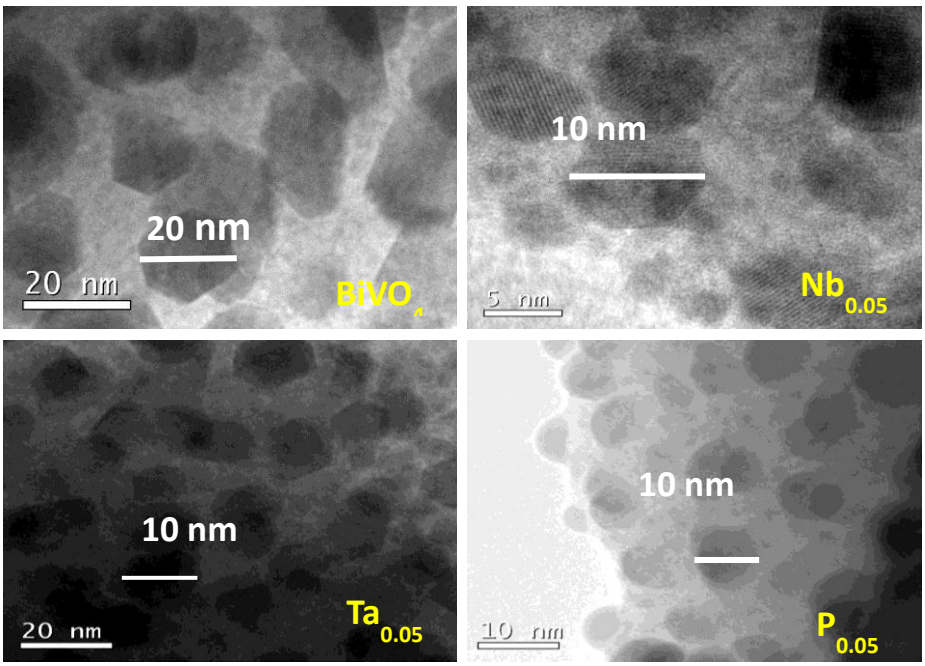

Fig. 5.6. HRTEM images of $BiVO_4$ and 5 mol % Nb, Ta and P substituted $BiVO_4$.

Even though microcystalline metal oxides are characterized by large grains, it could be an aggregate of small crystallites. HRTEM pictures (Fig. 5.6) show crystalline domains with a heterogeneous distribution of crystallite sizes between 10 and 40 nm. It is obvious from HRTEM studies that each particle (~ 5µm) of microcrystalline $BiVO_4$ consist of small crystallites in the nano regime (~20 nm) (Figure 5.6). Nb^{5+}, Ta^{5+} and P^{5+} substituted $BiVO_4$ is found to be composed of even smaller crystallites (~10 nm) which is evident from HRTEM images.

5.3.4 Diffuse reflectance and chromatic properties of niobium (Nb^{5+}) substituted $BiVO_4$

The colors of pure $BiVO_4$ and Nb^{5+} substituted $BiVO_4$ are shown in Fig. 5.7. As can be seen from the diffuse reflectance spectrum of $BiVO_4$ shown in Fig. 5.8, there exist a strong absorption band at 560 nm. The steep absorption at lower energy is attributable to the O_{2p}-V_{3d} transition. Substitution of Nb^{5+} for V^{5+} in $BiVO_4$ shifts the absorption edge towards the higher energy side. The spectra reveal strongest absorption up to 550 nm. The steep shape of the spectra indicated that the visible light absorption is not due to the transition from the impurity level but is due to the band to band transition. The substitution of Nb increases the band gap from 2.14 to 2.22 eV (Table 5.1). Thus the color of the pigment samples change from yellow to different shades of bright dark yellow (Fig. 5.7).

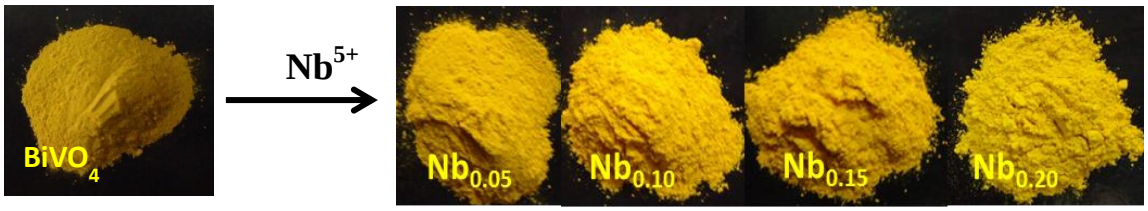

Fig. 5.7. Photograph of $BiV_{1-x}Nb_xO_4$ (x = 0, 0.05, 0.10, 0.15 and 0.2) pigments.

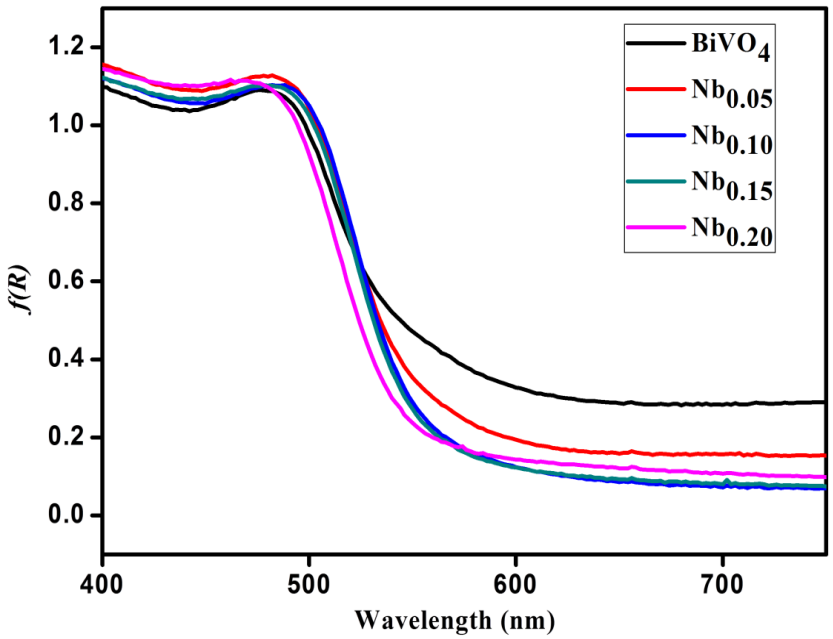

Fig. 5.8. Absorbance spectra of $BiV_{1-x}Nb_xO_4$ (x = 0, 0.05, 0.10, 0.15 and 0.2).

Table 5.1. Color co-ordinates and band gap of $BiV_{1-x}Nb_xO_4$ (x = 0, 0.05, 0.10, 0.15 and 0.2).

Sample	Color Co-ordinates					E_g (eV)
	*L**	*a**	*b**	*C**	*h°*	
$BiVO_4$	63.91	16.39	47.23	49.99	70.85	2.14
$Nb_{0.05}$	69.72	23.44	60.31	64.7	68.75	2.17
$Nb_{0.10}$	73.4	26.87	64.89	70.24	67.5	2.18
$Nb_{0.15}$	74.94	24.69	66.69	71.12	69.68	2.19
$Nb_{0.20}$	75.84	17.97	72.15	74.35	76.01	2.22

The chromatic properties of the synthesized $BiV_{1-x}Nb_xO_4$ (x = 0, 0.05, 0.10, 0.15 and 0.2) powder pigments can be assessed from their CIE 1976 color coordinate values depicted in Table 5.1. The systematic doping of niobium for V^{5+} in $BiVO_4$ (from 0 to 20 mol %) results in an increase in the b^* value regularly from 47.23 to 72.15, which indicates that the yellowness of the pigment sample enhances. On the other hand, the increase of Nb^{5+} substitution up to 15 mol % leads to an improvement in red hue of the pigment, which is again evident from the higher values of the color coordinate, a^* (increases from 16.39 to 24.69). However, substitution of niobium up to 20 mol % decreases the red component of the pigment samples (a^* value decreases from 24.69 to 17.97). As a consequence to the above, the C^* value which represents the richness of the color hue significantly increases. The observed hue angles of the developed pigments are found to be in the yellow region of the cylindrical color space ($h°$ = 70–105 for yellow), except for lower concentration of Nb^{5+} substituted compounds (Sulcova and Trojan 2008a). It is interesting to note that the chromatic properties of the typical pigment sample $BiV_{0.8}Nb_{0.2}O_4$ (L^* = 75.84, a^* = 17.97, b^* = 72.15, C^* = 74.35, $h°$ = 76.01) was found to be comparable to the chromatic properties of commercially available zircon yellow pigment reported elsewhere, especially the b^* value (L^* = 83.5, a^* = -3.2, b^* = 70.3) (Imanaka *et al.* 2008).

5.3.5 Diffuse reflectance and chromatic properties of tantalum (Ta^{5+}) substituted $BiVO_4$

The colors of Ta^{5+} substituted $BiVO_4$ are shown in Fig. 5.9. The UV-vis absorption spectra of the $BiVO_4$ and Ta substituted $BiVO_4$ samples are illustrated in Figure 5.10. For $BiVO_4$, absorption edge appeared near 550 nm corresponding to 2.14 eV. The ternary metal oxides $BiV_{1-x}Ta_xO_4$ were found to be relatively large band gap semiconductors with E_g = 2.20-2.23 eV (Table 5.2). The increase in band gap observed in Ta substituted $BiVO_4$ may account for the fact that antibonding character of the ‘e’ and ‘t_2’ MOs increases due to the contribution from the bigger Ta 5d orbital. The pentavalent

metal ion substitution at the vanadium site of bismuth vanadate steepened the absorption edge of $BiVO_4$ suggesting that prepared samples have a direct band gap and absorb visible light due to the band to band transition. In addition, absorption edge was blue shifted slightly as increasing amounts of Ta were incorporated. Absorption edge of Ta substituted $BiVO_4$ showed systematic increase with Ta concentration.

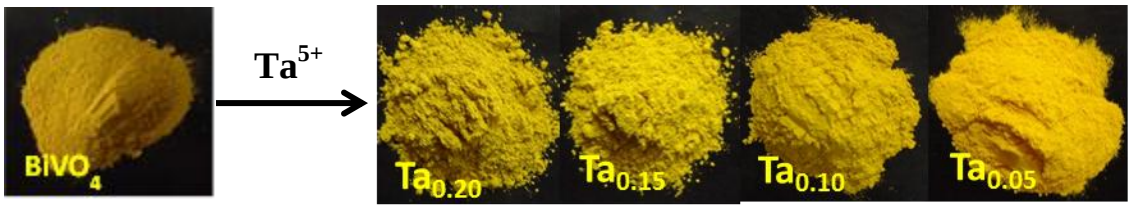

Fig. 5.9. Photograph of $BiV_{1-x}Ta_xO_4$ (x = 0, 0.05, 0.10, 0.15 and 0.2) pigments.

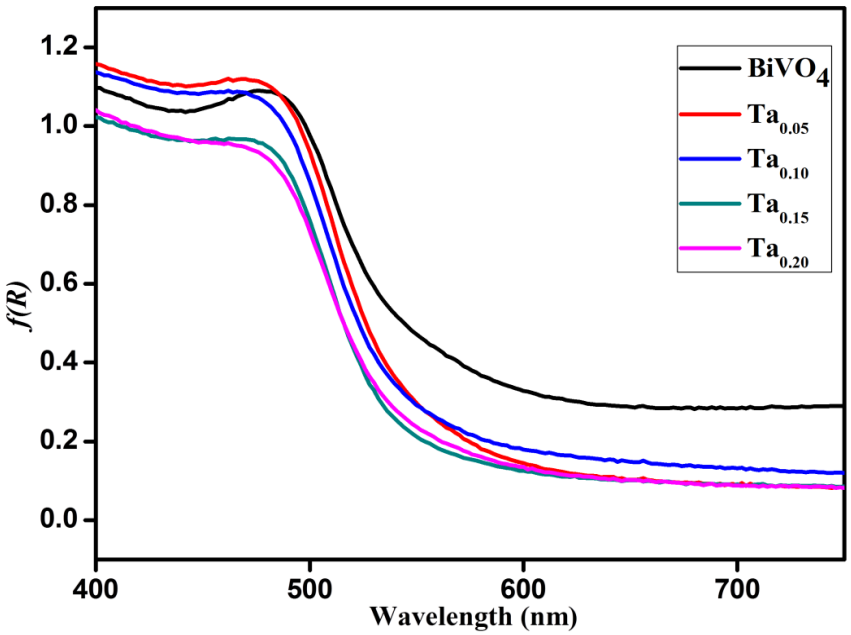

Fig. 5.10. Absorbance spectra of $BiV_{1-x}Ta_xO_4$ (x = 0, 0.05, 0.10, 0.15 and 0.2).

Table 5.2. Color co-ordinates and band gap of $BiV_{1-x}Ta_xO_4$ (x = 0, 0.05, 0.10, 0.15 and 0.20).

Sample	Color Co-ordinates					E_g (eV)
	*L**	*a**	*b**	*C**	*h°*	
$BiVO_4$	63.91	16.39	47.23	49.99	70.85	2.14
$Ta_{0.05}$	74.42	20.84	66.33	69.52	72.55	2.20
$Ta_{0.10}$	73.04	16.76	65.15	67.27	75.57	2.22
$Ta_{0.15}$	77.14	14.43	65.11	66.69	77.49	2.23
$Ta_{0.20}$	76.41	15.18	63.19	64.99	76.49	2.21

The color coordinates of the $BiV_{1-x}Ta_xO_4$ (x = 0, 0.05, 0.10, 0.15 and 0.2) powder pigment samples are summarized in Table 5.2. Replacing 5 mol % of Ta^{5+} for V^{5+} in $BiVO_4$ increases the yellow component (b*) significantly from 47.23 to 66.33 and red component (b*) is found to escalate. This is also reflected in its chroma value (C*) which gets enhanced from 49.99 to 69.52. A further increase in substituent concentration of the chromophore ion (up to 20 mol %) brings about a very slight decrease in the red and yellow hues. The hue angle values (h°) of the synthesized tantalum substituted $BiVO_4$ pigments lie in the yellow region of the cylindrical color space (h° = 70–105 for yellow).

5.3.6 Diffuse reflectance and chromatic properties of phosphorus (P^{5+}) substituted $BiVO_4$

P^{5+} substitution in $BiVO_4$ produces very good bright yellow (Fig. 5.11). The UV-vis absorption spectra of the $BiVO_4$ and P substituted $BiVO_4$ samples are illustrated in Figure 5.12. Substitution of 5 mol % of P^{5+} in bismuth vanadate blue shifts the optical absorption edge and gets steepened. The absorption maximum is shifted to wavelength shorter than 520 nm. As a result, the color of the samples is pure bright yellow, because

blue is a complementary color to yellow. This shift can be attributed to an increase in the intensity of the ligand field due to the decrease of the V-O distances produced by the substitution of P^{5+} by V^{5+} in bismuth vanadate due to higher electronegativity of phosphorus. As P atoms were incorporated, the band gap energy increased rapidly initially, and then slowly approached 2.25 eV (Table 5.3) as the absorption edge gets stabilized.

Fig. 5.11. Photograph of $BiV_{1-x}P_xO_4$ (x = 0, 0.05, 0.10, 0.15 and 0.20) pigments.

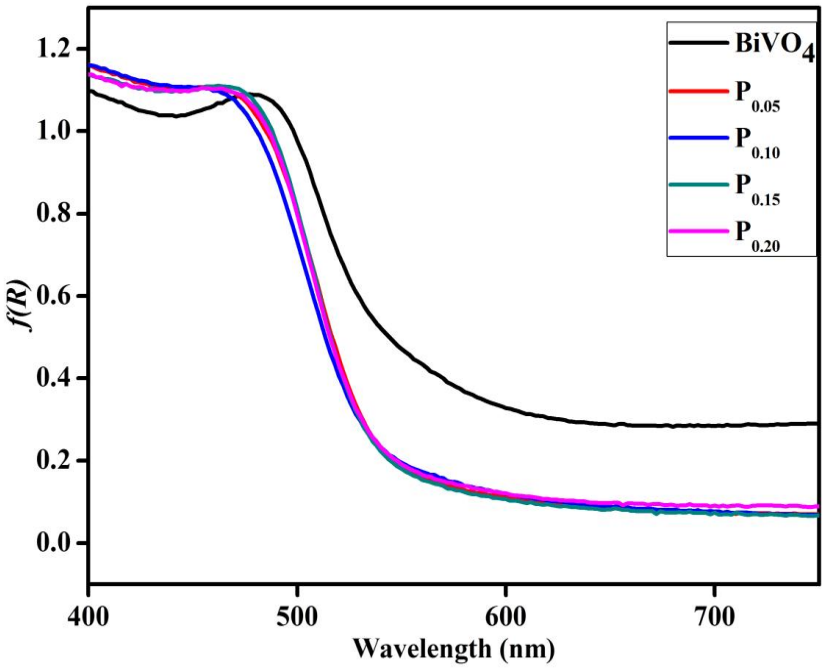

Fig. 5.12. Absorbance spectra of $BiV_{1-x}P_xO_4$ (x = 0-0.2).

It is clear from Table 5.3 that the substitution of 5 mol % of P^{5+} for V^{5+} in $BiVO_4$ drastically increases the yellow component (*b**) from 47.23 to 73.55, while there is not much change in the red component (*a**) as compared to the phosphorus free sample. In addition to the above, the chroma (C*) of the pigment has been significantly enhanced from 49.9 to 74.7. Substitution of P^{5+} in $BiVO_4$ is also found to increase the hue angle (h°) from 70.8 to 82.12. Improvement in lightness (*L**) has resulted in a change in the color of the pigment from dull yellow to bright yellow. Further increase in the dopant concentration of P^{5+} from 5 to 20 mol % progressively doesn't bring about systematic difference in the color co-ordinates. The color coordinates of the typical pigment sample $BiV_{0.85}P_{0.15}O_4$ (*L** = 78.57, *a** = 13.79, *b** = 75.79, C* = 77.04, hº = 79.68) was found to be comparable to the chromatic properties of commercially available zircon yellow pigment reported elsewhere, especially the *b** value (*L** = 83.5, *a** = -3.2, *b** = 70.3) (Imanaka *et al.* 2008).

Table 5.3. Color coordinates and band gap of $BiV_{1-x}P_xO_4$ (x = 0, 0.05, 0.10, 0.15 and 0.20).

Sample	Color Co-ordinates					E_g (eV)
	*L**	*a**	*b**	*C**	*h°*	
$BiVO_4$	63.91	16.39	47.23	49.99	70.85	2.14
$P_{0.05}$	78.73	13.09	73.55	74.7	79.9	2.23
$P_{0.10}$	79.76	10.08	72.94	73.63	82.12	2.25
$P_{0.15}$	78.57	13.79	75.79	77.04	79.68	2.25
$P_{0.20}$	77.7	13.08	73.95	75.1	79.96	2.26

5.3.7 Band gap engineering in M^{5+} (M = Nb, Ta and P) substituted $BiVO_4$

The band structure of a metal oxide semiconductor consists of metal nd/(n + 1)s and O_{2p} levels which form CB and VB, respectively. In the case of the monoclinic bismuth vanadate, the band gap energy is related to the energy difference between the valence band consisting of hybrid orbital of Bi_{6s} and O_{2p} and the conduction band derived from the primary V_{3d} orbitals in VO_4 tetrahedra and the secondary Bi_{6p} orbitals. The schematic band structure of bismuth vanadate and pentavalent metal ion substituted $BiVO_4$ is shown in Fig. 5.13. Band gap of monoclinic bismuth vanadate is calculated to be 2.14 eV. As Nb atoms were incorporated, the band gap energy increased to 2.22 eV. This means that the width or position of the conduction band is slightly modified by the incorporation of Nb^{5+}. It might be suggested that such modification in C.B. is originated from the hybridization between Nb_{4d} and V_{3d} orbitals. The increased band gap suggests formation of new conduction band edge made of only V_{3d} orbitals at a lower energy level than Nb_{4d} orbitals. Upon TaO_4 substitution Ta_{5d} orbitals were located at a higher energy level than V_{3d} orbital, contributing to the increase in width of the conduction band. Hence Ta substituted Bismuth vanadate exhibit a higher band gap of 2.23 eV. This is a reflection of the smaller crystal field splitting expected for a 3d transition metal ion, which in turn comes from the reduced spatial extension of the V_{3d} orbitals (relative to the Ta_{5d} orbitals). The greater the splitting of energy levels, the more hybridization with O_{2p} orbitals. A calculation of the V–O bond length for $BiVO_4$ from Raman spectra using the empirical expression suggested by Brown and Wu, and Hardcastle and Wachs (Brown and Wu 1976; Gotic *et al.* 2005; Hardcastle and Wachs 1991) reveals that the shorter and longer V–O bond length decreases with increasing the disparity between the two bond lengths by the substitution of Ta and P (Fig. 5.4 a and b). The slight distortion of the VO_4 tetrahedra inhibits the electron-hole pair recombination and enhances the optical properties (Zhao *et al.* 2011). Van-Vechten & Phillips assumed that spatial overlap is proportional to $d^{-2.5}$ (where d is the bond distance) (Van Vechten and Phillips 1970). Decreasing the bond distance increases the orbital overlap. The increased spatial overlap

has primary effect on increasing bonding-antibonding separation, E(σ∗)-E(σ) and secondary effect on increasing the bandwidth. The net effect is the increase of the band gap. The charge transfer energy of MO_4^{3-} increases in the order VO_4^{3-}< NbO_4^{3} < TaO_4^{3-}< PO_4^{3-} and this may also contribute to the shift in the absorption edge towards the higher energy side.

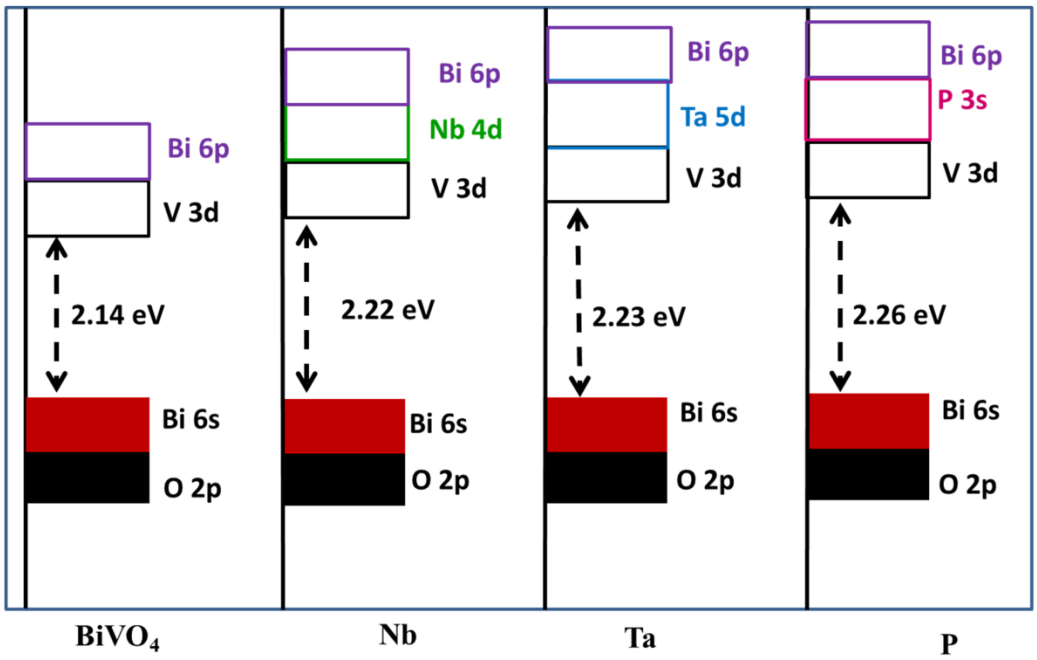

Figure 5.13. Band structure models of $BiV_{1-x}M_xO_4$ (M = Nb, Ta and P).

The increased electronegativity of the metal also translates into an increase in the covalency of the metal–oxygen bonds which tend to destabilize the energy of the antibonding 'e' levels and thereby raising the HOMO–LUMO gap as in the case of phosphate, sulfate, and perchlorate groups (Fierro 2006). Substitution of a highly electronegative phosphorus metal ion for vanadium in $BiVO_4$ increases the covalent antibonding destabilization and net result is an increase in the energy of the oxygen-to-metal charge transfer excitation from 2.14 eV to 2.26eV (Fig. 5.13). The increase in band gap observed in Nb and Ta substituted $BiVO_4$ may account for the fact that antibonding

character of the e and 't_2' MOs increases due to the contribution from the bigger Nb_{4d} and Ta_{5d} orbital compared to V_{3d}.

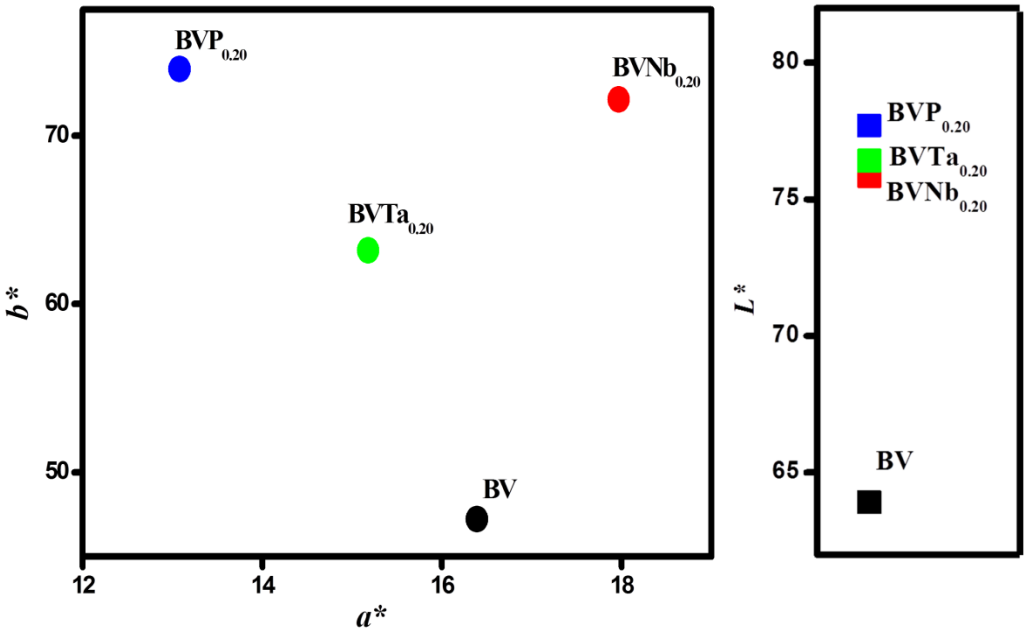

Figure 5.14. CIE *L*a*b** color parameters of $BiVO_4$ and 20 mol % M^{5+} (M = Nb, Ta and P) substituted bismuth vanadate.

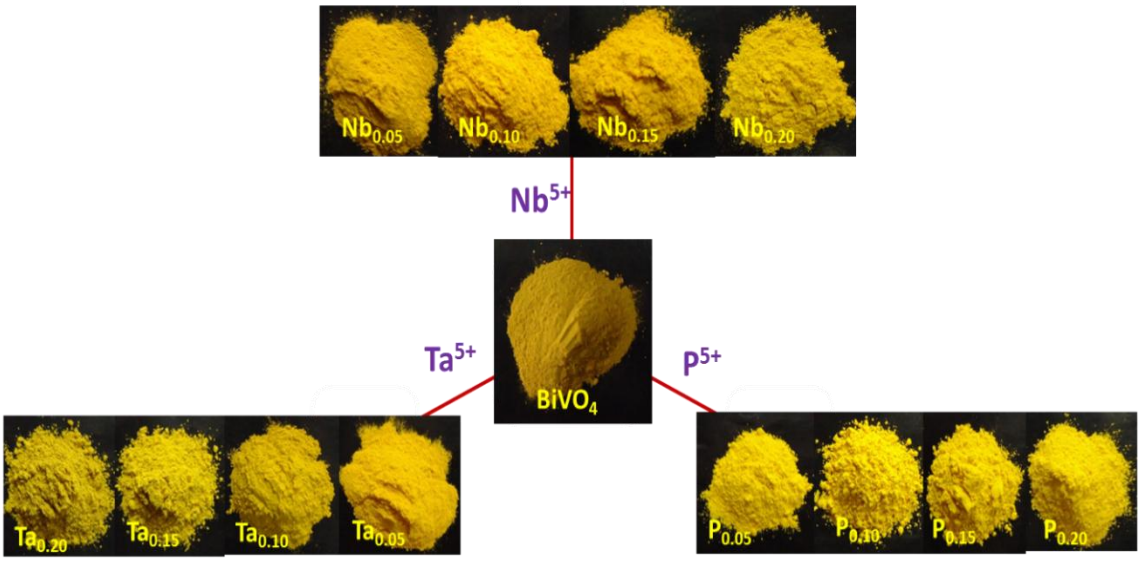

Fig. 5.15. Photographs of $BiVO_4$ and M^{5+} (M= Nb, Ta and P) substituted $BiVO_4$.

Corresponding to the band structure change in BiVO4 by the substitution of pentavalent metal ions, the color of bismuth vanadate is significantly altered as seen from Fig. 5. 15. CIE *L*a*b** color parameters of $BiVO_4$ and 20 mol% M^{5+} (M = Nb, Ta and P) substituted bismuth vanadate are shown in Fig. 5.14.

5.3.8 NIR reflectance of M^{5+} (M = Nb, Ta and P) substituted $BiVO_4$

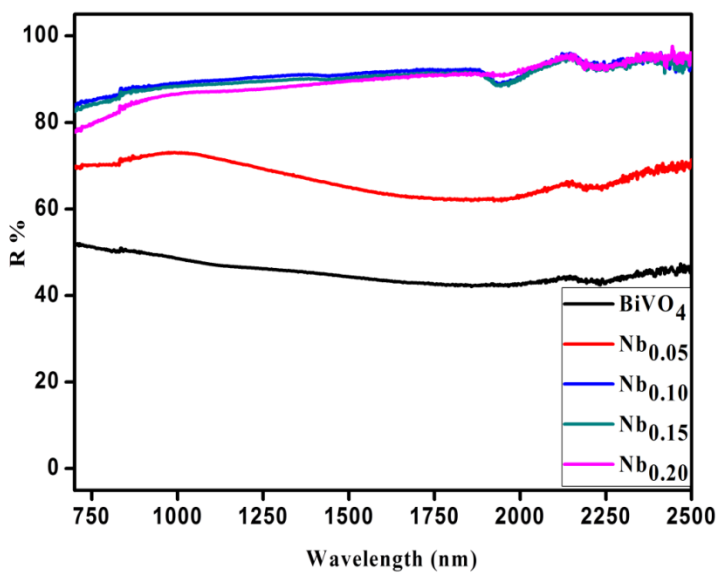

Fig. 5.15. NIR reflectance of $BiV_{1-x}Nb_xO_4$ (x = 0, 0.05, 0.10, 0.15 and 0.20).

Fig. 5.16 exemplifies the NIR reflectance spectra of the niobium substituted bismuth vanadate powder pigment samples. The substitution of Nb^{5+} for V^{5+} up to 5 mol % enhances the NIR solar reflectance to 70%. More substitution of Nb^{5+} in $BiVO_4$ increases the NIR reflectance of the pigment samples to 90%. The high NIR solar reflectance (~ 90%) displayed by all the newly designed yellow colored samples makes them interesting candidates for use as "cool colorants". Similar enhanced NIR reflectance was observed for Ta and P substituted bismuth vanadate. Figs. 5.16 and 5.17 show the NIR reflectance spectra of $BiV_{1-x}Ta_xO_4$ and $BiV_{1-x}P_xO_4$ (x = 0, 0.05, 0.10, 0.15 and 0.20) powder pigments. The NIR solar reflectance values increases to 90 % irrespective of the concentration of Ta^{5+} in bismuth vanadate. On the other hand, in the case of P^{5+}

substituted $BiVO_4$, NIR reflectance increases to 90% up to 15 mol% of the substituent and is found to decrease to 83% for 20 mol% of P^{5+}.

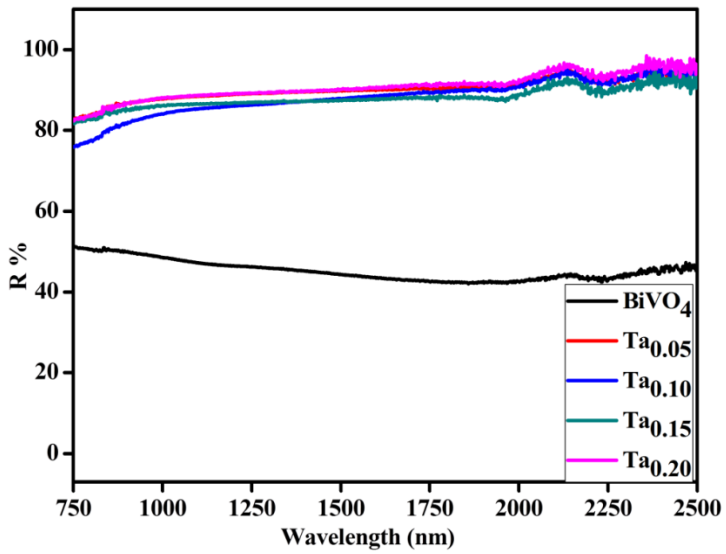

Fig. 5.16. NIR reflectance of $BiV_{1-x}Ta_xO_4$ (x = 0, 0.05, 0.10, 0.15 and 0.20).

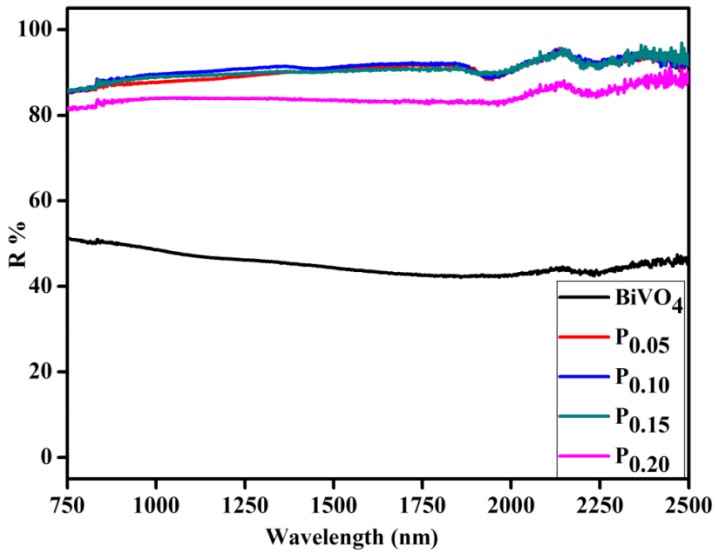

Fig. 5.17. NIR reflectance of $BiV_{1-x}P_xO_4$ (x = 0, 0.05, 0.10, 0.15 and 0.20).

Particle size of an oxide can affect its color which in turn can affect its reflectance property. According to the Kubelka-Munk theory, in general the reflectance of a material

increases as the particle size decreases. The reflectance of a material can be affected by a combination of factors such as mean particle size, particle size distribution, particle shape, particle porosity, packing density, surface texture, its chemical composition, and wavelength. Even though microcystalline metal oxides are characterized by large grains, it could be an aggregate of small crystallites. HRTEM pictures (Fig. 5.6) of $BiVO_4$ and M^{5+} substituted bismuth vanadate show crystalline domains with a heterogeneous distribution of crystallite sizes between 10 and 40 nm. It is obvious from HRTEM studies that each particle (~ 5µm) of microcrystalline $BiVO_4$ consists of small crystallites in the nano regime (~20 nm). Nb^{5+}, Ta^{5+} and P^{5+} substituted $BiVO_4$ is found to be composed of even smaller crystallites (~10 nm) which is evident from HRTEM images (Fig. 5.6). In the NIR region (750-2500 nm), the extinction of incident light due to scattering is usually larger than that due to absorption (Jeevanandam *et al.* 2007). It can be expected that the crystallites in the nano regime can scatter the incident NIR radiation and the dominant multiple scattering in metal ion substituted $BiVO_4$ helped to enhance the NIR reflectance to ~ 90 % for Nb, Ta and P substituted bismuth vanadate. From SEM analysis (Fig. 5.5), it can be noticed that even 5 mol % substitution of M^{5+} in bismuth vanadate destroyed the initial morphology of $BiVO_4$. Morphological evolution from smooth round particles ($BiVO_4$) to rough layer type particle shape (Nb, Ta and P substituted $BiVO_4$) can reflect the incident NIR radiation (Fig.5.5). The slight distortion of the VO_4 tetrahedra inhibits the electron-hole pair recombination and enhances the optical properties (Zhao *et al.* 2011). For $BiV_{1-x}M_xO_4$, the critical factor for enhanced NIR reflectance should be possibly due to the lattice distortion induced by the substitution of smaller/bigger ion and at the same time morphological evolution and small crystallites may also contribute.

5.3.9 Acid/Alkali resistance studies of the pigments

Chemical resistance studies were done using the typical pigments $BiVO_4$, $BiV_{0.8}Nb_{0.2}O_4$, $BiV_{0.8}Ta_{0.2}O_4$ and $BiV_{0.8}P_{0.2}O_4$. The acid/alkali resistance of the pigments was carried out in 10% HNO_3 and NaOH. A pre–weighed amount of the pigments were treated with acid/alkali and soaked for half an hour with constant stirring using a

magnetic stirrer. The pigment powders were then filtered, washed with water, dried and weighed. Negligible weight loss of pigments was noticed for the acid and alkali tested. The color coordinates of the resultant tested samples were measured and compared with the untreated samples. The total color difference was calculated and is summarized in Table 5.4. The negligible values of ΔE^*_{ab} reveal that the pigments are chemically stable towards the acid/alkali tested.

Table 5.4. The color coordinates (±0.1) of the $BiVO_4$ and $BiV_{0.8}M_{0.2}O_4$ (M = Nb, Ta and P) powder pigments after acid/alkali resistance tests.

Sample	Acid				Alkali			
	ΔL^*	Δa^*	Δb^*	ΔE^*_{ab}	ΔL^*	Δa^*	Δb^*	ΔE^*_{ab}
$BiVO_4$	0.33	0.52	0.16	0.63	0.99	0.67	0.53	1.30
$BiV_{0.8}Nb_{0.2}O_4$	0.64	0.81	0.21	1.05	0.81	0.56	0.74	1.23
$BiV_{0.8}Ta_{0.2}O_4$	0.76	0.37	0.58	1.02	1.5	0.31	0.83	1.74
$BiV_{0.8}P_{0.2}O_4$	1.2	0.91	0.78	1.69	1.2	0.66	0.91	1.64

$\Delta E^*_{ab} = [(\Delta L^*)^2+(\Delta a^*)^2+(\Delta b^*)^2]^{½}$

5.4 Conclusions

A series of potential NIR reflective inorganic pigments with the general formula $BiV_{1-x}M_xO_4$ (M = Nb, Ta and P; x = 0, 0.05, 0.10, 0.15 and 0.20) displaying a wide range of bright yellow colors have been successfully synthesized by calcination route. In summary, lattice distortion was induced into monoclinic bismuth vanadate crystal structure to enhance the optical properties by substituting pentavalent metal ions (Nb^{5+}, Ta^{5+} and P^{5+}) for V^{5+} in $BiVO_4$. The absorption edge was blue shifted with the

introduction of Nb^{5+} and Ta^{5+} in $BiVO_4$ by the destabilization of the conduction band from the bigger Nb_{4d} and Ta_{5d} orbital. P^{5+} substitution in bismuth vanadate increased band gap due to covalent antibonding destabilization by the introduction of highly electronegative post transition metal (P^{5+}) for vanadium. Most importantly, the pentavalent metal ion substitution in bismuth vanadate enhanced the NIR reflectance of to ~90 %. The smaller crystallites aggregated in the microcrystalline $BiV_{1-x}M_xO_4$ and morphological evolution from smooth round particles to rough layer type particle shape enable the multiple scattering of the incident NIR light and enhance the NIR reflection. The present results suggest that these pantavalent metal ion substituted bismuth vanadate can be a potential candidate for NIR reflecting yellow pigments to reduce the heat build-up.

CHAPTER 6

Conclusions and Future Scope

This chapter presents the general conclusions derived from the study of structure, microstructure and optical properties of rare earth – transition metal oxide based red and yellow pigments for coloring applications. These conclusions can serve as a guideline for the designing of new inorganic pigments by band gap engineering. The detailed investigation on optical properties can give a route to develop environmentally friendly, intense colored pigments with multifunctionality for a multitude of applications. The future scope of the present work is also discussed, to explore the band structure study for other applications like visible light photocatalysts, photochromic materials etc.

6.1 Significant Conclusions

Several series of rare earth transition metal mixed oxide based red and yellow inorganic pigments in different crystal systems have been designed based on different band gap engineering strategy like manipulating the band gap of the material by introducing substituents. The compounds were synthesized by calcination route and characterized for their structural and optical properties. The effect of substituents on the structure, microstructure and optical properties of these quarternary oxides has been studied and band structure model has been proposed for the developed pigments. The coloring performance of the pigments in a polymer matrix like PMMA is also highlighted. The NIR reflectance studies of a series of developed yellow pigments have been explored to use them as potential candidates for 'cool colorants' for multifunctional applications. The major conclusions drawn from the study is presented in this chapter.

- Thermally and chemically stable inorganic red and yellow pigments based on transition metal - rare earth mixed oxides were synthesized to replace currently using toxic ceramic pigments.

- It was found that small substitutions of transition metals (Fe, Zr, Mn, Sn and Si) into $Ce_{0.95}Pr_{0.05}O_2$ system shift their absorption edge towards the higher energy as the co-substitution of metal ion increases with change in band gap. The present investigations establish that various color hues can be achieved by the incorporation of suitable chromophore metal ions in CeO_2 host lattice by tuning the band gap. It can be concluded that substitution of transition metal ions in to Pr-CeO_2 helps to enhance the lightness and redness of ceria based red pigments.

- $TiCe_{1-x}Pr_xO_4$ (x= 0, 0.05, 0.10, 0.30, 0.50 and 0.70) solid solutions were synthesized by solid state method and they exhibit color change from white to brick red with the

increase in concentration of Pr^{4+}. Presence of Ti in the Pr - substituted ceria enhanced the lightness of the pigments retaining the redness of the pigments.

- In order to investigate the effect of RE ions on the optical properties of bismuth molybdate, $BiREMoO_6$ (RE= Y, Pr, Nd, Sm, Tb and Yb) solid solutions were synthesized and characterized to understand structure - property correlations. The substitution of rare earth for bismuth in Bi_2MoO_6 red shifted the absorption edge leading to yellow color for Y, Sm, Tb and Yb and greenish yellow color for Pr and light green color for Nd. Investigations on the optical properties of $BiREMoO_6$ reveal that the substitution of RE^{3+} in bismuth molybdate introduces addition energy level (*f* - band) in between the valence band and conduction band. The position of *f* - band depends on the no. of *f* electrons. The RE 4*f* level gradually becomes lowered with an increase of their atomic number, finally lying in the valence band, which results in increase of band gap energy. The developed pigments demonstrated good coloration to plastics and are chemically stable.

- $BiV_{1-x}M_xO_4$ (M = Nb, Ta and P; x = 0, 0.05, 0.10, 0.15 and 0.20) system was prepared by ceramic route and characterized to study the effect of pentavalent metal ion substitution on the optical properties. The substitution of M^{5+} for V^{5+} enhanced the yellow coloration of pure $BiVO_4$ by blue shifting the absorption edge of the colorants. Band gap engineering by replacing a 3d (V) metal ion with large 4d (Nb) and 5d (Ta) metal ion destabilized the antibonding conduction band and substitution of a higher electronegative metal ion (P) increased the metal-oxygen bond covalency and hence increased the band gap. The distortion produced by the substitution of M^{5+} in monoclinic $BiVO_4$ brought about special optical properties. Particle morphology and crystallite size influences the reflectance properties. Most importantly, the pentavalent metal ion substitution in bismuth vanadate enhanced the NIR reflectance to ~90 %. Morphological evolution from smooth round particles for $BiVO_4$ to rough

layer type particles for pentavalent metal ion substituted $BiVO_4$ enhanced reflectance in the NIR region. The newly designed $BiVO_4$ based yellow pigments exhibited high NIR solar reflectance, thus rendering them as excellent candidates for use as 'Cool Pigments'.

6.2 Future scope of this work

- Band structure studies of the developed pigments using Density Functional Theory.

- Most studies on photochromism of pigments seem to be carried out on vanadium and molybdenum based compounds. The photochromic behavior of Bi_2MoO_6 and $BiVO_4$ based colorants can be explored.

- The synthesized pigments having low band gap may exhibit good photocatalytic properties. The possibility of these compounds for Hydrogen production through photoelectrolysis of water and as photocatalyst for water purification can be explored.

LIST OF PUBLICATIONS IN SCI JOURNALS

Publications from the thesis

1. **Sandhya Kumari L**, Padala Prabhakar Rao, and Mundlapudi Lakshmipathi Reddy, "Environment-friendly red pigments from CeO_2-Fe_2O_3-Pr_6O_{11} solid solutions", *Journal of Alloys and Compounds 461* **(2007)** 509-515.

2. **Sandhya Kumari L**, Giable George, Padala Prabhakar Rao, and Mundlapudi Lakshmipathi Reddy, "Synthesis and characterization of environmentally benign praseodymium-doped $TiCeO_4$ pigments", *Dyes and Pigments 77* **(2008)** 427-431.

3. **Sandhya Kumari L.**, P. Prabhakar Rao, Peter Koshy, "Red Pigments based on CeO_2 – MO_2 – Pr_6O_{11} (M = Zr and Sn) Solid solutions for Coloration of Plastics", *Journal of the American Ceramic Society 93* [5] **(2010)** 1402–1408.

4. **Sandhya Kumari L.**, Thozhuthungal Haridasan Gayathri, Saithathul Fathimah Sameera, and Padala Prabhakar Rao, "Y-Doped Bi_2MoO_6 Yellow Pigments for the Coloration of Plastics", *Journal of the American Ceramic Society* 94 [2] **(2011)** 320–323.

5. **Sandhya Kumari L.**, P. Prabhakar Rao, S. Sameera, Peter Koshy, "Synthesis and Optical Properties of $Ce_{0.95}Pr_{0.05-x}M_xO_2$ (M = Mn, Si) as Potential Ecological Red Pigments for Coloration of Plastics", *Ceramics International 38* **(2012)** 4009–4016.

Publications out of the thesis

1. Giable George**, Sandhya Kumari L**, V.S. Vishnu, S. Ananthakumar, and Mundlapudi Lakshmipathi Reddy, "Synthesis and characterization of environmentally benign calcium-doped $Pr_2Mo_2O_9$: Application in plastic coatings", *Journal of Solid State Chemistry.181* **(2008)** 487-492.

2. **Sandhya Kumari L.**, P. Prabhakar Rao, Mariyam Thomas, Peter Koshy, ”Multiband Orange-Red-Emitting Phosphors, $SrY_3SiP_5O_{20}:Eu^{3+}$ under Near UV Irradiation”, *Journal of The Electrochemical Society 156* [8] **(2009)** P127-P131.

3. Saaithathul Fathima Sameera, Padala Prabhakar Rao, **Sandhya Kumari L.**, Peter Koshy, “New Scheelite-based Environmentally Friendly Yellow Pigments: $(BiV)_x(CaW)_{1-x}O_4$”, *Chemistry Letters 38* [11] (2009) 1088-1089.

4. Mariyam Thomas, Padala Prabhakar Rao, Sundaresan Pillai Kamalam Mahesh, **Sandhya Kumari L.** and Peter Koshy, “Luminescence properties of Eu^{3+}, Bi^{3+} co-activated $CaLaNbWO_8$ red phosphors under near UV and blue excitations”, *Phys. Status Solidi A 208* [9] **(2011)** 2170–2175.

LIST OF CONFERENCE PAPERS

1. **Sandhya Kumari L.**, P. Prabhakar Rao, and M. L. P. Reddy, "Environmentally benign red pigments from CeO_2-Fe_2O_3-Pr_6O_{11} solid solutions", in the National Seminar held by Indian Institute of Metals, Trivandrum Chapter.

2. **Sandhya Kumari L.**, Giable George, P. Prabhakar Rao, and M. L. P. Reddy, "Synthesis and characterization of environmentally benign red pigments: $TiCe_{1-x}Pr_xO_{4-\delta}$", in the International Seminar held by IIT Chennai, India.

3. **Sandhya Kumari L.**, P. Prabhakar Rao, M. Deepa, Mariyam Thomas, Peter Koshy, "Environmentally Benign Yellow Pigment Based on Samarium-doped Pr_2MoO_6 for Plastic Coating Applications", in the EMSI NC-2009 held by Bundelkhand university, Jhansi, India.

4. **Sandhya Kumari L.**, P. Prabhakar Rao, S. Sameera, Peter Koshy, "Novel Environmentally Friendly Yellow Pigments in Scheelite-based Oxides: $(BiV)_x(CaW)_{1-x}O_4$", in the ICAFM-2009 held by NIIST, Thiruvananthapuram, India.

5. **Sandhya Kumari L.**, Mariyam Thomas, P. Prabhakar Rao, A. N. Radhakrishnan, S. K. Mahesh, K. S. Sibi, Peter Koshy, "Structure, Microstructure and Luminescent Properties of Rare Earth Phosphors for WLED application" in the IASC-2009 held by The Indian Society of Analytical Scientists at Lonawala, Maharashtra, India.

6. **Sandhya Kumari L.**, P. Prabhakar Rao, S. Sameera, M.R. Chandran, Peter Koshy, "Effect of Tetravalent Metal Dopants on The Optical Properties of CeO_2–PrO_2 Pigments" in the STAR-2011 held by Rare Earth Association of India at Munnar, Kerala, India.

7. **Sandhya Kumari L.**, P. Prabhakar Rao, S. Sameera, M.R. Chandran, Peter Koshy, "Praseodymium - Doped Bi_2MoO_6 as Novel Environmentally Friendly Green and Yellow Pigment", in the IASC-2012 held by Indian Society of Analytical Scientists at Kanyakumari, Tamilnadu, India.

References

Abraham, F., Debreuille-Gresse, M. F., Mairesse, G.and Nowogrocki, G."Phase transitions and ionic conductivity in $Bi_4V_2O_{11}$ an oxide with a layered structure". *Solid State Ionics, 28-30*, **1988**, 529.

Adachi, G."*Science of Rare Earth*". Kagakudojin, **1999**.

Andrade, J., Villafuerte-Castrejon, M. E., Valenzuela, R.and West, A. R."Rutile solid solutions containing M^+ (Li), M^{2+} (Zn, Mg), M^{3+} (Al) and M^{5+} (Nb, Ta, Sb) ions". *Journal of Materials Science Letters, 5*, **1986**, 147.

Aruna, S. T., Ghosh, S.and Patil, K. C."Combustion Synthesis and Properties of $Ce_{1-x}Pr_xO_{2-\delta}$ Red Ceramic Pigments". *Int. J. Inorg. Mater, 3*, **2001**, 387.

Arvela, P."Toxicity of rare earths". *Progress in Pharmacology, 2*, **1979**, 69.

Badenes, J. A., Vicent, J. B., Llusar, M., Tena, M. A.and Monros, G."The nature of Pr–$ZrSiO_4$ yellow ceramic pigment". *Journal of Mateial Science, 37*, **2002**, 1413.

Baidya, T., Gayen, A., Hegde, M. S., Ravishankar, N.and Dupont, L."Enhanced Reducibility of $Ce_{1-x}Ti_xO_2$ Compared to That of CeO_2 and Higher Redox Catalytic Activity of $Ce_{1-x-y}Ti_xPt_yO_{2-\delta}$ Compared to That of $Ce_{1-x}Pt_xO_{2-\delta}$". *The Journal of Physical Chemistry B, 110*, **2006**, 5262.

Berke, H."The invention of blue and purple pigments in ancient times". *Chemical Society Reviews, 36*, **2007**, 15.

Blonski, R. P."Stable heavy metal free zircon pigments for use in plastics and paints and method for coloring thereof." *U.S. Patent No. 5,316,570*, **1994**.

Bondioli, F., Ferrari, A. M., Leonelli, C.and Manfredini, T."Syntheses of Fe_2O_3/Silica Red Inorganic Inclusion Pigments for Ceramic Applications". *Materials Research Bulletin, 33*, **1998**, 723.

Bondioli, F., Ferrari, A. M., Lusvarghi, L., Manfredini, T., Nannerone, S., Pasquali, L."Synthesis and Characterization of Praseodymium-Doped Ceria Powders by a Microwave-Assisted Hydrothermal Route". *J. Mater. Chem., 15*, **2005**, 1061.

Borgarello, E., Kiwi, J., Graetzel, M., Pelizzetti, E.and Visca, M."Visible light induced water cleavage in colloidal solutions of chromium-doped titanium dioxide particles". *Journal of the American Chemical Society, 104*, **1982**, 2996.

Bornick, R. M.and Stacy, A. M."Intermediate Valence in $EuCo_{2-x}Ni_xP_2$: Interdependence of Structure and Energetics". *Chemistry of Materials, 6*, **1994**, 333.

Bosacka, M., Kurzawa, M., Rychlowska-Himmel, I.and Szkoda, I."Phase relations in the system ZnO-$BiVO_4$: the synthesis and properties of $BiZn_2VO_6$". *Thermochimica Acta, 428*, **2005**, 51.

Brown, I. D.and Wu, K. K."Empirical parameters for calculating cation–oxygen bond valences". *Acta Crystallographica Section B, 32*, **1976**, 1957.

Bunzli, J.-C. G.and Piguet, C."Taking advantage of luminescent lanthanide ions". *Chemical Society Reviews, 34*, **2005**, 1048.

Busnot, S.and Macaudiere, P."Composition based on samarium sesquisulphide, preparation method and use as coloring pigment". *U.S. Patent No. 6,419,735*, **2002**.

Buxbaum."*Introduction to Inorganic High Performance Pigments*". Wiley-VCH Verlag GmbH & Co. KGaA, **2003**.

Buxbaum, G."*Industrial inorganic pigments*". Weinheim; New York, Wiley-VCH, **1998**.

Buxbaum, G.and Pfaff, G."*Industrial inorganic pigments*". Weinheim, Wiley-VCH Verlag GmbH & Co, **2005**.

Buxhaum, G." *Industrial inorganic pigments*". Germany, VCH, **1993**.

Byong K, C."Chemical modification of catalyst support for enhancement of transient catalytic activity: nitric oxide reduction by carbon monoxide over rhodium". *Journal of Catalysis, 131*, **1991**, 74.

Candeia, R. A., Souza, M. A. F., Bernardi, M. I. B., Maestrelli, S. C., Santos, I. M. G., Souza, A. G."$MgFe_2O_4$ pigment obtained at low temperature". *Materials Research Bulletin, 41*, **2006**, 183.

Cavalcante, P. M. T., Dondi, M., Guarini, G., Raimondo, M.and Baldi, G."Colour performance of ceramic nano-pigments". *Dyes and Pigments, 80*, **2009**, 226.

Chaminade, J. P., Olazcuaga, R., Le Polles, G., Le Flem, G.and Hagenmuller, P."Crystal growth and characterization of $Ce_{1-x}Pr_xO_2$ (x =0.05) single crystals". *Journal of Crystal Growth, 87*, **1988**, 463.

Christie, R. M."*Colour chemistry*". UK, Royal Society of Chemistry, **2001**.

Connell, M. O.and Morris, M. A."New ceria-based catalysts for pollution abatement". *Catalysis Today, 59*, **2000**, 387.

Coster, M., Arnould, X., Chermant, J. L., Chermant, L.and Chartier, T."The use of image analysis for sintering investigations: The example of CeO_2 doped with TiO_2". *Journal of the European Ceramic Society, 25*, **2005**, 3427.

Dohnalova, Z., Sulcova, P.and Trojan, M."Synthesis and characterization of $LnFeO_3$ pigments". *Journal of Thermal Analysis and Calorimetry, 91*, **2008**, 559.

Dohnalova, Z., Sulcova, P.and Trojan, M."Effect of Er^{3+} substitution on the quality of Mg-Fe spinel pigments". *Dyes and Pigments, 80*, **2009**, 22.

Dondi, M., Matteucci, F., Zama, I.and Cruciani, G."High-performance yellow ceramic pigments $Zr(Ti_{1-x-y}Sn_{x-y}V_yM_y)O_4$ (M = Al, In, Y): Crystal structure, colouring mechanism and technological properties". *Materials Research Bulletin, 42*, **2007**, 64.

Emiliani, G.and Corbara, F."*Tecnologia Ceramica: Le Materie Prime (CeramicTechnology: Raw Materials)*". Faenza, Italy, Grupo Editoriale Faenza Editrice S.P.A. (Italia), **1999**.

Eppler, R. A."*Ullmann's encyclopedia of industry*". A5. Germany, Weinheim: VCH, **1998**.

Erkens."Bismuth vanadate pigment powder mixtures". *U.S. Patent 5976238*, **1999**.

Escribano, P., Carda, J. B.and Cordoncillo, E."*Esmaltes y Pigmentos Cerámicos. Enciclopedia Cerámica*". 3, Faenza Editrice Ibérica, **2001**.

Fernandez-Gonzalez, R., Julian-Lopez, B., Cordoncillo, E.and Escribano, P."New insights on the structural and optical properties of Ce-Ti mixed oxide nanoparticles doped with praseodymium". *Journal of Materials Chemistry, 21*, **2011**, 497.

Fierro, J. L. G."*Metal oxides: chemistry and applications*". Boca Raton, FL, Taylor & Francis, **2006**.

Furukawa, S., Masui, T.and Imanaka, N."Synthesis of new environment-friendly yellow pigments". *Journal of Alloys and Compounds, 418*, **2006**, 255.

García, A., Llusar, M., Calbo, J., Tena, M. A.and Monrós, G."Low-toxicity red ceramic pigments for porcelainised stoneware from lanthanide–cerianite solid solutions". *Green Chemistry, 3*, **2001**, 238.

Gauthier, G., Jobic, S., Evain, M., Koo, H. J., Whangbo, M. H., Fouassier, C."Syntheses, Structures, and Optical Properties of Yellow Ce_2SiS_5, $Ce_6Si_4S_{17}$, and $Ce_4Si_3S_{12}$ Materials". *Chemistry of Materials, 15*, **2003**, 828.

George, G., George, G., Rao, P. P.and Reddy, M. L."Synthesis and Characterization of Environmentally Benign Nontoxic Pigments: $RE_2Mo_2O_9$ (RE = La or Pr)". *Chemistry Letters, 34*, **2005**, 1702.

George, G., Rao, P. P.and Reddy, M. L. P."Synthesis and Characterization of CeO_2-TiO_2-Pr_6O_{11} Solid Solutions for Environmentally Benign Nontoxic Red Pigments". *Chemistry Letters, 35*, **2006**, 1412.

George, G., Sandhya Kumari, L., Vishnu, V. S., Ananthakumar, S.and Reddy, M. L. P."Synthesis and characterization of environmentally benign calcium-doped $Pr_2Mo_2O_9$ pigments: Applications in coloring of plastics". *Journal of Solid State Chemistry, 181*, **2008**, 487.

George, G., Vishnu, V. S.and Reddy, M. L. P."The synthesis, characterization and optical properties of silicon and praseodymium doped Y_6MoO_{12} compounds: Environmentally benign inorganic pigments with high NIR reflectance". *Dyes And Pigments, 88*, **2011**, 109.

Giable, G., Rao, P. P.and Reddy, M. L. P."Synthesis and Characterization of CeO_2-TiO_2-Pr_6O_{11} Solid Solutions for Environmentally Benign Nontoxic Red Pigments". *Chemistry Letters, 35*, **2006**, 1412.

Glerup, M., Nielsen, O. F.and Poulsen, F. W."The structural transformation from the pyrochlore structure, $A_2B_2O_7$, to the fluorite structure, AO_2, studied by Raman spectroscopy and defect chemistry modeling". *J. Solid State Chem., 160*, **2001**, 25.

Gonzalvo, B., Romero, J., Fernández, F.and Torralvo, M. J."$(Bi,R)_2O_3$ (R: Nd, Sm and Dy) oxides as potential pigments". *Journal of Alloys and Compounds, 323-324*, **2001**, 372.

Gorte, R. J."What do we know about the acidity of solid acids?" *Catalysis Letters, 62*, **1999**, 1.

Gotic, M., Music, S., Ivanda, M., Soufek, M.and Popovic, S."Synthesis and characterisation of bismuth(III) vanadate". *Journal of Molecular Structure, 744-747*, **2005**, 535.

Goubin, F., Rocquefelte, X., Whangbo, M.-H., Montardi, Y., Brec, R.and Jobic, S."Experimental and Theoretical Characterization of the Optical Properties of CeO_2, $SrCeO_3$, and Sr_2CeO_4 Containing Ce^{4+} (f^0) Ions". *Chemistry of Materials, 16*, **2004**, 662.

Gupta, A., Kumar, A., Waghmare, Umesh, V.and Hegde, M. S."Origin of activation of Lattice Oxygen and Synergistic Interaction in Bimetal-Ionic $Ce_{0.89}Fe_{0.1}Pd_{0.01}O_2$ Catalyst". *Chemistry of Materials, 21*, **2009**, 4880.

Gupta, K. K., Nishkam, A.and Kasturiya, N."Camouflage in the Non-Visible Region ". *Journal of Industrial Textiles, 31*, **2001**, 27-42.

Haley, T. J."Pharmacology and toxicology of the rare earth elements". *Journal of Pharmaceutical Sciences, 54*, **1965**, 663.

Hardcastle, F. D.and Wachs, I. E."Determination of vanadium-oxygen bond distances and bond orders by Raman spectroscopy". *The Journal of Physical Chemistry, 95*, **1991**, 5031.

Hill, K., Lehman, R.and Swiler, D."Effects of Selected Processing Variables on Color Formation in Praseodymium-Doped Zircon Pigments". *Journal of the American Ceramic Society, 83*, **2000**, 2177.

Hiroshi, T., Junji, K., Masahisa, N.and Shinobu, S."Europium chelate solid laser based on morphology - dependent resonances ". *Applied Physics Letters, 67*, **1995**, 1060.

Hoefdraad, H. E."Charge-transfer spectra of tetravalent lanthanide ions in oxides". *Journal of Inorganic and Nuclear Chemistry, 37*, **1975**, 1917.

Hoffart, L., Heider, U., Jörissen, L., Huggins, R. A.and Witschel, W."Transport properties of materials with the scheelite structure". *Solid State Ionics, 72*, **1994**, 195.

Imamura, S., Shono, M., Okamoto, N., Hamada, A.and Ishida, S."Effect of cerium on the mobility of oxygen on manganese oxides". *Applied Catalysis A: General, 142*, **1996**, 279.

Imanaka, N., Masui, T.and Furukawa, S."Novel Nontoxic and Environment-friendly Inorganic Yellow Pigments". *Chemistry Letters, 37*, **2008**, 104.

Jansen, M.and Letschert, H. P."Inorganic yellow-red pigments without toxic metals". *Nature, 404*, **2000**, 980.

Jatia, A., Chang, C., MacLeod, J. D., Okubo, T.and Davis, M. E."ZrO_2 promoted with sulfate, iron and manganese: a solid superacid catalyst capable of low temperature n-butane isomerization". *Catalysis Letters, 25*, **1994**, 21.

Jeevanandam, P., Mulukutla, R. S., Phillips, M., Chaudhuri, S., Erickson, L. E.and Klabunde, K. J."Near infrared reflectance properties of metal oxide nanoparticles". *Journal of Physical Chemistry C, 111*, **2007**, 1912.

Jorgensen, C. K."*Oxidation Numbers and oxidation states*". Berlin, Springer, **1969**.

Jørgensen, C. K.and Rittershaus, E."Powder-Diagram and Spectroscopic Studies of Mixed Oxides of Lanthanides and Quadrivalents Metals". *Mat. Fys. Medd. K. Dan. Vidensk. Selsk., 35*, **1967**, 1.

Kato, E. "Synthesis of yellow Pr-$ZrSiO_4$ pigments". *Keram. Zeit., 13*, **1961**, 617.

Kepinski, L., Hreniak, D.and Strek, W."Microstructure and luminescence properties of nanocrystalline cerium silicates". *Journal of Alloys and Compounds, 341*, **2002**, 203.

Kido, J.and Okamoto, Y."Organo Lanthanide Metal Complexes for Electroluminescent Materials". *Chemical Reviews, 102*, **2002**, 2357.

Koebrugge, G. W., Winnubst, L.and Burggraaf, A. J."Thermal stability of nanostructured titania and titania-ceria ceramic powders prepared by the sol-gel process". *Journal of Materials Chemistry, 3*, **1993**, 1095.

Koelling, D. D., Boring, A. M.and Wood, J. H."The electronic structure of CeO_2 and PrO_2". *Solid State Communications, 47*, **1983**, 227.

Krishna Reddy, J., Srinivas, B., Durga Kumari, V.and Subrahmanyam, M."Sm^{3+}-Doped Bi_2O_3 Photocatalyst Prepared by Hydrothermal Synthesis". *ChemCatChem, 1*, **2009**, 492.

Kudo, A., Omori, K.and Kato, H."A Novel Aqueous Process for Preparation of Crystal Form-Controlled and Highly Crystalline $BiVO_4$ Powder from Layered Vanadates

at Room Temperature and Its Photocatalytic and Photophysical Properties". *Journal of the American Chemical Society, 121*, **1999**, 11459.

Kumari, L. S., George, G., Rao, P. P.and Reddy, M. L. P."The synthesis and characterization of environmentally benign praseodymium-doped $TiCeO_4$ pigments". *Dyes and Pigments, 77*, **2008**, 427.

Levinson, R., Akbari, H.and Reilly, J. C."Cooler tile-roofed buildings with near-infrared-reflective non-white coatings". *Building and Environment, 42*, **2007a**, 2591.

Levinson, R., Berdahl, P.and Akbari, H."Solar spectral optical properties of pigments-Part I: model for deriving scattering and absorption coefficients from transmittance and reflectance measurements". *Solar Energy Materials and Solar Cells, 89*, **2005a**, 319.

Levinson, R., Berdahl, P.and Akbari, H."Solar spectral optical properties of pigments-Part II: survey of common colorants". *Solar Energy Materials and Solar Cells, 89*, **2005b**, 351.

Levinson, R., Berdahl, P., Akbari, H., Miller, W., Joedicke, I., Reilly, J."Methods of creating solar-reflective nonwhite surfaces and their application to residential roofing materials". *Solar Energy Materials and Solar Cells, 91*, **2007b**, 304.

Li, H., Li, K.and Wang, H."Hydrothermal synthesis and photocatalytic properties of bismuth molybdate materials". *Materials Chemistry and Physics, 116*, **2009**, 134.

Liu, J., Zhao, Z., Xu, C., Duan, A., Wang, L.and Zhang, S."Synthesis of nanopowder Ce-Zr-Pr oxide solid solutions and their catalytic performances for soot combustion". *Catalysis Communications, 8*, **2007**, 220.

Llusar, M., Calbo, J., Badenes, J. A., Tena, M. A.and Monros, G."Synthesis of iron zircon coral by coprecipitation routes". *Journal of Materials Science, 36*, **2001**, 153.

Llusar, M., Vitaskova, L., Sulcova, P., Tena, M. A., Badenes, J. A.and Monros, G."Red ceramic pigments of terbium-doped ceria prepared through classical and non-conventional coprecipitation routes". *Journal of the European Ceramic Society, 30*, **2010**, 37.

Lopez, T., Rojas, F., Alexander-Katz, R., Galindo, F., Balankin, A.and Buljan, A."Porosity, structural and fractal study of sol-gel TiO_2-CeO_2 mixed oxides". *Journal of Solid State Chemistry, 177*, **2004**, 1873.

Martos, M., Julian-Lopez, B., Cordoncillo, E.and Escribano, P."Structural and Spectroscopic Study of a Novel Erbium Titanate Pink Pigment Prepared by Sol-Gel Methodology". *The Journal of Physical Chemistry B, 112*, **2008**, 2319.

Masui, T., Furukawa, S.and Imanaka, N."Synthesis and Characterization of CeO_2-ZrO_2-Bi_2O_3 Solid Solutions for Environment-friendly Yellow Pigments". *Chemistry Letters, 35*, **2006**, 1032.

Masui, T., Tategaki, H.and Imanaka, N."Preparation and characterization of SiO_2-CeO_2 particles applicable for environment-friendly yellow pigments". *Journal of Materials Science, 39*, **2004**, 4909.

Matteucci, F., Cruciani, G., Dondi, M., Gasparotto, G.and Tobaldi, D. M."Crystal structure, optical properties and colouring performance of karrooite $MgTi_2O_5$ ceramic pigments". *Journal of Solid State Chemistry, 180*, **2007**, 3196.

Miki, T., Ogawa, T., Haneda, M., Kakuta, N., Ueno, A., Tateishi, S."Enhanced oxygen storage capacity of cerium oxides in cerium dioxide/lanthanum

sesquioxide/alumina containing precious metals". *The Journal of Physical Chemistry, 94*, **1990**, 6464.

Mizoguchi, H., Hosono, H., Kawazoe, H., Yasukawa, M., Fujitsu, S.and Fukumi, K."Valence states of bismuth in new mixed-valence oxides: $Bi_{1-x}Y_xO_{1.5+\delta}$ (x = 0.4) by XANES". *Materials Research Bulletin, 34*, **1999**, 373.

Modly, Z. M."Pigment consisting of a mixture of chromium oxide and iron oxide useful in high infra red reflectance gray vinyl composition ". *U.S. Patent No. 4,624,710*, **1986**.

Nahum, M., Hector, B., Raquel, M., Beatriz, J., Juan, B. C.and Purificacion, E."Optimization of Praseodymium-Doped Cerium Pigment Synthesis Temperature". *J. Am. Ceram. Soc, 86*, **2003**, 425.

Neves, M. C., Lehocky, M., Soares, R., Lapcik, L.and Trindade, T."Chemical bath deposition of cerium doped $BiVO_4$". *Dyes and Pigments, 59*, **2003**, 181.

Nunes, M. G. B., Cavalcante, L. S., Santos, V., Sczancoski, J. C., Santos, M. R. M. C., Santos-Junior, L. S."Sol-gel synthesis and characterization of Fe_2O_3 - CeO_2 doped with Pr ceramic pigments". *Journal of Sol-Gel Science and Technology, 47*, **2008**, 38.

Odaki, T., Hashimoto, K.and Toda, Y."The Color Sift of Cerium Molybdenum Sheelite by Substituting Bi^{3+} or W^{6+} Ion". *Journal of the Japan Society of Colour Material, 81*, **2008**, 73.

Ohno, Y."CIE Fundamentals for Color Measurements". *INTERNATIONAL CONFERENCE ON DIGITAL PRINTING TECHNOLOGIES*, **2000**, 540.

Olazcuaga, R., El Kira, A., Le Flem, G.and Hagenmuller, P."Pr-CeO_2 red pigment". *Rev. Chim. Miner., 21*, **1984**, 221.

Pailhe, N., Gaudon, M.and Demourgues, A."(Ca^{2+}, V^{5+}) co-doped $Y_2Ti_2O_7$ yellow pigment". *Materials Research Bulletin, 44*, **2009**, 1771.

Pailhe, N., Wattiaux, A., Gaudon, M.and Demourgues, A."Correlation between structural features and vis-NIR spectra of α-Fe_2O_3 hematite and AFe_2O_4 spinel oxides (A=Mg, Zn)". *Journal of Solid State Chemistry, 181*, **2008**, 1040.

Perrin, M. A.and Wimmer, E."Color of pure and alkali-doped cerium sulfide: A local-density-functional study". *Physical Review B, 54*, **1996**, 2428.

Petoud, S., Cohen, S. M., Bunzli, J.-C. G.and Raymond, K. N."Stable Lanthanide Luminescence Agents Highly Emissive in Aqueous Solution: Multidentate 2-Hydroxyisophthalamide Complexes of Sm^{3+}, Eu^{3+}, Tb^{3+}, Dy^{3+}". *Journal of the American Chemical Society, 125*, **2003**, 13324.

Philips, J. C."*Bonds and bands in semiconductors*". New York, **1973**.

Pijolat, M., Prin, M., Soustelle, M., Touret, O.and Nortier, P."Thermal stability of doped ceria: experiment and modelling". *Journal of the Chemical Society, Faraday Transactions, 91*, **1995**, 3941.

Prabhakar Rao, P.and Reddy, M. L. P."Synthesis and characterisation of $(BiRE)_2O_3$ (RE: Y, Ce) pigments". *Dyes and Pigments, 63*, **2004**, 169.

Prokofiev, A. V., Shelykh, A. I.and Melekh, B. T."Periodicity in the band gap variation of Ln_2X_3 (X = O, S, Se) in the lanthanide series". *Journal of Alloys and Compounds, 242*, **1996**, 41.

Radostin, S. P., Juan, B. C., Vicente, B. M.and Hohembergerger, J. M."New Red Shade Ceramic Pigments Based on $Y_2Sn_{2-x}Cr_xO_{7-\delta}$ Pyrochlore Solid Solutions". *J Am Ceram Soc, 85*, **2002**, 1197.

Rao, P. P.and Reddy, M. L. P."$(TiO_2)_1$ $(CeO_2)_{1-x}$ $(RE_2O_3)_x$ - novel environmental secure pigments". *Dyes and Pigments, 73*, **2007**, 292.

Reddy, B. M.and Khan, A."Nanosized CeO_2–SiO_2, CeO_2–TiO_2, and CeO_2–ZrO_2 mixed oxides: influence of supporting oxide on thermal stability and oxygen storage properties of ceria". *Catalysis Surveys from Asia, 9*, **2005**, 155.

Reddy, B. M., Khan, A., Lakshmanan, P., Aouine, M., Loridant, S.and Volta, J.-C."Structural Characterization of Nanosized CeO_2-SiO_2, CeO_2-TiO_2, and CeO_2-ZrO_2 Catalysts by XRD, Raman, and HREM Techniques". *The Journal of Physical Chemistry B, 109*, **2005**, 3355.

Reddy, B. M., Khan, A., Yamada, Y., Kobayashi, T., Loridant, S. p.and Volta, J.-C."Raman and X-ray Photoelectron Spectroscopy Study of CeO_2-ZrO_2 and V_2O_5/CeO_2-ZrO_2 Catalysts". *Langmuir, 19*, **2003a**, 3025.

Reddy, B. M., Khan, A., Yamada, Y., Kobayashi, T., Loridant, S. p.and Volta, J.-C."Structural Characterization of CeO_2-MO_2 (M = Si^{4+}, Ti^{4+}, and Zr^{4+}) Mixed Oxides by Raman Spectroscopy, X-ray Photoelectron Spectroscopy, and Other Techniques". *The Journal of Physical Chemistry B, 107*, **2003b**, 11475.

Reddy, J., Lalitha, K., Durga Kumari, V.and Subrahmanyam, M."Photocatalytic Study of Bi-ZSM-5 and Bi_2O_3-HZSM-5 for the Treatment of Phenolic Wastes". *Catalysis Letters, 121*, **2008**, 131.

Richard, A. E.and Douglas, R. E."Which Colors Can and Cannot Be Produced in Ceramic Glazes ". *Ceram Eng Sci Proc, 15*, **1994**, 281.

Romero, S., Mosset, A., Macaudière, P.and Trombe, J. C."Effect of some dopant elements on the low temperature formation of γ-Ce_2S_3". *Journal of Alloys and Compounds, 302*, **2000**, 118.

Roncari, E., Galassi, C., Ardizzone, S.and Bianchi, C. L."Vanadium-doped TiO_2 catalysts. A unifying picture of powders and suspensions". *Colloids and Surfaces A: Physicochemical and Engineering Aspects, 117*, **1996**, 267.

Rynkowski, J., Farbotko, J., Touroude, R.and Hilaire, L."Redox behaviour of ceria-titania mixed oxides". *Applied Catalysis A: General, 203*, **2000**, 335.

Sakoske, George, E., Sarver, Joseph, E., Novotnyand Miroslav."Bismuth manganese oxide pigments". *US Patent 6221147*, **2001**.

Santos, S. F., de Andrade, M. C., Sampaio, J. A., da Luz, A. B.and Ogasawara, T."Synthesis of ceria-praseodymia pigments by citrate-gel method for dental restorations". *Dyes and Pigments, 75*, **2007**, 574.

Shannon, R."Revised effective ionic radii and systematic studies of interatomic distances in halides and chalcogenides". *Acta Crystallographica Section A, 32*, **1976**, 751.

Shia, M. L., Kalkanoglu, H. M.and Hong, K. C."Colored roofing granules with increased solar heat reflectance, solar heat-reflective shingles, and process for producing same ". *7,241,500*, **2007**.

Shimodaira, Y., Kato, H., Kobayashi, H.and Kudo, A."Photophysical Properties and Photocatalytic Activities of Bismuth Molybdates under Visible Light Irradiation". *The Journal of Physical Chemistry B, 110*, **2006a**, 17790.

Shimodaira, Y., Kato, H., Kobayashi, H.and Kudo, A."Photophysical Properties and Photocatalytic Activities of Bismuth Molybdates under Visible Light Irradiation". *The Journal of Physical Chemistry B, 110*, **2006b**, 17790.

Shuk, P., Greenblatt, M.and Croft, M."Hydrothermal Synthesis and Properties of Mixed Conducting $Ce_{1-x}Tb_xO_{2-\delta}$ Solid Solutions". *Chemistry of Materials, 11*, **1999**, 473.

Silversmith, A. J., Boye, D. M., Brewer, K. S., Gillespie, C. E., Lu, Y.and Campbell, D. L."$^5D_3$-->^7F_J emission in terbium-doped sol-gel glasses". *Journal of Luminescence, 121*, **2006**, 14.

Sivakumar, V.and Varadaraju, U. V."Environmentally benign novel green pigments: $Pr_{1-x}Ca_xPO_4$ (x=0-0.4)". *Material Science, 28*, **2005**, 299.

Sleight, A. W."Heterogeneous Catalysts". *Science, 208*, **1980**, 895.

Sleight, A. W., Chen, H. y., Ferretti, A.and Cox, D. E."Crystal growth and structure of $BiVO_4$". *Materials Research Bulletin, 14*, **1979**, 1571.

Sliwinsky, T. R., Pipoly, R. A.and Blonski, R. P."Infrared reflective color pigment ". *U.S. Patent No. 6,454,848*, **2002**.

Smith, H. M."*High Performance Pigments*". Wiley-VCH, **2002**.

Sreeram, K. J., Aby, C. P.and Nair, B. U."Synthesis and characterization of doped rare earth oxides for environmentally benign nontoxic reddish-yellow pigments". *Chemistry Letters, 37*, **2008a**, 902.

Sreeram, K. J., Aby, C. P., Nair, B. U.and Ramasami, T."Colored cool colorants based on rare earth metal ions". *Solar Energy Materials and Solar Cells, 92*, **2008b**, 1462.

Sreeram, K. J., Srinivasan, R., Meena Devi, J., Unni Nair, B.and Ramasami, T."Cerium molybdenum oxides for environmentally benign pigments". *Dyes and Pigments, 75*, **2007**, 687.

Stengl, V., Bakardjieva, S.and Murafa, N."Preparation and photocatalytic activity of rare earth doped TiO2 nanoparticles". *Materials Chemistry and Physics, 114*, **2009**, 217.

Sulcova, P.and Prokleskova, E."The effect of lanthanides on colour properties of the $(Bi_2O_3)_{0.7}(Ln_2O_3)_{0.3}$ compounds". *J. of Mining and Metallurgy, 44*, **2008**, 27.

Sulcova, P., Prokleskova, E., Bystrzycki, P.and Trojan, M."Thermal analysis of the $(Bi_2O_3)_{1-x}(Lu_2O_3)_x$ compounds". *Journal of Thermal Analysis and Calorimetry, 100*, **2010a**, 65.

Sulcova, P.and Trojan, M."Synthesis of $Ce_{1-x}Pr_xO_2$ pigments with other lanthanides". *Dyes and Pigments, 40*, **1999**, 87.

Sulcova, P.and Trojan, M."Thermal Analysis of Pigments Based on CeO_2". *Journal of Thermal Analysis and Calorimetry, 65*, **2001**, 399.

Sulcova, P.and Trojan, M."Study of $Ce_{1-x}Pr_xO_2$ Pigments". *Themochim. Acta, 395*, **2003a**, 251.

Sulcova, P.and Trojan, M."The synthesis and analysis of $Ce_{0.95-y}Pr_{0.05}Sm_yO_{2-y/2}$ pigments". *Dyes and Pigments, 58*, **2003b**, 59.

Sulcova, P.and Trojan, M."Thermal Synthesis of the CeO_2–PrO_2–La_2O_3 Pigments". *J. Therm. Anal. Calorim., 77*, **2004**, 99.

Sulcova, P.and Trojan, M."Thermal synthesis and properties of the $(Bi_2O_3)_{1-x}(Ho_2O_3)_x$ pigments". *Journal of Thermal Analysis and Calorimetry, 83*, **2006**, 557.

Sulcova, P.and Trojan, M."Thermal synthesis of the $(Bi_2O_3)_{1-x}(Er_2O_3)_x$ pigments". *Journal of Thermal Analysis and Calorimetry, 88*, **2007**, 111.

Sulcova, P.and Trojan, M."Thermal analysis of the $(Bi_2O_3)_{1-x}(Y_2O_3)_x$; pigments". *Journal of Thermal Analysis and Calorimetry, 91*, **2008a**, 151.

Sulcova, P.and Trojan, M."Thermal analysis of the Bi_2O_3-Er_2O_3-ZrO_2 pigments". *Journal of Thermal Analysis and Calorimetry, 91*, **2008b**, 805.

Sulcova, P.and Trojan, M."Thermal analysis of the Bi_2O_3-Y_2O_3-ZrO_2 pigments". *Journal of Thermal Analysis and Calorimetry, 93*, **2008c**, 795.

Sulcova, P., Trojan, M.and Solc, M."Cerium Dioxide Fluorite Type Pigments". *Dyes and Pigments, 37*, **1998**, 65.

Sulcova, P., Vitaskova, L.and Trojan, M."Thermal analysis of the $Ce_{1-x}Tb_xO_2$ pigments". *Journal of Thermal Analysis and Calorimetry, 99*, **2010b**, 409.

Suzuki, K.and Kijima, K."Optical Band Gap of Barium Titanate Nanoparticles prepared by RF-plasma Chemical Vapor Deposition. " *Jpn. J. Apply. Phys., 44*, **2005**, 2081.

Swilerand Axtell, E. A."Rare earth manganese oxide pigments ". *U.S. Patent No. 6,541,112*, **2003**.

Swiler, D."Manganese vanadium oxide pigments". *U.S. Patent No. 6,485,557*, **2002**.

Synnefa, A., Santamouris, M.and Apostolakis, K."On the development, optical properties and thermal performance of cool colored coatings for the urban environment". *Solar Energy, 81*, **2007**, 488.

Tabora, J. E.and Davis, R. J."Structure of Fe, Mn-promoted sulfated zirconia catalyst by X-ray and IR absorption spectroscopies". *Journal of the Chemical Society, Faraday Transactions, 91*, **1995**, 1825.

Tago, T., Tashiro, S., Hashimoto, Y., Wakabayashi, K.and Kishida, M."Synthesis and Optical Properties of SiO_2-Coated CeO_2 Nanoparticles". *Journal of Nanoparticle Research, 5*, **2003**, 55.

Takahashi, T.and Iwahara, H."Oxide ion conductors based on bismuthsesquioxide". *Materials Research Bulletin, 13*, **1978**, 1447.

Tokunaga, S., Kato, H.and Kudo, A."Selective Preparation of Monoclinic and Tetragonal $BiVO_4$ with Scheelite Structure and Their Photocatalytic Properties". *Chemistry of Materials, 13*, **2001**, 4624.

Trojan, M., Solc, Z.and Novotny, M."*Pigments, Kirk-Othmer Encyclopedia of Chemical Technology*". 19. New York, Wiley and Sons, **1996**.

Tung, L.-C., Chen, J. C., Wu, M. K.and Guan, W."Ion-size effect on superconducting transition temperature T_c in $R_{1-x-y}Pr_xCa_yBa_2Cu_3O_{7-z}$ systems (R=Er, Dy, Gd, Eu, Sm, and Nd)". *Physical Review B, 59*, **1999**, 4504.

Van Vechten, J. A.and Phillips, J. C."New Set of Tetrahedral Covalent Radii". *Physical Review B, 2*, **1970**, 2160.

Vishnu, V. S.and Reddy, M. L."Near-infrared Reflecting Yellow Inorganic Pigments Based on Molybdenum-doped Yttrium Cerate: Synthesis, Characterization, and Optical Properties". *Chemistry Letters, 39*, **2010**, 820.

Vishnu, V. S.and Reddy, M. L."Near-infrared reflecting inorganic pigments based on molybdenum and praseodymium doped yttrium cerate: Synthesis, characterization and optical properties". *Solar Energy Materials and Solar Cells, 95*, **2011**, 2685.

Volz, H. G."*Industrial color testing: fundamentals and techniques*". Weinheim [u.a.], Wiley-VCH, **2001**.

Walsh, A., Yan, Y., Huda, M. N., Al-Jassim, M. M.and Wei, S.-H."Band Edge Electronic Structure of $BiVO_4$: Elucidating the Role of the Bi s and V d Orbitals". *Chemistry of Materials, 21*, **2009**, 547.

West, A. R."*Solid State Chemistry and its Applications*". John Wiley &Sons, **1989**.

Yashima, M., Arashi, H., Kakihana, M.and Yoshimura, M."Raman Scattering Study of Cubic–Tetragonal Phase Transition in $Zr_{1-x}Ce_xO_2$ Solid Solution". *Journal of the American Ceramic Society, 77*, **1994**, 1067.

Yu, J.and Kudo, A."Hydrothermal Synthesis and Photocatalytic Property of 2-Dimensional Bismuth Molybdate Nanoplates". *Chemistry Letters, 34*, **2005**, 1528.

Zhang, L., Wang, W., Yang, J., Chen, Z., Zhang, W., Zhou, L."Sonochemical synthesis of nanocrystallite Bi_2O_3 as a visible-light-driven photocatalyst". *Applied Catalysis A: General, 308*, **2006**, 105.

Zhao, Z., Li, Z.and Zou, Z."Electronic structure and optical properties of monoclinic clinobisvanite $BiVO_4$". *Physical Chemistry Chemical Physics, 13*, **2011**, 4746.

Zhou, L., Yu, M., Yang, J., Wang, Y.and Yu, C."Nanosheet-Based $Bi_2Mo_xW_{1-x}O_6$ Solid Solutions with Adjustable Band Gaps and Enhanced Visible-Light-Driven Photocatalytic Activities". *The Journal of Physical Chemistry C, 114*, **2010**, 18812.

Zhu Zhen-Feng, Wang bao-Liand MA., J.-Z."Characterization of Pr-CeO_2 nano crystallites prepared by low-temperature combustion & hydrothermal synthesis. " *Chinese J. Struct. Chem, 25*, **2006**, 1270.

Zhukov, V., Mauricot, R., Gressier, P.and Evain, M."Band Electronic Structure Study of Some Doped and Undoped γ-Ln_2S_3(Ln=La, Ce, Pr, and Nd) Rare Earth Sulfides through LMTO-TB Calculations". *Journal of Solid State Chemistry, 128*, **1997**, 197.

Zou, Z., Ye, J.and Arakawa, H."Role of R in Bi_2RNbO_7 (R = Y, Rare Earth): Effect on Band Structure and Photocatalytic Properties". *The Journal of Physical Chemistry B, 106*, **2001**, 517.